Internal Pore-Water Pressure Measurements and Effective Stress Analysis in Partially Frozen Soil

by

Yawu Liang

A thesis submitted in partial fulfillment of the requirements for the degree of

Doctor of Philosophy

in

Geotechnical Engineering

Department of Civil and Environment Engineering
University of Alberta

Abstract

The thawing of permafrost is one of the major challenges facing coastal and northern communities in Canada's North as it is associated with the deterioration of overlying infrastructures. In addition, the industrial development and expansion of Inuit communities demand more climate-resilient infrastructures. However, current engineering design practice utilized in cold permafrost regions is less robust in warm permafrost regions (i.e., > –2 ºC). The "near surface" soils in these warm regions, particularly in ice-rich and/or saline areas, are at a partially frozen state with unfrozen water and ice coexisting in the pore space. Further, if there is sufficient unfrozen water to provide a continuous water phase within the pore network, the effective stress that controls the strength and deformation of a soil, should be established via pore water pressure (PWP) measurement. For the prediction of behavior of existing infrastructures and the design for new soil structures to withstand climate change, the measurement of PWP and conducting an effective stress analysis are desirable to properly understand the mechanical properties of partially frozen soil. Thus, the main focus of this study is to develop a new method for measuring internal PWP and establishing the effective stress within the partially frozen soil.

Firstly, a new triaxial testing method for internal PWP measurement within soil using the filter-less rigid piezometers (FRPs) is developed. Then, this method is extended to partially frozen soil in order to examine the continuity in the water phase. A series of consolidated undrained and drained triaxial tests were performed on both dense and loose sand with a salinity of 30 ppt, at different temperatures (-3, -5, and -10 ºC) and strain rates (1 %/min and 0.1%/min). Continuity in

the unfrozen water phase was confirmed by comparing PWP measurements between the FRPs and the base transducer, at -3 and -5 °C. During shear, the decreases in PWP of partially frozen, loose and dense sand are mainly attributed to the shear-induced dilation of the pore ice and the soil skeleton respectively. It was shown that the temperature only affects the effective cohesion, not the effective friction angle of sand. The pore ice stress and its relationship with PWP were also estimated using Ladanyi and Morel's (1990) postulate on the internal stresses within frozen soil. Based on Ladanyi and Morel's (1990) concept of internal confinement in frozen sand, a Mohr–Coulomb model that uses effective failure and residual friction angles from unfrozen sand to estimate the strength of partially frozen sand is presented.

Finally, a unique CSL is established in both stress (q-p') and void ratio (e-p') space for the partially frozen sand at -3 °C. The results also show that the critical state friction angle (φ'_{cs}) is not affected by temperature while the critical state cohesion (c'_{cs}) is a function of temperature, strain rate, and failure mode. In e-p' space, the slope λ_d represents the dilatancy of partially frozen sand, which increases with decreasing temperature and increasing strain rate.

Keywords: warm permafrost, partially frozen soil, continuous water phase, effective stress, pore-water pressure, pore ice stress, shear strength, critical state line

Preface

Several chapters of this thesis were reproduced from publications (with modifications). The experimental apparatus referred to chapters 2-5 was designed by myself, with the assistance of technological staff Lucas Duerksen, Christine Hereygers, and Dr. Ahlam Abdulnabi. The publications and author contributions for each chapter, included the following:

Chapter 2:

Liang Y, Beier N, and Sego DC. 2022. New method for internal pore-water pressure measurements. Geotechnical Testing Journal, 45(2): 490-502.

I was responsible for the lab tests and data analysis as well as the manuscript composition. Dr. Nicholas Beier and Dr. D. C. Sego edited and reviewed the manuscript.

Chapter 3:

Liang Y, Beier N, and Sego DC. 2022. Continuity of pore-water pressure measurements in partially frozen sand. (Manuscript submitted for publication)

I was responsible for the lab tests and data analysis as well as the manuscript development. Dr. Nicholas Beier and Dr. D. C. Sego edited and reviewed the manuscript.

Chapter 4:

Liang Y, Beier N, and Sego DC. 2022. Strength of partially frozen sand under triaxial

compression. 75th Canadian Geotechnical Conference (GeoCalgary 2022), Calgary, Canada. Accepted.

This manuscript was further expanded and submitted to a Journal for publication. I was responsible for the lab tests and data analysis as well as the manuscript development. Dr. Louis Kabwe contributed to the French abstract. Vivian Giang proofread the manuscript. Dr. Nicholas Beier and Dr. D. C. Sego edited and reviewed the manuscript.

Chapter 5:

Liang Y, Beier N, and Sego DC. 2022. Determination of the critical state line in partially frozen sand (Manuscript submitted for publication).

I was responsible for the lab tests and data analysis as well as the manuscript development. Dr. Nicholas Beier and Dr. D. C. Sego edited and reviewed the manuscript.

Dedication

I would like to dedicate this thesis to my parents, whose love and unselfish support laid the foundation for me to complete this work.

Acknowledgement

I would like to thank all the people who have helped and inspired me during the doctoral study. First, I am extremely grateful to my supervisors, Dr. Nicholas Beier and Dr. D. C. Sego for their invaluable guidance, continuous support, patience, and for going through the numerous versions of this dissertation. I hope to continue doing research with them. Additionally, an appreciation is also acknowledged to the committee member, Dr. Michael Hendry for his constructive comments about this work.

I am grateful to Lucas Duerksen, Christine Hereygers, Ryan Lewis and Dr. Ahlam Abdulnabi for their technical support on my lab tests. I am also immensely thankful to the staff in the Geotechnical Centre, Jennifer Stogowski, Vivian Giang, David Barsi, and Dr. Louis Kabwe for their help and support. Special thanks are dedicated to my fellow lab mates for their assistance and encouragement, especially during the COVID pandemic. I particularly would like to thank Tony Zheng, Xin xu, Chao Liu, Yunhai Zhang, and Dr. Huawei Xu.

Finally, I would like to thank my parents. Without their tremendous understanding and constant love in the past few years, it would be impossible for me to complete my program.

This work was financially supported by the Natural Sciences and Engineering Research Council of Canada (NSERC) Discovery Grant Program (RGPIN-2019-04573) and China Scholarship Council (CSC).

Contents

List of Tables

List of Figures

List of Symbols

$\boldsymbol{B}$: Skempton's B pore-water pressure parameter;

$\boldsymbol{c_D}$: cohesion caused by pore ice in partially frozen, dense sand;

$\boldsymbol{c_L}$: cohesion caused by pore ice in partially frozen, loose sand;

$\boldsymbol{c'_{cs}}$: critical state cohesion caused by the pore ice;

$\boldsymbol{D_{50}}$: median diameter;

$\boldsymbol{e}$: void ratio;

$\boldsymbol{K'_p}$: passive earth pressure coefficient;

$\boldsymbol{p'}$: effective mean stress;

$\boldsymbol{p_i}$: mean stress of pore ice;

$\boldsymbol{q}$: deviator stress;

$\boldsymbol{q_i}$: shear strength of pore ice;

$\boldsymbol{q_{FS}}$: peak strength of frozen sand;

$\boldsymbol{q_{PLS}}$: peak strength of partially frozen, loose sand;

$\boldsymbol{q_{PLS(low)}}$: peak strength of partially frozen, loose sand at a lower strain rate;

$\boldsymbol{q_{PDS}}$: is the peak strength of partially frozen, dense sand;

$\boldsymbol{T_i}$: tension stress provided by pore ice due to dilatancy hardening;

$\boldsymbol{T_w}$: measured suction of the pore water;

$\boldsymbol{T_i}$: tensile stress of pore ice, which is equal to the measured suction of pore water;

$\boldsymbol{V_0}$: initial volume of pore water;

$\boldsymbol{V_f}$**:** final volume of pore water;

$\Delta\boldsymbol{V_c}$**:** volume change during the consolidation;

$\Delta\boldsymbol{V_s}$**:** volume change during the shear;

$\boldsymbol{M}$**:** critical state parameter, slope of critical state line in q-p' plane;

$\boldsymbol{\alpha'}$**:** angle of the failure line or effective failure angle of unfrozen, dense sand;

$\boldsymbol{\beta'}$**:** angle of the ultimate line or effective residual angle of unfrozen sand;

$\boldsymbol{\sigma_{3cell}}$**:** cell pressure;

$\boldsymbol{\sigma_{3(i)}}$**:** minor principal stress of pore ice;

$\boldsymbol{\varphi'_{cs}}$**:** critical state friction angle;

$\boldsymbol{\lambda}$**:** critical state parameter of unfrozen sand, slope of critical state line in e-p' plane;

$\boldsymbol{\lambda_d}$**:** critical state parameter of partially frozen sand, slope of critical state line in e-p' plane;

$\boldsymbol{\Gamma}$**:** critical state parameter, intercept of critical state line in e-p' plane.

1. Introduction

1.1 Definition of the problems

1.1.1 Background

Permafrost is defined as the ground that remains at or below 0 ºC for at least two consecutive years and underlays about 25 % of exposed land in the Northern Hemisphere and nearly 50 % of Canada's land surface (Heginbottom et al. 1995; Muller 1947). In the past few decades, the temperature of permafrost has gradually increased between 0.5 and 2 ºC due to climate warming and the trend is expected to continue in the future (Romanovsky et al. 2010). As a consequence, the extent and thickness of permafrost decrease with increasing ground temperature, which is so called permafrost degradation.

With the increase in permafrost temperature with time, the permafrost will eventually thaw and become unstable, particularly in the warm regions (i.e., > –2 ºC). The thawing of permafrost is one of the major challenges faced by the coastal and northern communities because it is associated with the deterioration of overlying infrastructures including (Lewkowicz and Harris 2005a and 2005b; Government of the NWT, 2008; PIEVC 2008; Holubec 2008; Laxton and Coates 2010; Allard et al. 2012; Boyle et al. 2013; Damm and Felderer 2013; Kokelj et al. 2015; Shiklomanov et al. 2017; Vincent et al. 2017):

- differential thaw settlement of building's foundation and linear structures (e.g., pipelines, roads, and railways);

- reduction in bearing capacity of foundations (e.g., pile, and footings) and
- instability of slopes triggered by releasing of melt water at thawing front (e.g., debris flows, thaw slumps, and embankments).

An amount of the unfrozen water exists within the soil in most permafrost regions (i.e., ice-rich and/or saline) when the ground temperature is close to 0 ºC, and hence these soils are in a partially frozen state. Further, if there is sufficient unfrozen water to provide a continuous water phase within the soil pore network, the effective stress that controls the strength and deformation of a soil should be established by measuring the pore water pressure (PWP) in these warm permafrost regions. In this study, the soil with a continuous water phase at subzero temperatures is defined as partially frozen soil (Kia 2012).

In northern Canada, industrial development (e.g., mining) and the expansion of Inuit communities demand more long-lasting infrastructures (Allard et al. 2009; Allard et al. 2012). In addition, a growing body of reports provide evidences that the engineering design practices utilized in cold permafrost regions are less robust in warm permafrost regions (Linell and Johnston 1973; Holubec 2008; Laxton and Coates 2010; Swanson et al. 2021). The current design method relies on the total stress approach while the effective stress approach is not applied to analyze the mechanical behavior and stability of partially frozen soils. Therefore, the prediction of behavior of existing infrastructures and the design for new soil structures to withstand climate change call for a better understanding of effective stress behavior of partially frozen soil.

1.1.2 Need to measure the internal PWP in partially frozen soil

The continuity in the water phase is a prerequisite for measuring PWP at subfreezing temperatures to establish the effective stress approach within the partially frozen soil. If the internal water phase is not continuous, the stress of the water phase would not be independent of other phases of partially frozen soil, such as ice and solid grains, and thus the effective stress approach is not applicable in this case.

Typically, there are two methods to examine the continuity in the water phase: one is checking the continuity of electrical conductivity, and the other is monitoring the PWP response at different zones within the soil by changing the back pressure. However, the former is an indirect measurement, and the electrical resistance is likely affected by the thickness of water film, salinity, and temperature. Therefore, Kia (2012) recommended to use the latter to confirm the continuity in the water phase of partially frozen soil. Since this method requires multipoint PWP measurements within a soil sample, the traditional method in a laboratory, which only measures PWP at the boundary (top or bottom) of the sample, is not capable of examining the continuity in the water phase. Therefore, there is a need to develop a new method for measuring PWP in different zones within partially frozen soil, which is called internal PWP measurements.

Distribution and response of pore water pressure in freezing, thawing, or frozen soils is of interest for investigating the mechanism of frost heave and thaw settlement. Numerous research studies have been conducted to investigate the process of phase change induced water migration, ice segregation, thawing consolidation, and solifluction by measuring PWP during

freezing, thawing or cyclic freezing and thawing (Penner 1959; Williams 1966; Konrad 1989; Seto and Konrad 1994; Eigenbrod et al. 1996; Harris and Davies 1998; Tsarapov 2007; Zhang et al. 2014; Zhang et al. 2015). Some effort has also been made to study the PWP response of the soil near 0 ^{o}C under different loading conditions (Arenson and Springman 2005; Hazirbaba et al. 2011; Zhang et al. 2016; Lyu et al. 2021). In these investigations, the PWP was often measured via a base transducer where an antifreeze liquid was used to ensure the hydraulic connection between the water phase and the external measuring system, a miniature pressure transducer embedded at the bottom of the specimen, or tubes with antifreeze liquid jointed to the pressure transducers which were installed at the surface of the specimen (one-dimensional test). However, the continuity in the water phase could not be examined in the tests, so the measured PWP may not be confirmed as representative of the whole sample. To the authors' knowledge, only Kia (2012) validated continuity in the water phase using the Filter-less Rigid Piezometers (FRPs) for correctly measuring PWP in partially frozen soil. Kia's (2012) test was limited to a one-dimension condition. As is well known, the triaxial test is the most common procedure performed in geotechnical laboratories to evaluate the constitutive behavior of soils under axisymmetric (in situ) stress condition, so there is also a need for measuring internal PWP in triaxial tests.

When permafrost thaws and the ground ice melts, the unfrozen water content increases and can lead to excess PWP generation when drainage is blocked, resulting in reduced shear strength of soil and thus potential instability of slopes. The internal PWP measurement will be extremely

helpful to ascertain the conditions close to the failure surface for either back analyze or stability analysis.

1.1.3 Need to investigate the mechanical properties of partially frozen soil

Knowledge of mechanical properties of frozen soil is of great importance for the design and construction of soil structures. The frozen soil normally consists of solid grains, pore ice, pore water, and air, so the factors that influence the properties of these four constituents will therefore impact on the mechanical properties of frozen soil, such as temperature, strain rate, confining pressure, and salinity (Chamberlain et al. 1972; Alkire and Andersland 1973; Sayles 1974; Parameswaran 1980; Bragg and Andersland 1980; Parameswaran and Jones 1981; Baker et al. 1981; Kuribayshi 1985; Enokido and Kameta 1987; Hivon and Sego 1995; Andersen et al. 1995; Chae et al. 2015; Du et al. 2016; Xu et al. 2016; Xu et al. 2017).

The compressive strength of the soil, either under confined or unconfined conditions, is the most important value for the design of bearing capacity of foundations. However, it has been noted that considerably lower strengths were observed when the temperature of permafrost soil was close to the thawing point, probably due to the loss of ice cementing of soil particles as result of the presence of high unfrozen water content (Parameswaran 1980; Yamamoto and Springman 2014). Furthermore, the continuous water phase might exist at such a warm temperature, but the PWP, which is associated with effective strength parameters, was not measured during these studies. Thus the previous researches were limited to use the total stress approach, and the effective stress behavior of partially frozen soil was not established.

The large difference in strength between frozen and unfrozen soil is associated with the ice matrix, which is a temperature and strain rate dependent material. For a saturated frozen sand, which is simplified as a sand-ice system, when the volume concentration of sand is less than about 42 %, the mechanical behavior and measured strength is dependent on the properties of the ice matrix, because the soil particles are, to a lager extent, separated by ice, while at the higher sand concentration, the internal friction and dilatancy hardening come into effect (Goughnour and Andersland 1968). Ting et al. (1983) concluded that the mechanics of saturated frozen sand is mainly controlled by the following mechanisms: (1) ice strength; (2) soil strength, including frictional component, dilatancy effects, and particle interference; (3) mechanical interactions between the ice and soil through dilatancy hardening; and (4) structural hindrance. However, whether this is also true in the soil at a partially frozen state, where the internal stresses from the pore ice and pore water coexist, is not understood. Further, the inability to measure the internal stresses directly and separately makes it difficult to assess their respective effects on the overall strength of partially frozen sand, particularly the ice strength and related effects.

In addition, the current constitutive models that simulate the mechanical behavior of frozen soil often assume the distribution of the pore ice or water pressure by volume or thermodynamic equilibrium（Li et al. 2008; Nishimura et al. 2009; Zhang and Michalowski 2015), but these assumptions have never been experimentally proven. For example, the Clausius–Clapeyron equation that represents the phase equilibrium of the pore ice and pore water pressure under isothermal conditions, has not been validated when soil is under external loading conditions

(Biermans et al. 1978; Miyata and Akagawa 1997; Henry 2000; Li et al. 2001; Dash et al. 2006; Thomas et al. 2009).

To better understand the mechanical properties and mechanisms of partially frozen soil, it is necessary to investigate the relationship between the pore ice and pore water pressure and to evaluate their respective contributions to the overall measured strength.

1.1.4 Need to investigate the critical state behavior of partially frozen soil

The critical (or steady) state theory has been widely used in soil constitutive models to represent the fundamental behaviour of the unfrozen soil and for the design of soil structures (Hanzawa 1980; Poulos et al. 1981; Poulos et al. 1985; Ishihara 1993; Jefferies 1993; Imam et al. 2005; Anderson and Eldridge 2012; Jefferies and Been 2015). In the state diagram (e-p' space), soil with a state above the critical state line (CSL) exhibits contractive behavior, e.g., liquefaction, whilst the state below the CSL exhibit dilative behavior, e.g., stain localization. The practical use of the concept of critical (or steady) state can also be extended to permafrost engineering.

By the definition of critical state in which the soil undergoes a continuous deformation at the constant effective stress and volume, establishing the effective stress is a prerequisite for determining the conditions of critical state. However, due to technical difficulty in measuring the PWP and pore ice pressure to ascertain the effective stress, the total stress was adopted in some critical-state-based constitutive models to capture features of frost heave and thaw settlement (Nishimura and Wang 2019; Ghoreishian Amiri et al. 2016; Zhang and Michalowski 2015; Yu et al.2021). Besides, the design method to evaluate short- and long (creep)-term

strength and deformation of permafrost soil rely on the total stress approach, while the critical state approach is rarely applied in frozen ground engineering, especially in warm permafrost regions. This is probably due to the lack of the understanding of critical state behavior of partially frozen soil. Thus, a reliable method to establish the relationship between critical void ratio and mean effective stress (i.e., critical state line) for facilitating understanding of critical state behavior of partially frozen is required.

1.2 Objective

The main-focus of this thesis is to measure the pore water pressure (PWP) and establish the effective stress within the partially frozen soil. Particular objectives are:

1) Development of a new triaxial testing method for measuring internal PWP within a soil;
2) Measure the PWP response and examine the continuity in the water phase within partially frozen soil;
3) Determine the effective strength parameters of partially frozen soil;
4) Evaluate the stress distribution between the soil skeleton, pore ice, and pore internal water;
5) Investigate the individual effect of pore matrix (ice and unfrozen water) on the overall strength of partially frozen sand;
6) Establish the critical state line (CSL) in partially frozen sand and study the influence of temperature and strain rate on critical state parameters.

To achieve the above objectives, two main hypotheses are involved in this study:

1) The continuous water phase exists in a soil at subfreezing temperatures;
2) The soil skeleton carries the same amount of stress in both frozen and unfrozen states when the soil has undergone the same strain history (Ladanyi and Morel, 1990).

1.3 Description of the study

In Chapter 2, a new triaxial testing method for internal PWP measurement within soil using the filter-less rigid piezometers (FRPs) is outlined. The effectiveness and capability of this novel method are validated by comparing PWP measurements between the FRPs and a traditional transducer on saturated, unfrozen loose and dense sand. Then, in Chapter 3, this method is extended in partially frozen sand with a salinity of 30 ppt to measure the internal PWP and examine the continuity in the water phase throughout the consolidated, undrained triaxial tests, at -3 ºC. Also, the Skempton's B values are determined in the tests.

In Chapter 4, the effective stress path is established in partially frozen sand with the continuity of PWP measurements. Using Ladanyi and Morel's (1990) postulate on the unique relationship between the stress and strain of the soil skeleton, the stress distribution between the soil skeleton, pore ice, and pore water in partially frozen sand are evaluated. The individual effect of each component of the pore matrix (ice and unfrozen water) on the overall strength of partially frozen sand is also investigated in this chapter.

In Chapter 5, a new test method to establish CSL in partially frozen sand is developed to study the influence of temperature and strain rate on critical state parameters. Chapter 6 summarizes

the findings of this research and their practical significance. The recommendation for future research was provided in Chapter 7.

1.4 Reference

Anderson, D.M., and Morgenstern, N.R. 1973. Physics, chemistry, and mechanics of frozen ground : a review. In 2nd International Conference on Permafrost. National Academy of Science, Washington, D.C., Yakutsk, USSR, pp. 257-288.

Anderson, C.D. and Eldridge, T.L. 2012. Critical state liquefaction assessment of an upstream constructed tailings sand dam. 14th International Conference on Tailings and Mine Waste, Vail, CO, United states, pp. 101-112.

Alkire, B.D., and Andersland, O.B. 1973. The effect of confining pressure on the mechanical properties of sand–ice materials. Journal of Glaciology, 12(66): 469-481.

Allard, M., Lemay, M., Barrette, C., L'Hérault, E., Sarrazin, D., Bell, T., and Doré, G. 2012. Permafrost and climate change in Nunavik and Nunatsiavut: Importance for municipal and transportation infrastructures. Nunavik and Nunatsiavut: From science to policy. An Integrated Regional Impact Study (IRIS) of climate change and modernization: 171-197.

Allard, M., Gibéryen, T., L'Hérault, E., and Sarrazin, D. 2009. L'impact des changements climatologiques sur laproblématique de la fonte du pergélisol au village de Salluit, Nunavik Rapport d'étape au MAMROT, pp. 41.

Andersen, G.R., Swan, C.W., Ladd, C.C., and Germaine, J.T. 1995. Small-strain behavior of frozen sand in triaxial compression. Canadian Geotechnical Journal, 32(3): 428-451.

Arenson, L.U., and Springman, S.M. 2005. Triaxial constant stress and constant strain rate tests on ice-rich permafrost samples. Canadian Geotechnical Journal, 42(2): 412-430.

Baker, T., Jones, S., and Parameswaran, V. 1981. Confined and unconfined compression tests on frozen sands. The Roger JE Brown Memorial Volume. In Proc. 4th Canadian Permafrost Conference, Calgary, Alberta, pp. 2-6.

Biermans, M.B.G.M., Dijkema, K.M. and De Vries, D.A. 1978. Water movement in porous media towards an ice front. Journal of Hydrology, 37(1-2):137-148.

Boyle, J., Cunningham, M., and Dekens, J. 2013. Climate Change Adaptation and Canadian Infrastructure: A review of the literature. International Institute for Sustainable Development,

Manitoba, Canada.

Bragg, R.A., and Andersland, O. 1980. Strain rate, temperature, and sample size effects on compression and tensile properties of frozen sand. Engineering Geology, 18(1-4):35-46.

Chae, D., Hwang, B., and Cho, W. 2015. Stress-strain-strength characteristics of frozen sands with various fine contents. Journal of the Korean GEO-environmental Society, 16(6): 31-38.

Chamberlain, E., Groves, C., and Perham, R. 1972. The mechanical behaviour of frozen earth materials under high pressure triaxial test conditions. Géotechnique, 22(3): 469-483.

PIEVC. 2008. Adapting to climate change, Canada's first national engineering vulnerability assessment of public infrastructure. Canadian Council of Professional Engineers.

Damm, B., and Felderer, A. 2013. Impact of atmospheric warming on permafrost degradation and debris flow initiation: A case study from the eastern European Alps. E and G Quaternary Science Journal, 62(2): 136-149.

Dash, J.G., Rempel, A.W. and Wettlaufer, J.S. 2006. The physics of premelted ice and its geophysical consequences. Reviews of modern physics, 78(3): 695-741.

Du, H., Ma, W., Zhang, S., Zhou, Z., and Liu, E. 2016. Strength properties of ice-rich frozen silty sands under uniaxial compression for a wide range of strain rates and moisture contents. Cold Regions Science and Technology, 123: 107-113.

Eigenbrod, K.D., Knutsson, S., and Sheng, D. 1996. Pore-Water Pressures in Freezing and Thawing Fine-Grained Soils. Journal of Cold Regions Engineering, 10(2): 77-92.

Enokido, M., and Kameta, J. 1987. Influence of water content on compressive strength of frozen sands. Soils and Foundations, 27(4): 148-152.

Ghoreishian Amiri, S., Grimstad, G., Kadivar, M., and Nordal, S. 2016. Constitutivemodel for rate-independent behavior of saturated frozen soils. Canadian Geotechnical Journal, 53(10): 1646-1657.

Government of the Northwest Territories. (2008). NWT climate change impacts and adaptation report. Yellowknife, NWT: Environment and Natural Resources.

Goughnour, R.R., and Andersland, O. 1968. Mechanical properties of a sand-ice system. Journal of the Soil Mechanics and Foundations Division, 94(4): 923-950.

Harris, C., and Davies, M.C.R. Pressures recorded during laboratory freezing and thawing of

a natural silt-rich soil. In Seventh International Conference on Permafrost, Yellowknife, NWT, Canada, June. 1998. pp. 23-27.

Hanzawa, H. 1980. Undrained strength and stability analysis for a quick sand. Soils and Foundations , 20(2):17-29.

Hazirbaba, K., Zhang, Y., and Hulsey, J.L. 2011. Evaluation of temperature and freeze–thaw effects on excess pore pressure generation of fine-grained soils. Soil dynamics and earthquake engineering, 31(3): 372-384.

Heginbottom, J., Dubreuil, M., and Harker, P. 1995. Canada, Permafrost. National Atlas of Canada. Geomatics Canada, National Atlas Information Service, and Geological Survey of Canada: Ottawa; Plate 2.1 (MCR 4177).

Henry, K.S. 2000. A review of the thermodynamics of frost heave. Cold Regions Research and Engineering Laboratory, US Army Corps of Engineers. Report ERDC/CRREL TR-0016.

Hivon, E., and Sego, D. 1995. Strength of frozen saline soils. Canadian Geotechnical Journal, 32(2): 336-354.

Holubec, I. 2008. Flat loop thermosyphon foundations in warm permafrost. Government of the Northwest Territories Asset Management Division of Public Works and Services and the Climate Change Vulnerability Assessment of the Canadian Council of Professional Engineers.

Imam, S.R., Morgenstern, N.R., Robertson, P.K. and Chan, D.H. 2005. A critical-state constitutive model for liquefiable sand. Canadian geotechnical journal, 42(3): 830-855.

Ishihara, K. 1993. Liquefaction and flow failure during earthquakes. Géotechnique, 43(3): 351-451.

Jefferies, M.G. 1993. Nor-Sand: a simle critical state model for sand. Géotechnique, 43(1): 91-103.

Jefferies, M., and Been, K. 2015. Soil liquefaction: a critical state approach. CRC press.

Kia, M. 2012. Measuring Pore-water Pressure in Partially Frozen Soils. Ph.D. thesis, Faculty of Graduate Studies and Research, University of Alberta, Edmonton, AB.

Kokelj, S., Tunnicliffe, J., Lacelle, D., Lantz, T., Chin, K., and Fraser, R. 2015. Increased precipitation drives mega slump development and destabilization of ice-rich permafrost terrain, northwestern Canada. Global and Planetary Change, 129: 56-68.

Konrad, J.M. 1989. Pore water pressure at an ice lens: Its measurement and interpretation. Cold Regions Science and Technology, 16(1): 63-74.

Kuribayashi, E. 1985. Stress-strain characteristics of an artificially frozen sand in uniaxially compressive tests. Proceedings of the Fourth International Symposium on Ground Freezing, Sapporo, Japan, 2:177-182.

Ladanyi, B., and Morel, J.-F. 1990. Effect of internal confinement on compression strength of frozen sand. Canadian Geotechnical Journal, 27(1): 8-18.

Laxton, S., and Coates, J. 2010. Geophysical and borehole investigations of permafrost conditions associated with compromised infrastructure in Dawson and Ross River, Yukon. Yukon Exploration and Geology: 135-148.

Lewkowicz A. G., and Harris C. 2005a. Frequency and magnitude of active-layer detachment failures in discontinuous and continuous permafrost, northern Canada.Permafrost and Periglacial Processes, 16(1): 115-130

Lewkowicz A. G., and Harris C. 2005b. Morphology and geotechnique of active-layer detachment failures in discontinuous and continuous permafrost, northern Canada. Geomorphology , 69 (1-4): 275-297.

Li, N., Chen, F., Xu, B., and Swoboda, G. 2008. Theoretical modeling framework for an unsaturated freezing soil. Cold Regions Science and Technology, 54(1): 19-35.

Li, N., Cheng, G.D. and Xu, X.Z. 2001. The advance and review on frozen soil mechanics. Advances in Mechanics, 31(1): 95-102.

Lian-hai, Z., Wei, M.A., and Cheng-song, Y. 2015. Pore water pressure measurement for soil subjected to freeze-thaw cycles. Rock and Soil Mechanics, 36(7): 1856-1864.

Linell, K.A. and Johnston, G.H. 1973. Engineering design and construction in permafrost regions: A review. Permafrost: North American Contribution to the Second Internationl Conference , National Academy of Sciences, pp. 553-575.

Lyu, C., Nishimura, S., Amiri, S.A.G., Zhu, F., Eiksund, G.R., and Grimstad, G. 2021. Pore-water pressure development in a frozen saline clay under isotropic loading and undrained shearing. Acta Geotechnica, 16(12): 3831-3847.

Miyata, Y. and Akagawa, S. 1997. An experimental study on static solid-liquid phase

equilibrium in the pores of a porous medium. Heat Transfer-Japanese Research: Co-sponsored by the Society of Chemical Engineers of Japan and the Heat Transfer Division of ASME, 26(2): 69-83.

Muller, S.W. 1946. Permafrost and related engineering problems. AAPG Bulletin, 30(12): 2089-2089.

Nishimura, S., and Wang, J. 2019. A simple framework for describing strength of saturated frozen soils as multi-phase coupled system. Géotechnique, 69(8): 659-671.

Nishimura, S., Gens, A., Olivella, S., and Jardine, R. 2009. THM-coupled finite element analysis of frozen soil: formulation and application. Géotechnique, 59(3): 159-171.

Parameswaran, V. 1980. Deformation behaviour and strength of frozen sand. Canadian Geotechnical Journal, 17(1): 74-88.

Parameswaran, V., and Jones, S. 1981. Triaxial testing of frozen sand. Journal of Glaciology, 27(95): 147-155.

Penner, E. 1959. Pressures developed in a porous granular system as a result of ice segregation. Highway Research Board Special Report, (40): 191-199.

Poulos, S.J. 1981. The steady state of deformation. Journal of the Geotechnical Engineering Division, 107(5): 553-562.

Poulos, S.J., Castro, G., and France, J.W. 1985. Liquefaction evaluation procedure. Journal of Geotechnical Engineering, 111(6): 772-792.

Romanovsky, V.E., Smith, S.L., and Christiansen, H.H. 2010. Permafrost thermal state in the polar Northern Hemisphere during the international polar year 2007–2009: a synthesis. Permafrost and Periglacial processes, 21(2): 106-116.

Sayles, F.H. 1974. Triaxial constant strain rate tests and triaxial creep tests on frozen Ottawa sand. Corps of Engineers, US Army Cold Regions Research and Engineering Laboratory. Technical Report 253.

Seto, J., and Konrad, J.-M. 1994. Pore pressure measurements during freezing of an overconsolidated clayey silt. Cold regions science and technology, 22(4): 319-338.

Shiklomanov, N.I., Streletskiy, D.A., Swales, T.B., and Kokorev, V.A. 2017. Climate change and stability of urban infrastructure in Russian permafrost regions: prognostic assessment based on GCM climate projections. Geographical review, 107(1): 125-142.

Swanson, D., Murphy, D., Temmer, J., and Scaletta, T. 2021. Advancing the Climate Resilience of Canadian Infrastructure: A Review of Literature to Inform the Way Forward. International Institute for Sustainable Development.

Thomas, H.R., Cleall, P., Li, Y.-C., Harris, C., and Kern-Luetschg, M. 2009. Modelling of cryogenic processes in permafrost and seasonally frozen soils. Géotechnique, 59(3): 173-184.

Ting, J.M., Torrence Martin, R., and Ladd, C.C. 1983. Mechanisms of strength for frozen sand. Journal of Geotechnical Engineering, 109(10): 1286-1302.

Tsarapov, M. 2007. Use of pore pressure to determine strength characteristics of thawing soils. Soil Mechanics and Foundation Engineering, 44(4): 132-136.

Vincent, W.F., Lemay, M., and Allard, M. 2017. Arctic permafrost landscapes in transition: towards an integrated Earth system approach. Arctic Science, 3(2): 39-64.

Williams, P.J. 1966. Pore Pressures at a Penetrating Frost line and their prediction. Géotechnique, 16(3): 187-208.

Xu, J., Liu, H., and Zhao, X. 2017. Study on the strength and deformation property of frozen silty sand with NaCl under tri-axial compression condition. Cold Regions Science and Technology, 137: 7-16.

Xu, X., Wang, Y., Bai, R., Fan, C., and Hua, S. 2016. Comparative studies on mechanical behavior of frozen natural saline silty sand and frozen desalted silty sand. Cold Regions Science and Technology, 132: 81-88.

Yamamoto, Y., and Springman, S.M. 2014. Axial compression stress path tests on artificial frozen soil samples in a triaxial device at temperatures just below 0℃. Canadian Geotechnical Journal, 51(10): 1178-1195.

Yu, F., Guo, P., and Na, S. 2022. A framework for constructing elasto-plastic constitutive models for frozen and unfrozen soils. International Journal for Numerical and Analytical Methods in Geomechanics, 46(2): 436-466.

Zhang, H., Zhang, J., Zhang, Z., and Chai, M. 2016. Investigation of the pore-water pressure of saturated warm frozen soils under a constant load. Journal of Offshore Mechanics and Arctic Engineering, 138(6): 062001

Zhang, L., Ma, W., Yang, C., and Yuan, C. 2014. Investigation of the pore water pressures of

coarse-grained sandy soil during open-system step-freezing and thawing tests. Engineering Geology, 181: 233-248.

Zhang, Y., and Michalowski, R.L. 2015. Thermal-hydro-mechanical analysis of frost heave and thaw settlement. Journal of geotechnical and geoenvironmental engineering, 141(7): 04015027.

2. New Method for Internal Pore-Water Pressure Measurements

(This chapter has been published in Geotechnical Testing Journal, Liang et al. 2022)

Abstract: The triaxial test is the most common procedure performed in a geotechnical laboratory to investigate the mechanical behavior of soils. However, often only the global pore-water pressure (PWP) is measured at the bottom of specimen during conventional triaxial tests, which cannot detect the variation in internal pore-water pressures to represent the true effective stress path adjacent to the failure surface. Here, a modified triaxial testing apparatus capable of measuring internal PWP within the soil using a filter-less rigid piezometer (FRP) is outlined. To validate the effectiveness and capability of this novel test method, a series of consolidated undrained tests were conducted on saturated loose and dense sand. The FRPs measurements provide a reliable PWP response, especially at pressure above 400 kPa where the FRPs have a faster response than the base transducer. Moreover, the internal PWP measured by the FRPs during the initiation of shearing in loose sand can capture the rapid development of excess PWP before liquefaction or failure. The results also show that there are increases of 25 % in average peak strength of the loose specimen and 8 % in average residual strength of the dense specimen with internal PWP measurement, respectively, compared with using only global PWP measurement due to the internal FRP installation. While FRP installation appears to have no apparent effect on average peak strength of the dense specimen and average residual strength of the loose specimen. The new triaxial testing method can be applied to study the response and distribution of PWP at specific zones within the soil.

Keywords: local scale, internal pore-water pressure (PWP) measurement, filter-less rigid piezometer (FRP), enhanced response, select internal test zones

2.1 Introduction

The determination of pore-water pressure (PWP) is essential for effective stress analysis in geotechnical engineering. Typically, the PWP in a triaxial test is measured at the boundary (top or/and bottom) of the specimen, termed the global PWP in respect to the global stress and strain. However, the global measurement does not capture changes in PWP at the local scale, such as the local shear-induced PWP that contributes to the strain softening during the formation and propagation of shear band (Atkinson and Richardson 1987; Thakur et al. 2005; Thakur 2007; Gylland et al. 2013), and hence cannot represent the true internal effective stress. Consequently, the effective cohesion and friction angle obtained from global PWP measurement are not representative when estimating the shear strength along the shear band or failure surface. It is therefore of importance to carry out the internal PWP measurement at a local scale to ascertain the condition along the failure surface.

Although the excess PWP produced within a shear band is theorized and numerically observed in clays (Shuttle and Smith 1990; Schrefler et al. 1998; Thakur 2007; Thakur 2011), little experimental evidence has been reported. Typical examples of this type of work are limited to the plain strain tests as presented by Viggiani et al. (1994), Cheng (2004), Marello (2005), Yuan et al. (2013), and Thakur et al. (2018). They placed miniature pore pressure probes on the external side of the specimens (stiff, quick, and silty clays) to measure the PWP at the edge of

the specimens and found a variation in the build-up of PWP at different distances from the shear band, and that the highest excess PWP existed within the shear band because of contraction inside the band. In coarse grained soils, internal fluid flow and formation of a local undrained shear band in saturated sands were theoretically discussed but has not yet been experimentally proven because of a lack of internal PWP measurement (Vardoulakis 1996a; Vardoulakis 1996b). Based on the previous plain strain test results, Han and Vardoulakis (1991) concluded that the development of PWP shocks across shear-band boundaries is impossible to be measured in conventional experiments where PWP has enough time to equalize throughout the specimen.

Triaxial test is the most common procedure performed in geotechnical laboratories to evaluate the constitutive behavior of soils under axisymmetric (in-situ) stress condition, however, measuring local PWP in a triaxial test is a very challenging task as the disturbance to the stress field due to the installation of pressure probes on the surface of specimens is inevitable. One such modified triaxial equipment was developed by Sheahan (1991), who placed a surgical tubing with a paddle of epoxy against the mid-side of the clay specimen to measure the mid-height PWP on the surface of the specimen, but he mentioned that the measurement may be affected by the cell pressure acting on the surgical tubing. In addition, this method is not applicable to cohesionless soil such as sand where a low vacuum is required to maintain specimen integrity while the split mold is removed, which conflicts with mounting of the tube. Zhou et al. (1995) embedded two micro transducers into the middle and near the bottom of samples of sand and silt. They observed uniform distribution of PWP in sand but nonuniform

PWP distribution in normally consolidated silt. However, the performance of micro transducers was not assessed in denser samples. To measure PWP distribution within partially frozen sand under laterally confined condition, Kia (2012) designed a filter-less rigid piezometer (FRP) and examined its applicability to measure positive and negative PWP during triaxial tests. But the testing points were quite close to the bottom transducer, and the impact of tubes on the mechanical behavior of soil was not evaluated.

In this paper, we proposed a new triaxial testing method for internal PWP measurement of soil using the FRPs. The new apparatus can be utilized to track the response and distribution of PWP at specific zones within a sample. The effectiveness of the apparatus was examined by comparing PWP measurements between the FRPs and a traditional transducer on saturated loose and dense sand under undrained shear condition.

2.2 Testing apparatus

The modified triaxial testing apparatus for internal PWP measurement is based on using the FRP developed and presented in Kia (2012). The FRP includes four main components: (i) a miniature, high sensitivity fiber optic pressure sensor (FOP, fig. 2-1); (ii) low compressible piezometer fluid (heavy mineral oil); (iii) low volume connectors; and (iv) a small diameter of flexible PeekSil tube. After injecting a minimal volume of heavy mineral oil, the oil droplet formed at the tip of the PeekSil tube can transfer the fluid pore pressure via intimate contact between the oil in the piezometer and the pore-water in the soil.

Contrasting with conventional triaxial devices, which only measure PWP response at the base

of sample, the modified triaxial testing apparatus (fig. 2-2A and 2-2B) has three PeekSil tubes with inner diameter of 0.53 mm embedded at different heights within the specimen (8cm, 10cm, and 12cm from the base) and connected to three FOPs (model FOP-M-NP-R3) by a multiconductor feed through the metal base of the cell for measuring the internal PWP. Universal Multichannel Instrument (UMI) with a recording rate of 1 Hz collected the data. Cell, back, and pore pressure at the bottom of the specimen were recorded using conventional pressure transducers (model PLC 250PSI). All these transducers were connected to the QuantumX Amplifier Device (model MX1615B) with the same recording rate as the UMI.

In this study, the cylindrical sand specimen was prepared at approximately 10 cm in diameter and 20 cm in height. All the triaxial compression tests were carried out on a Digital Tritest 50 machine. An external load cell (model LCHD-10k) with capacity of 4500 kg was used to monitor the axial load. The axial displacement was measured using a linear potentiometer displacement (LP) with 5 cm axial translation range (model TR50). The heavy mineral oil (model 8042-47-5) was supplied through a syringe pump (model 500D) at a constant flow rate of 0.5 ml/min.

The main purpose of this study is to propose and validate the new testing method. Since the sand has high permeability and less heterogeneity than clay, the PWP will adjust relatively fast, and the effectiveness of this method will be confirmed if the FRPs and the transducer show the same response. To validate the effectiveness of this internal PWP testing method in both contractive and dilative materials, experimental investigations were conducted using dense and

loose sand. Also, the effect of tubes within the specimen on the mechanical behavior of soil was examined by comparing test specimens with and without tubes.

2.3 Experiments

2.3.1 Material

The material used in this research is a uniformly graded fine sand (D_{50} = 0.25 mm) with a specific gravity of 2.66. The grain size distribution of sand is presented in Figure 2-3. This article is part of the first author's PhD research on the relationship between PWP measurement in unfrozen and partially frozen saline sand. For consistency, 30 ppt salinity representing high-salinity pore fluid in arctic coastal communities (Hivon and Sego 1993) was used in this test program.

2.3.2 Procedures

Prior to the preparation of the specimen, the three PeekSil tubes were mounted through the pedestal to the desired height and filled with mineral oil using a syringe pump. Two reconstitution techniques were used to achieve the desired initial void ratios of the sand specimens. A moist tamping method (Jefferies and Been 2015) was used to reconstitute loose samples. A known amount of dry sand was mixed with 5 % saline water by weight and then tamped into membrane-lined split mold in five equal layers at the target void ratio. Then carbon dioxide followed by de-aired saline water was percolated from the bottom to the top of the samples before the saturation stage. The dense samples were prepared by slurry deposition

(Kuerbis 1989). The mixture of sand and saline water was poured into split mold and densified to desired void ratio using gentle vibration. Only de-aired saline water was flushed throughout the dense samples prior to the saturation step. To fully saturate the samples, a back pressure of 400 kPa was incrementally applied until the Skempton's B value reached 0.97 or greater, while an effective confining pressure of approximately 30 kPa was maintained.

After saturation, each sample was isotropically consolidated at confining pressure of 200 kPa and then sheared at a constant displacement (strain) rate. Since the rate of PWP change is associated with deformation rate, a high strain rate of 1 %/min was selected throughout the shearing stage to better examine the performance of the new testing method. Confirmation of this method at the high strain rate will confirm its application at the lower strain rates. A series of consolidated, undrained triaxial tests was conducted on specimens with and without tubes and a summary of the testing program is shown in Table 2-1.

2.4 Results and discussion

2.4.1 Calibration of FRPs and transducer

To compare the PWP measurements between the base transducer and the FRPs, all the sensors were calibrated prior to conducting each test. First, the transducer was calibrated with a portable pressure calibrator (model DPI 603). Then, the transducer was used to verify the factory calibration of the FOPs in the water-filled cell by changing cell pressure (loading and unloading). Note that the oil droplet was always created at the tip of the tube (fig. 2-4) ahead of the calibration to ensure the contact between the oil and surrounding water.

Comparison of pressure measurement between the transducer and FRPs during calibration is displayed in Figure 2-5. During the loading stage, the pressure measured by the FRPs (dash lines) increases and reaches the equilibrium state more rapidly than by transducer (solid line) at each loading step for pressures above 100 kPa. Likewise, the FRPs show a faster drop before the pressure falls below 300 kPa; however, the response of FRPs starts lagging compared to the transducer when pressure is less than 130 kPa during unloading. The difference in pressure response observed in loading and unloading curves may be associated with gas bubbles that dissolves in or comes out from the mineral oil at different pressures, resulting in the change of the rigidity and conductivity of the piezometer fluid and hence affects the speed of pressure transfer. The lag initiation point for the FRP is largely affected by the amount of gas bubbles dissolved in the piezometer fluid and by the unloading rate.

2.4.2 Internal PWP measurement in loose and dense sand

The stress-strain and PWP response of loose and dense specimens are presented in Figures 2-6 and 2-7. Figure 2-6A presents a typical contractive nature of the loose sand in which the initial increase of PWP measured at different elevations within the samples is followed by a progressive stabilization at the steady state. It is observed that each internal PWP measurement using FRPs increases faster than the transducer measured global PWP up to 2 % axial strain with the largest difference being 35 kPa at the same axial strain (fig. 2-6B). The global PWP gradually approaches the internal PWP at higher strains, excluding PWP recorded by FRP-8 cm (red line) that is around 5 kPa above the transducer presumably because of the error in

calibration. So, the measurement of internal PWP with the FRPs reflects well how the excess PWP develops to trigger liquefaction compared to the base transducer measurement.

In contrast to fig. 2-6A, fig. 2-7A shows that after the development of excess PWP at the initial contraction stage, the PWP decreases continuously to the negative value compared to atmospheric pressure and stabilizes until the critical state is reached. This is the typical dilative nature of dense sand. At the contraction stage, the internal PWP increases and reaches the peak slightly earlier than the global PWP with the greatest difference being almost 15 kPa, in the FRP-10 cm and FRP-12 cm (fig. 2-7B). When dilation begins, the internal and global PWP values gradually approach one another, indicating a more rapid drop in the internal PWP. However, the FRPs start lagging the base transducer after the PWP drops down to 120 kPa. This FRP's lag is consistent with the calibration curve (fig. 2-5) and the lag initiation point for each FRP is mainly controlled by the rigidity and conductivity of the piezometer fluid, the rate of pressure drops, and the local granular structure at the tip of the tube. The surface tension of the water in contact with the transducer is larger than that of the mineral oil used in the FRPs; therefore, the water sustains larger suction. This can explain why the global PWP exhibits 20 kPa lower PWP at the critical state.

The results from loose and dense specimens (L-1 and D-1) demonstrate the findings observed from the calibration curve (fig. 2-5) that FRPs exhibit a reliable PWP response during loading and unloading at higher pressure (above 130 kPa), especially when the pressure is above 400 kPa where FRPs have a faster response than the base transducer.

2.4.3 Incremental change of PWP response in loose and dense sand

Because the faster response of the FRP was demonstrated above and can capture the variation of PWP on a short time scale, this section presents an incremental change of internal PWP over strain compared to global PWP (fig. 2-8). As shown in figs. 2-8A and 2-8C, the incremental global PWP progresses relatively smoothly in response to the change of deviator stress on both loose and dense sand. In contrast, figs. 2-8B and 2-8D show a clear variation of the incremental internal PWP prior to 2 % strain in loose sand and between 1 and 3 % strain in dense sand, respectively, particularly with FRP-10 cm where the most dramatic changes are recorded. It is believed that the PWP change responds to the change of stress, and hence the variation of the incremental internal PWP can reflect the local stress variation within a short time, corresponding to the local movement of particles such as sliding.

2.4.4 Effect of tubes on the behavior of loose and dense sand

Although the volume fraction of PeekSil tubes within the specimen is only 0.07% with respect to solid particles, it is necessary to consider its effect on the stress-strain and PWP response of soil. For this reason, two groups of specimens (with and without tubes) were tested under the same conditions as specimens L-1 and D-1. Figures 2-9A and 2-10A show three sets of stress-strain curves at each of the test configuration. The stress-strain responses of different sets are similar, particularly at the initial stage where stress increases rapidly and a slight difference in response will result in a high mean absolute percent error (MAPE) of stress. In this case, the test repeatability is quantified by calculating the MAPE of peak strength between the peak

strength of each specimen and the average peak strength. As shown in Table 2-2, a good repeatability of both loose and dense specimens is indicated, and two different test configurations present a similar repeatability.

According to the Figure 2-9A, the stress–strain curves of each group of loose specimens are nearly identical, with a maximum of 8 % difference in the measured peak stress but a similar large strain response. The average peak stress of loose specimens with tubes is higher than that of non-tubes loose specimens, 127.7 kPa versus 101.9 kPa (Table 2-2), while both groups of specimens have almost the same average residual value at steady state. This 25 % difference in peak stress exceeds the degree of test repeatability (about 5.6 %, MAPE), and hence it is most likely because of the resistance associated with the embedded tubes. The tube is compressed along with the increase in axial deformation of the soil before failure and thereafter the compressive deformation of the tube recovers during flow deformation of the soil. As a result, the difference is only present at the peak strength and not at the residual strength. For comparison purposes, only global PWP measured by the base transducer is shown in fig. 2-9B. Although the minor differences in the initial excess PWP generation are recorded, equal global PWP are developed at the end of tests. Therefore, measuring the internal PWP with this method does not affect the determination of a steady state line (or critical state line) in loose sand.

Figure 2-10 compares stress-strain behavior and global PWP response of two groups of dense specimens, with a repeatability of around 2 % (MAPE) for each group. For specimens with initial void ratio around 0.599, both stress and PWP curves of specimens D-1 and D-3 start

lagging the curve of non-tubes specimen D-4 after the initiation of dilation. This phenomenon could be the result for two reasons: first, difference in sample uniformity related to the process of preparation and consolidation; and second, the deformation of the tubes accompanied by the shear deformation in the upper part of the specimen. However, specimens D-2, D-5, and D-6 whose void ratio are close to 0.596 exhibit almost the same stress and PWP response without any lag being observed before the failure. This implies that the different pre-peak response among D-1, D-3, and D-4 is unlikely attributed to the deformation of the tubes, and the variation is within the test repeatability. Moreover, the average peak strength of specimens with tubes is 73 kPa (3 %) less than that of specimens without tubes (Table 2-2). This is close to the degree of test repeatability and therefore the effect of tubes on the peak strength of the dense specimen can be negligible.

The images (figs. 2-11A and 2-11C) of specimens D-1 and D-4 display almost identical types of shear bands both of which run from the top left to the bottom right. Additionally, the deformation of the tubes is recorded in fig. 2-11B after being extracted from the bottom of the sample. In this case, only one tube (FRP-12 cm) was sheared and kinked at the height of 10.8 cm and 10.3 cm, matching with the upper and lower shear boundary shown in fig. 2-11A, respectively. Moreover, these images indicate that the layout of tubes can measure the PWP above, close to, and below the shear plane. Since part of the deformation of tubes was recovered during extraction, another example with minimal disturbance to the distortion of the tubes is presented in figs. 2-12A and 2-12B, which clearly illustrates how the tubes were sheared when the shear plane was fully developed. Further, the results may also explain why the average

residual strength of specimens with tubes is around 140 kPa (8 %) higher than that of non-tubes specimens.

2.5 Conclusion

This study presents a modified triaxial testing apparatus to measure the internal PWP within soil. A series of consolidated, undrained experiments were performed on dense and loose sand to validate the effectiveness and capability of the testing method. By comparing the PWP measurements between the FRPs and a traditional transducer in saturated specimens, it is demonstrated that the FRPs provide a reliable PWP response during loading and unloading at higher pressure (above 130 kPa), especially when the pressure is above 400 kPa where the FRPs have a faster response than the base transducer. Thus, a higher back pressure is recommended when using this new testing method. In loose specimens, the substantial initial increase of internal PWP recorded by the FRPs demonstrates how the excess PWP develops before liquefaction. On the other hand, a clear variation of the incremental internal PWP was observed in both loose and dense sand, which can reflect the local stress variation within a short time. The differences in behavior observed between specimens with and without tubes reveal that the average peak strength of the loose specimens and the average residual strength of dense specimens with tubes are about 25 % and 8 % higher than that of specimens without tubes, respectively. However, there is no apparent effect of the FRP installation on the average peak strength of the dense specimen and the average residual strength of the loose specimen.

The new testing method offers a range of capabilities to measure the internal PWP at specific

zones within the soil under the triaxial condition. For future analysis of the relationship between PWP response and progressive development of shear band, the different elevations of tubes enable to measure the PWP above, close to, and below the shear plane.

2.6 Tables

Table 2-1 Summary of testing program

Group	Test ID	Preparation	Initial Height (cm)	Initial Void Ratio	Condition of PWP Measurements (with /without tubes)
I	L-1	Moist Tamping	19.61	0.836	with
	L-2	Moist Tamping	19.59	0.835	with
	L-3	Moist Tamping	19.59	0.835	with
	D-1	Slurry Deposition	19.62	0.599	with
	D-2	Slurry Deposition	19.58	0.596	with
	D-3	Slurry Deposition	19.62	0.599	with
II	L-4	Moist Tamping	19.60	0.836	without
	L-5	Moist Tamping	19.60	0.835	without
	L-6	Moist Tamping	19.59	0.835	without
	D-4	Slurry Deposition	19.62	0.600	without
	D-5	Slurry Deposition	19.57	0.595	without
	D-6	Slurry Deposition	19.59	0.597	without

Note: L, loose; D, dense.

Table 2-2 Comparison of strength of specimen

Test ID	Peak Strength (kPa)	Average of Peak Strength (kPa)	MAPE of Peak Strength (%)	Residual Strength (kPa)	Average of Residual Strength (kPa)
L-1	117.4	127.7	5.4	6.3	8.8
L-2	127.9			11.2	
L-3	137.8			9	
L-4	93.6	101.9	5.8	9	9.1
L-5	101.4			7.8	
L-6	110.7			10.5	
D-1	2159	2206.6	1.9	1779.5	1787.4
D-2	2268.2			1811.2	
D-3	2191.9			1771.4	
D-4	2205.4	2280.0	2.2	1648.9	1651.8
D-5	2348.6			1706.3	
D-6	2286.1			1600.1	

2.7 Figures

FIG 2-1 Fiber optic pressure sensor

FIG 2-2 Illustration of testing apparatus: (A) schematic of apparatus and (B) close-up view

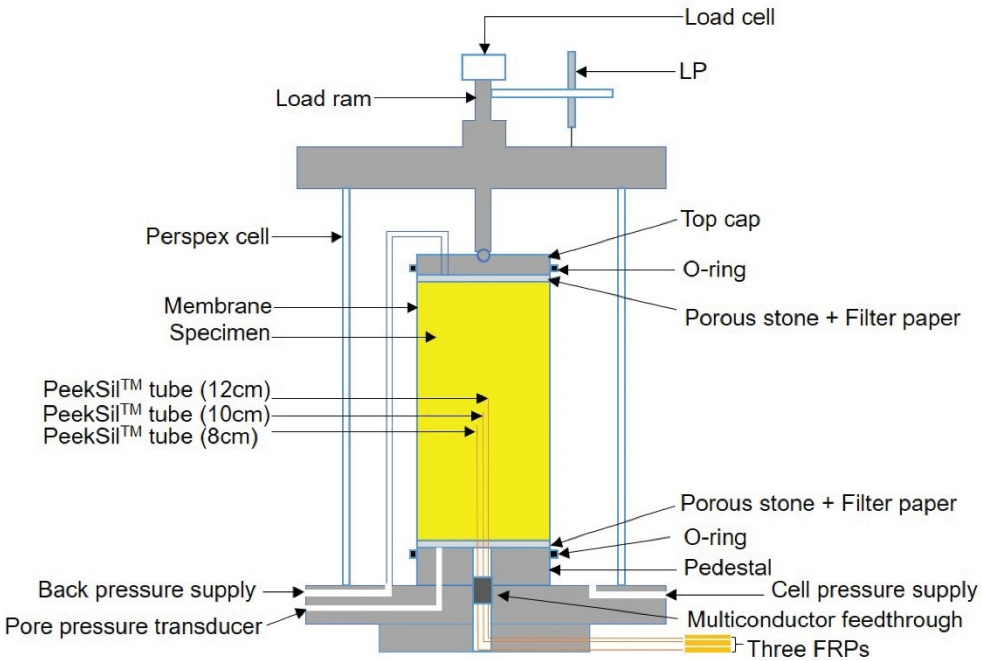

(A)

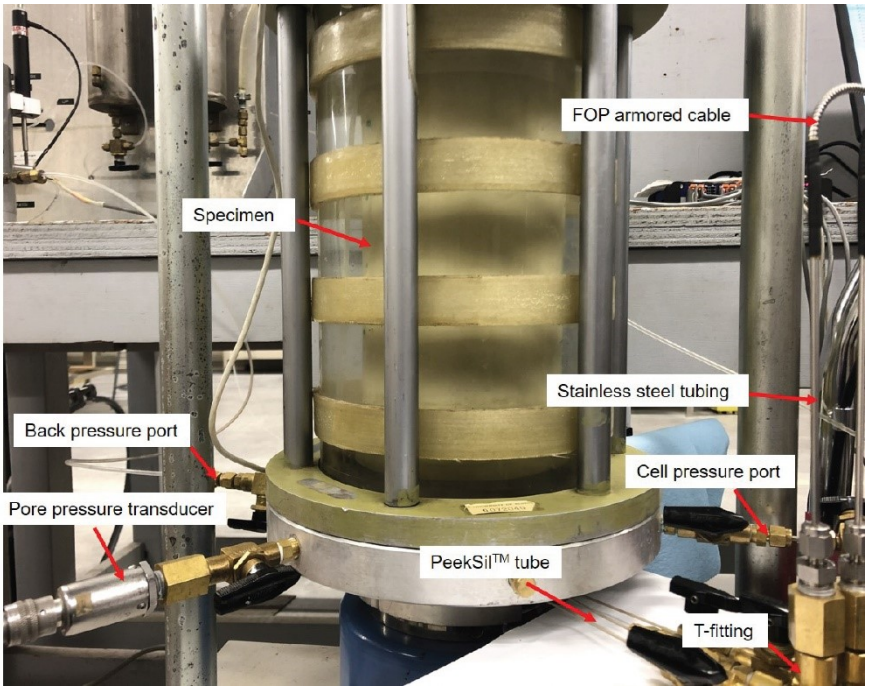

(B)

FIG 2-3 Grain size distribution of sand

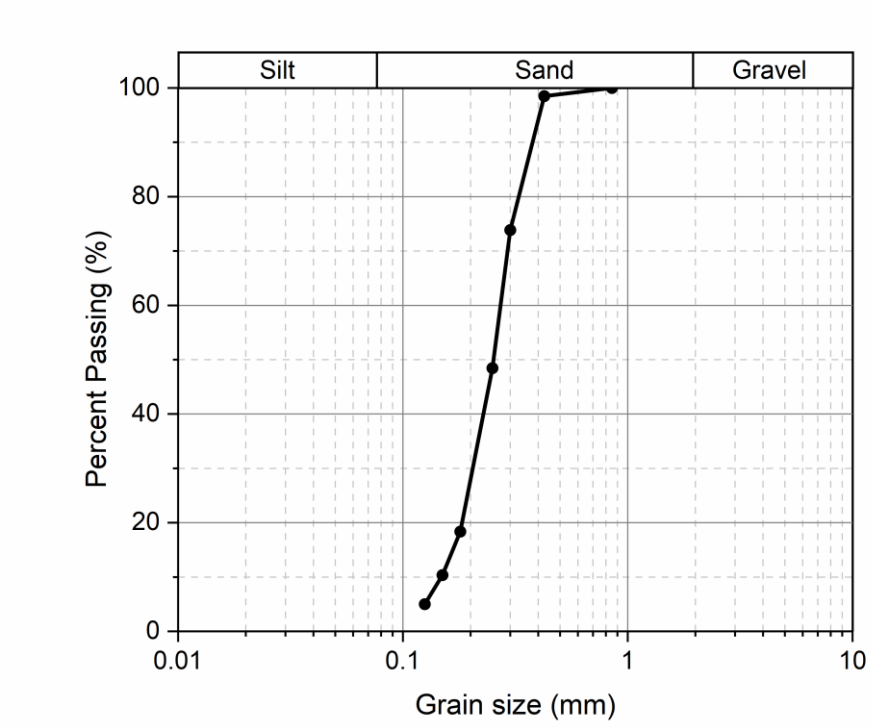

FIG 2-4 Oil droplet at the tip of the tube

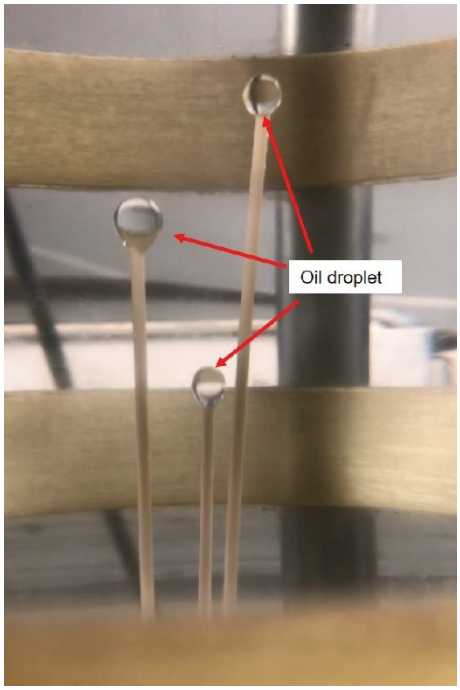

FIG 2-5 Results of calibration: pressure response of all sensors under loading and unloading conditions

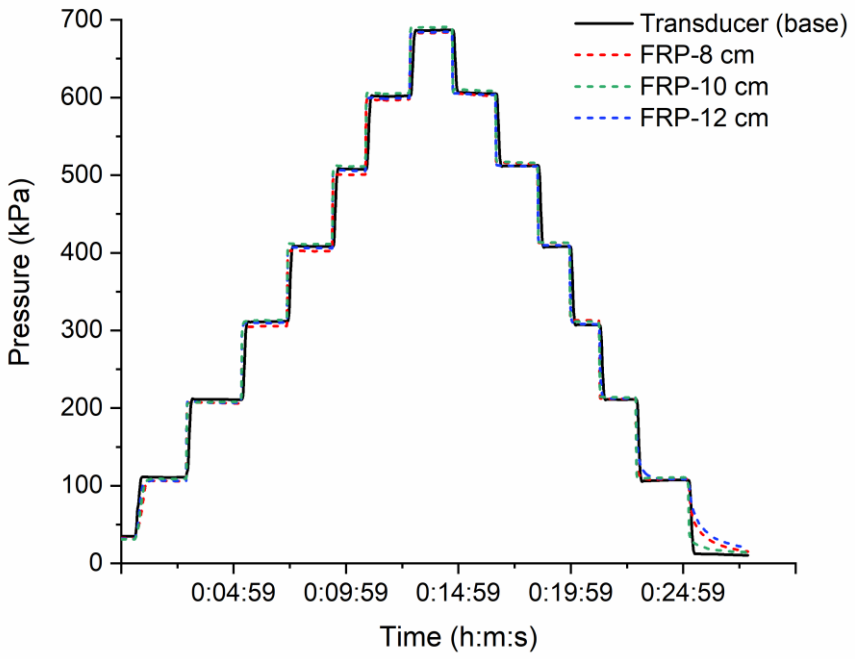

FIG 2-6 Stress-strain curves of loose specimen L-1: (A) stress and pore pressure response and (B) pore pressure change (current PWP subtracts initial PWP)

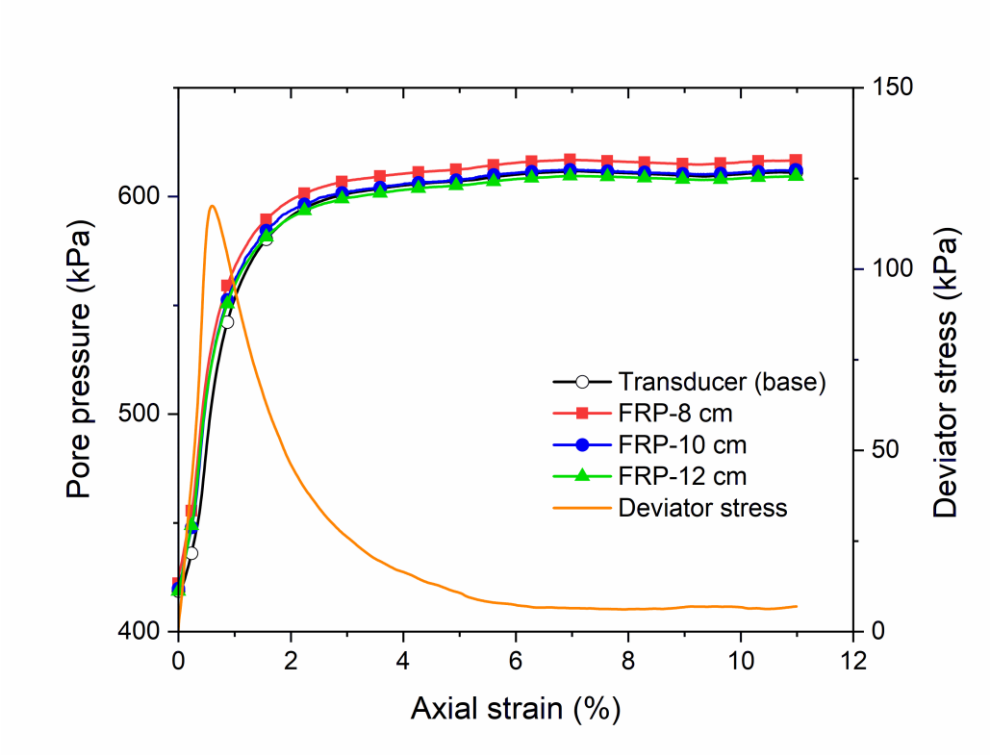

(A)

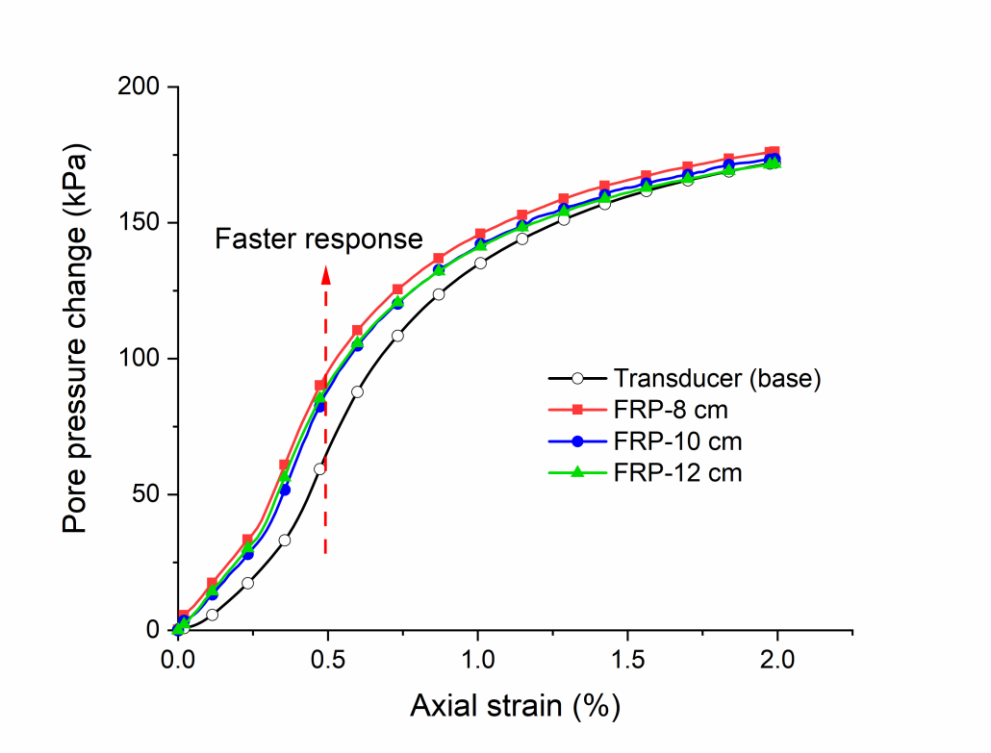

(B)

FIG 2-7 Stress-strain curves of dense specimen D-1: (A) stress and pore pressure response and (B) pore pressure change (current PWP subtracts initial PWP)

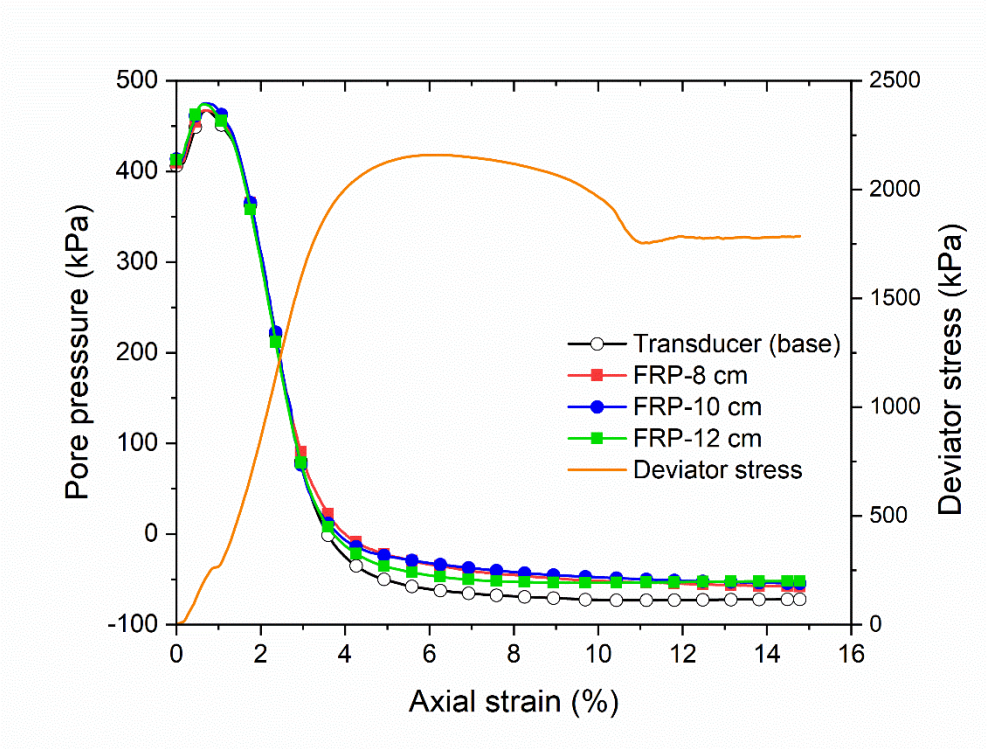

(A)

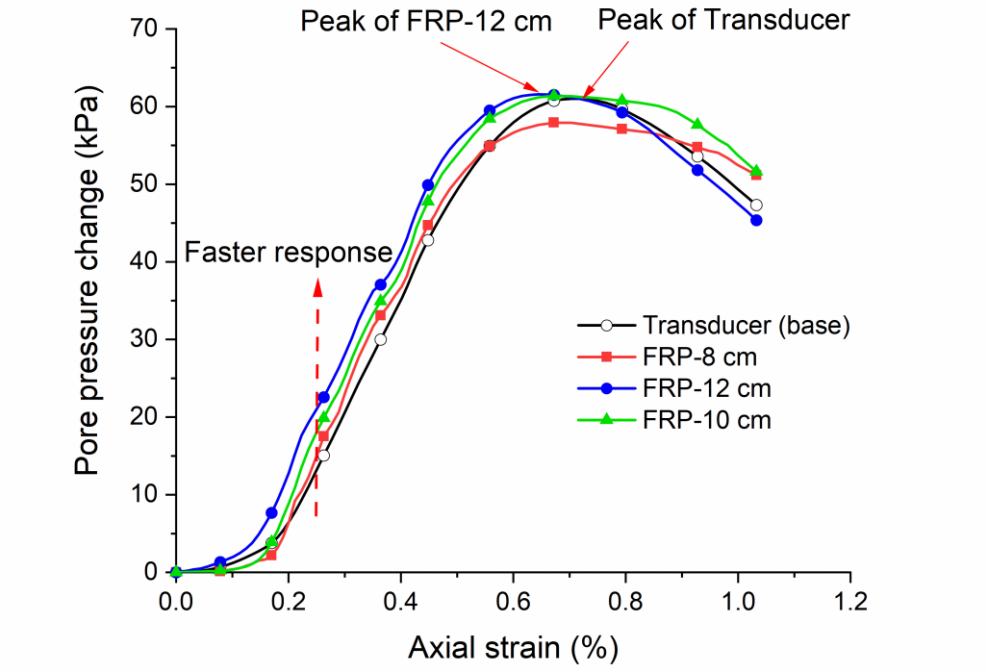

(B)

FIG 2-8 Incremental pwp and deviator stress versus strain: (A) global pwp (loose sand),(B) internal pwp (loose sand), (C) global pwp (dense sand), and (D) internal pwp (dense sand)

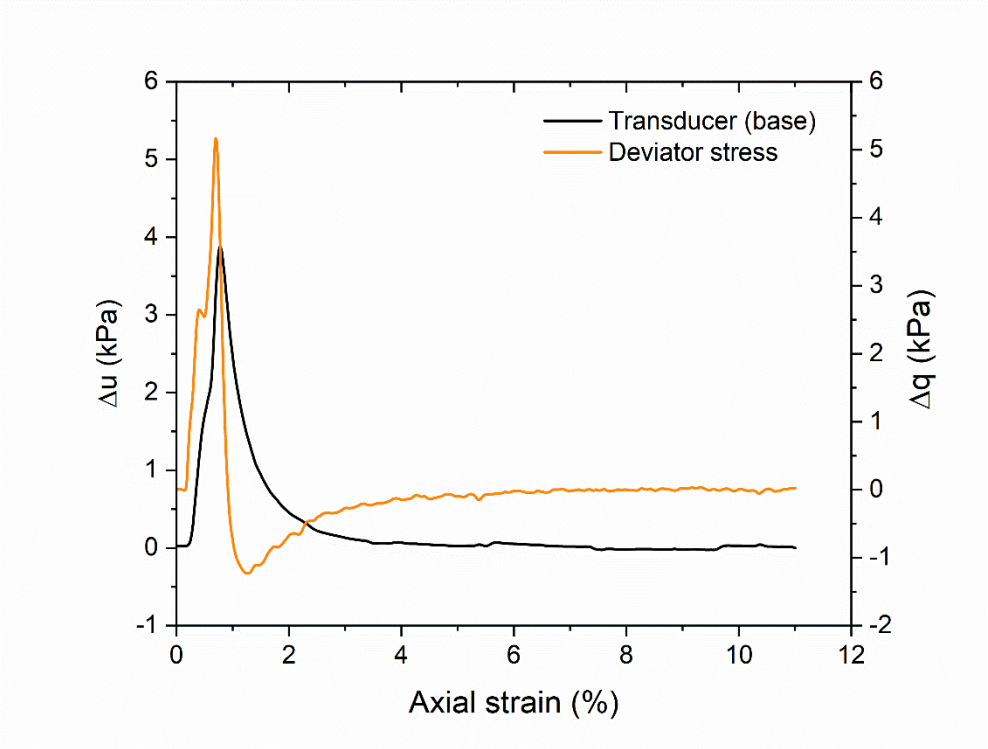

(A)

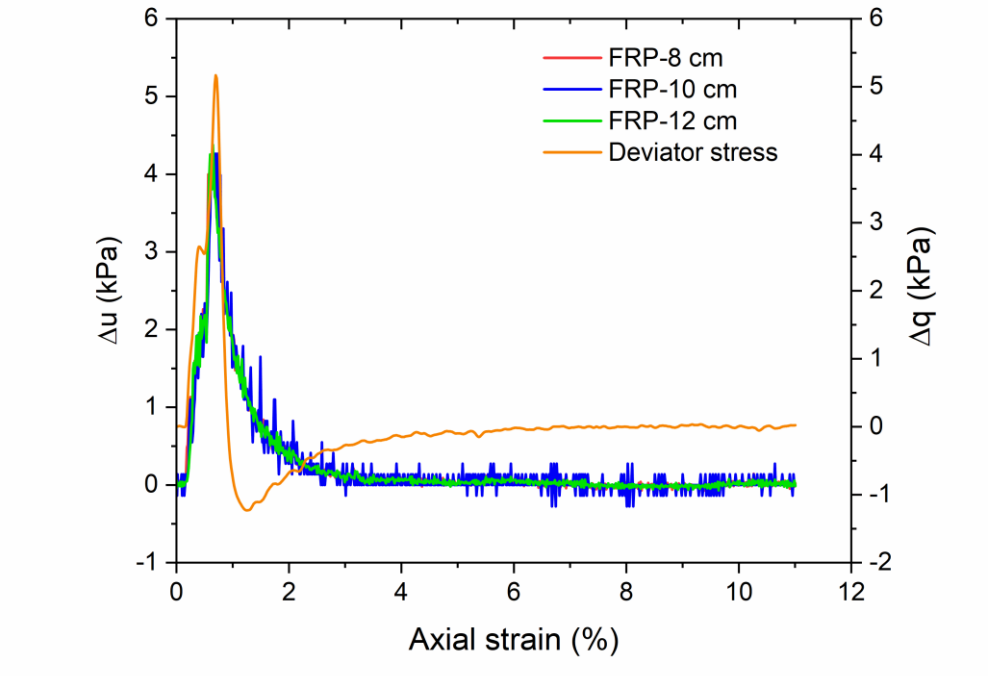

(B)

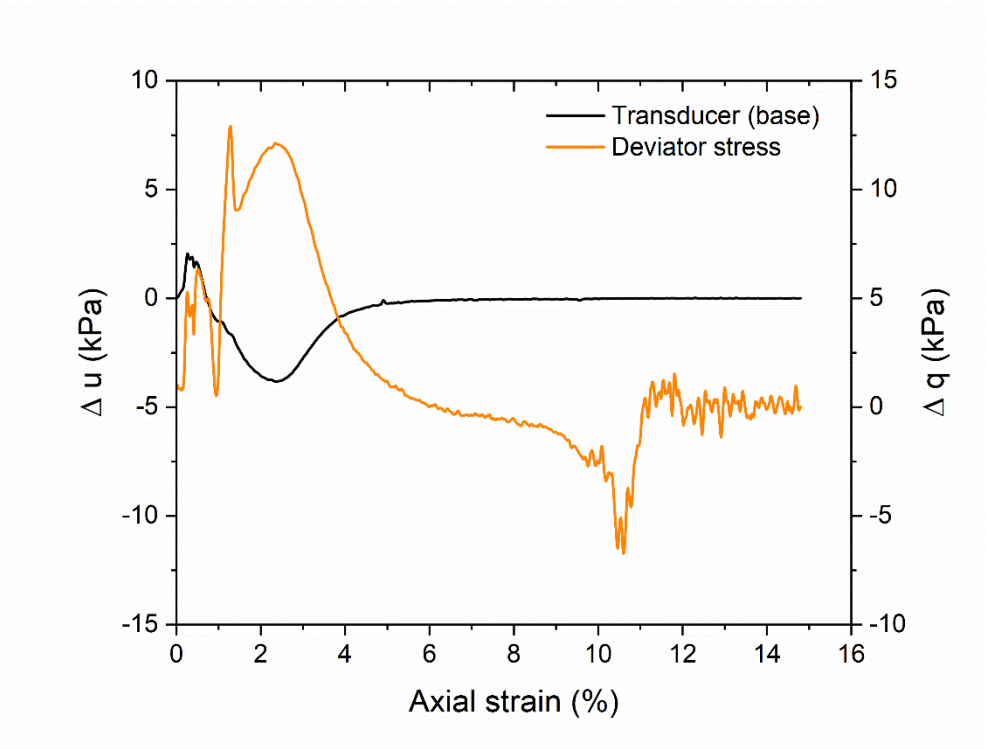
Transducer (base)
Deviator stress
Δ u (kPa)
Δ q (kPa)
Axial strain (%)
10
5
0
-5
-10
-15
15
10
5
0
-5
-10
0
2
4
6
8
10
12
14
16

(C)

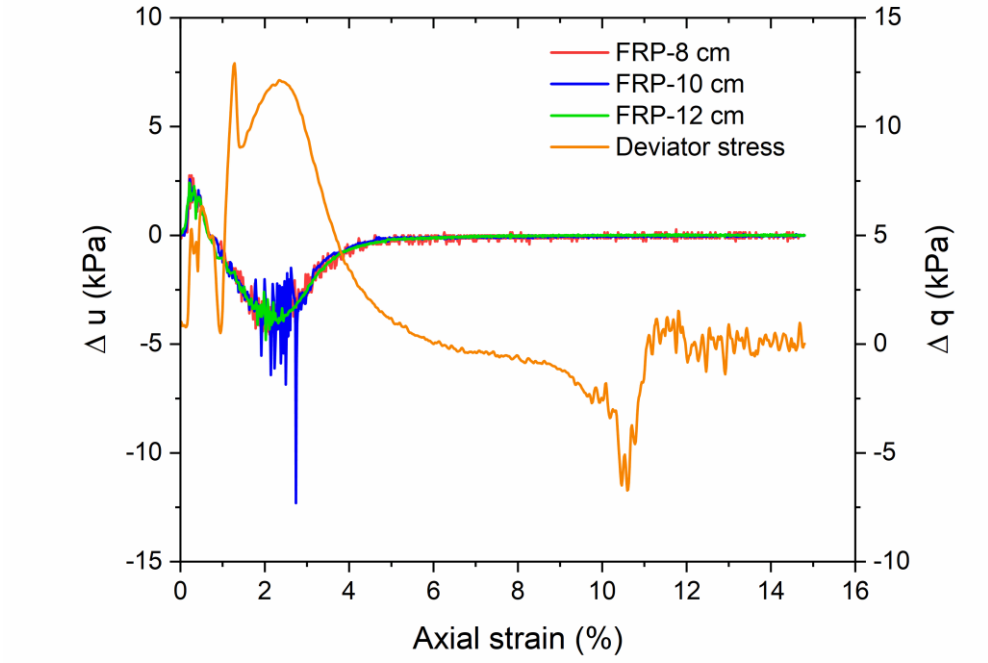
FRP-8 cm
FRP-10 cm
FRP-12 cm
Deviator stress
Δ u (kPa)
Δ q (kPa)
Axial strain (%)
10
5
0
-5
-10
-15
15
10
5
0
-5
-10
0
2
4
6
8
10
12
14
16

(D)

FIG 2-9 Effect of tubes on the behavior of loose specimens: (A) shear stress and (B)global pore pressure (transducer at base)

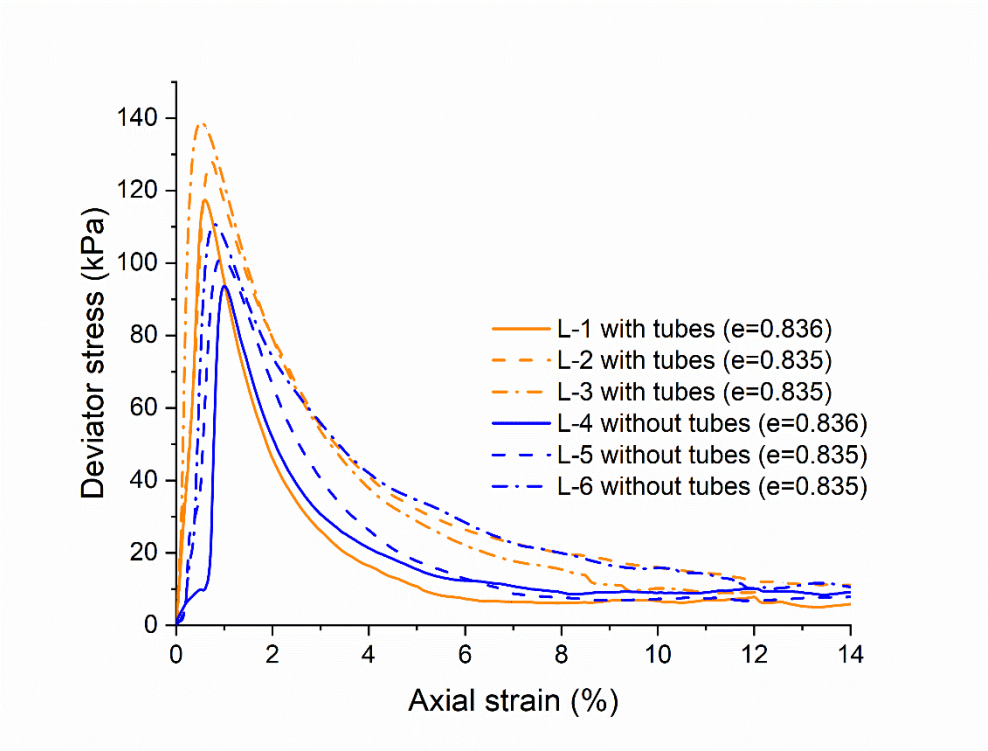

(A)

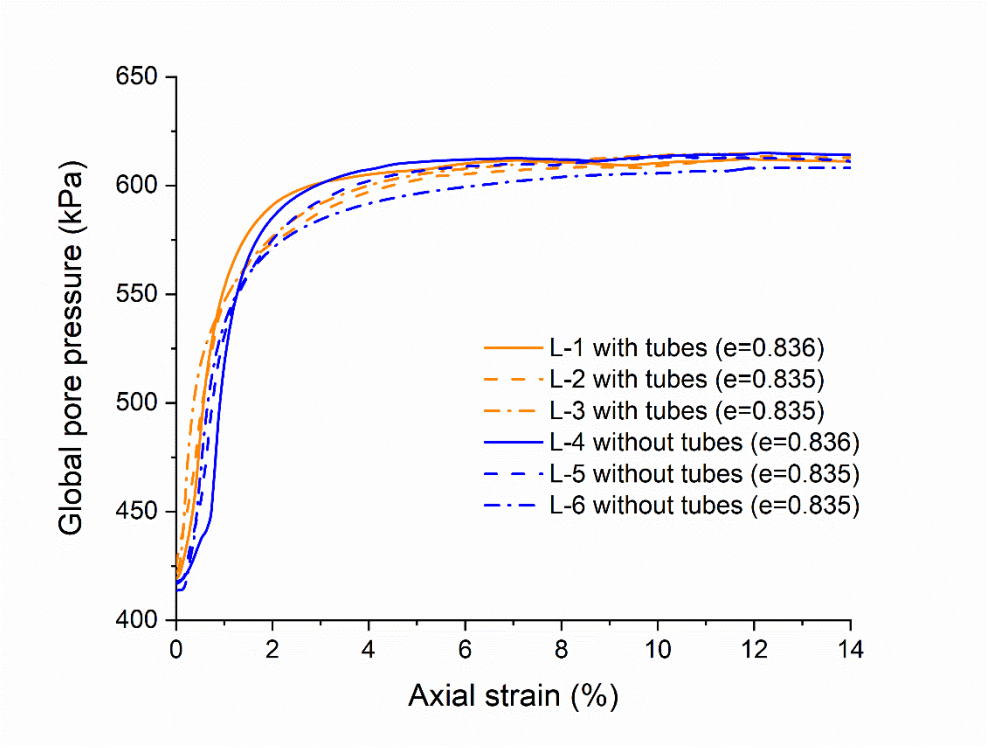

(B)

FIG 2-10 Effect of tubes on the behavior of dense specimens: (A) shear stress and (B) global pore presssure (transducer at base)

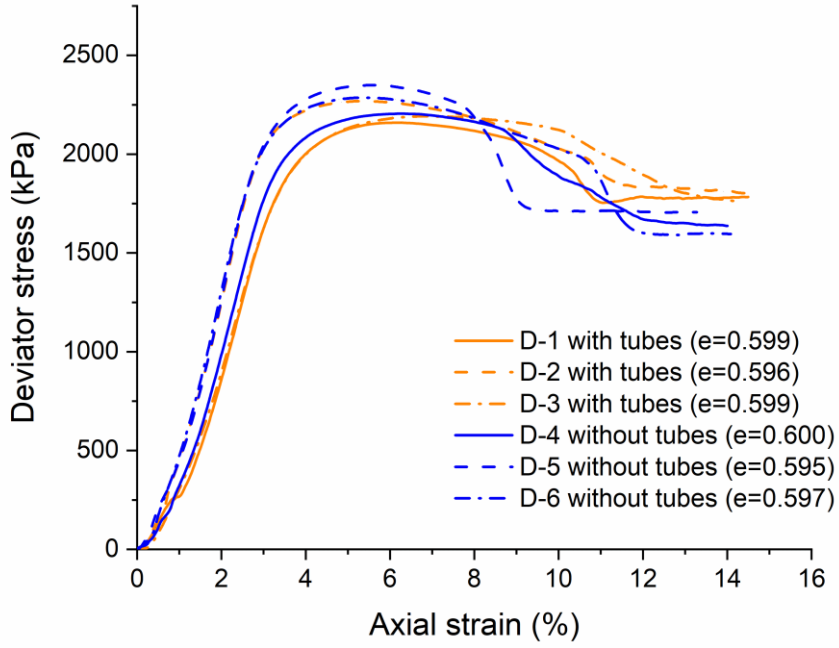

(A)

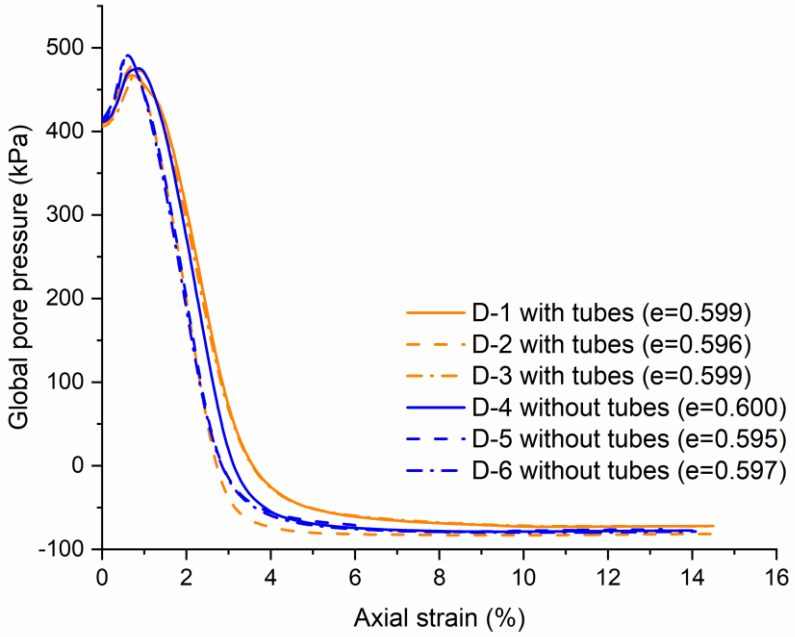

(B)

FIG 2-11 Images of specimens after failure: (A) shear plane of specimen D-1, (B) deformation of tubes of specimen D-1 , and (C) shear plane of specimen D-4

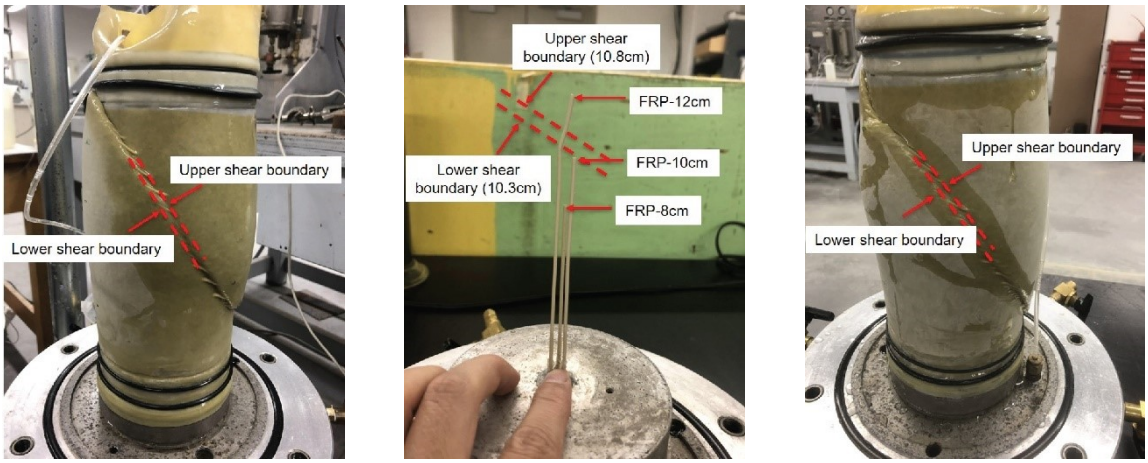

(A) (B) (C)

FIG 2-12 Images of specimen with 400 kPa confining pressure after failure: (A) shear plane and (B) deformation of tubes

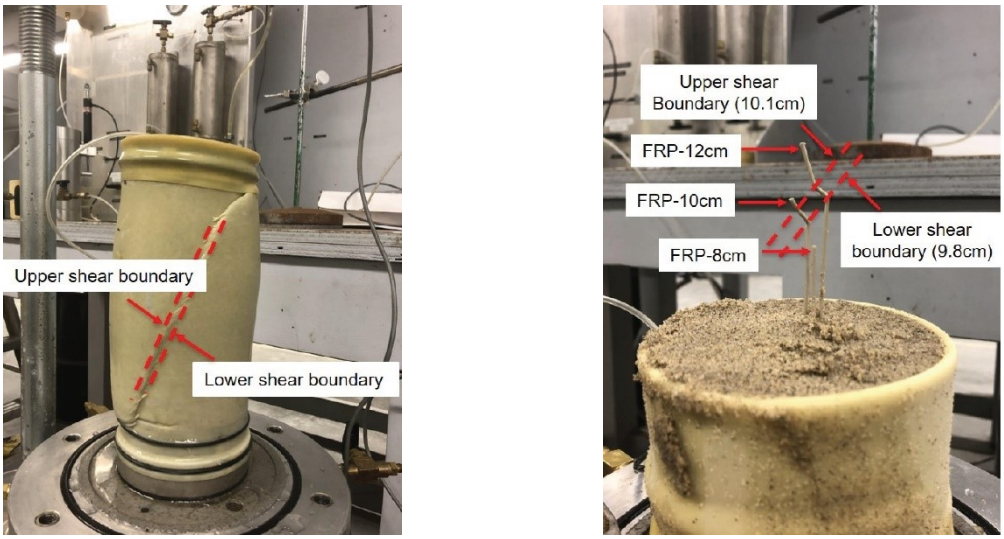

(A) (B)

2.8 References

Atkinson, J. H, and D. Richardson. 1987. The Effect of Local Drainage in Shear Zones on the Undrained Strength of Overconsolidated Clay, Géotechnique 37(3): 393–403.

Cheng, X. H. 2004. Localization in Dutch Dune Sand and Organic Clay. PhD diss., Delft University of Technology.

Gylland, A. S., H. P. Jostad, and S. Nordal. 2013. Experimental Study of Strain Localization in Sensitive Clays. Acta Geotechnica. 9(2): 227–40.

Han, C, and I. G. Vardoulakis. 1991. Plane-Strain Compression Experiments on Water-Saturated Fine- Grained Sand. Géotechnique 41 (1): 49–78.

Hivon, E.G. and D.C. Sego. 1993. Distribution of Saline Permafrost in the Northwest Territories, Canada. Canadian Geotechnical Journal. 30(3): 506–14.

Jefferies, M. and K. Been. 2015. Soil Liquefaction: A Critical State Approach. 2nd ed. Boca Raton, CRC press. US.

Kia, M. 2012. Measuring Pore-water Pressure in Partially Frozen Soils. Ph.D. thesis, Faculty of Graduate Studies and Research, University of Alberta, Edmonton, AB.

Kuerbis, R. H. 1989. The Effect of Gradation and Fines Content on the Undrained Loading Response of Sand. Ph.D. thesis, University of British Columbia.

Marello, S. 2005. Experimental Study of Shear Bands in Fine Grained Soils. In Proceedings of the 11th International Conference on Computer Methods and Advances in Geomechanics, IACMAG, Torino, Italy, 2:119–26.

Schrefler, B. A., H. W. Zhang, M. Pastor, and O. C. Zienkiewicz. 1998. Strain Localisation Modelling and Pore Pressure in Saturated Sand Samples. Computational Mechanics, 22 (3): 266–80.

Sheahan, T. C. 1991. An experimental study of the time-dependent undrained shear behavior of resedimented clay using automated stress path triaxial equipment. Ph.D. thesis, Massachusetts Institute of Technology.

Shuttle, D.A, and I. M. Smith. 1990. Localisation in the Presence of Excess Porewater Pressure. Computers and Geotechnics, 9(1): 87–99.

Thakur, V., S. Nordal, H. P. Jostad, and L. Andresen. 2005. Study on Pore Water Pressure Dissipation during Shear Banding in Sensitive Clays. In 11th International Conference on Computer Methods and Advances in Geomechanics, IACMAG, Torino, Italy, 4: 289- 296.

Thakur, V. 2007. Strain Localization in Sensitive Soft Clays. PhD diss., Norwegian University of Science and Technology.

Thakur, V. 2011. Numerically Observed Shear Bands in Soft Sensitive Clays. Geomechanics and Geoengineering: An International Journal, 6(2): 131–46.

Thakur, V., S. Nordal, G. Viggiani, and P. Charrier. 2018. Shear Bands in Undrained Plane Strain Compression of Norwegian Quick Clays. Canadian Geotechnical Journal, 55 (1): 45-56.

Vardoulakis, I. 1996a. Deformation in Water-Saturated Sand: II. Effect of Pore Water Flow and Shear Banding. Géotechnique, 46(3): 457–72.

Vardoulakis, I. 1996b. Deformation of Water-Saturated Sand: I. Uniform Undrained Deformation and Shear Banding. Géotechnique, 46 (3): 441–56.

Viggiani, G, R J Finno, and W. W. Harris. 1994. Experimental Observations of Strain Localisation in Plane Strain Compression of a Stiff Clay. Localization and Bifurcation Theory for Soils and Rocks, 189–98.

Yuan, J., Q. Zhang, B. Li, and X. Zhao. 2013. Experimental Analysis of Shear Band Formation in Plane Strain Tests on Shanghai Silty Clay. Bulletin of Engineering Geology and the Environment, 72(1): 107–14.

Zhou, J., Lee, W. and Zhou, K. 1995. Dynamic properties and liquefaction potential of silts. Proceedings of the International Conference on Earthquake Geotechnical Engineering, Tokyo, Japan, 2:833-838.

3. Continuity of Pore-Water Pressure Measurements in Partially Frozen Sand

Abstract: A continuous water phase is a prerequisite for measuring pore-water pressure (PWP) within partially frozen soil to establish the effective stress within the test material. A new triaxial apparatus and test method is presented to examine continuity of the water phase and measure the internal PWP in partially frozen soil. A series of consolidated, undrained tests with Skempton's B values determined following consolidation and then measurements of internal PWP were conducted for both dense and loose saline sand at temperatures of 23 °C and -3 °C. This unique set of measurements established continuity in the internal water phase in the sample of a partially frozen soil. Continuity was confirmed using measurements between the internal Filter-less Rigid Piezometers and the base PWP transducer. Hence, the base transducer measured PWP was validated to be representative of the whole sample. Pore ice was found to have minimal impact on the B value for a sample with the continuous water phase. During shear, a continuous decrease in PWP observed in partially frozen, loose samples suggested dilatancy occurred associated with the pore ice that surrounds the sand particles and partially occupies the pore spaces.

Keywords: continuous water phase, pore-water pressure (PWP), partially frozen soil, B value, pore ice.

3.1 Introduction

The geotechnical community have long raised concerns about the impact of climate change on permafrost degradation in Northern communities related to the stability of their infrastructure. The soil in permafrost (e.g., ice rich or saline area) will gradually warm to a “partially frozen” state due to the coexistence of unfrozen water and ice phases in the pore space (Kia 2012). As is well known, it is the effective stress that controls the strength and deformation of a soil. If there is sufficient unfrozen water to provide a continuous water phase at sub-zero temperatures, the effective stress can also be established in these partially frozen soils. This raises two questions: whether the continuous water phase exists in a soil at subfreezing temperatures, and if so, how to measure and prove it experimentally.

In fine-graded soil an unfrozen water film interlayer exists between the particle surface and the pore ice. The water phase would be continuous if the water film, that depends on the temperature and salinity, is thick enough (Anderson and Morgenstern 1973; Sheeran and Yong 1975). In contrast, ice crystals directly grow from the solid particles, and the unfrozen water is trapped within the ice matrix in saline coarse-graded soil (Sheeran and Yong 1975). Further, Arenson and Sego (2006) observed interconnected unfrozen water channels between the ice crystals in a saline sand by using a fluorescent tracer dye. However, confirmation of the continuous water phase along with the PWP measurement in frozen soil has rarely been reported. In some situations where the local PWP at freezing and thawing fringes is of interest for investigating the mechanism of frost heave and thaw settlement (Penner 1959; Williams

1966; Konrad 1989; Eigenbrod et al. 1996; Harris and Davies 1998; Tsarapov 2007; Zhang et al. 2014; Zhang et al. 2015), a continuous water phase throughout the entire specimen is not the essential condition for the tests. On the other hand, there is a challenge in examining continuity in the water phase due to the lack of experimental methods to measure the internal PWP in frozen soil.

To the authors' knowledge, only Kia (2012) validated continuity in the water phase using the Filter-less Rigid Piezometers (FRPs) in partially frozen sand. This study was limited to a one-dimension test. Arenson and Springman (2005) attempted to measure PWP in the ice-rich frozen soil in a triaxial test in which an antifreeze liquid was used to ensure the hydraulic connection between the water phase and the external measuring system. Recently, Lyu et al. (2021b) adopted the same method to monitor PWP using a base transducer in the frozen saline clay. Both Arenson and Springman (2005) and Lyu et al. (2021b) did not examine continuity in the internal water phase during the tests. High air-content was found in ice-rich samples (unsaturated) and low PWP coefficients of B values (less than 0.5) were recorded in frozen saline clay (Arenson and Springman 2005; Lyu et al. 2021b). In general, the water phase would not be continuous when the degree of saturation is lower than 50% (Barden 1965), therefore the measured PWP in these studies cannot be representative of the whole sample as these samples were not saturated and hence the water phase was likely discontinuous.

The objective of this study is to present a test method for examining the continuity in the water phase within partially frozen sand. A series of consolidated, undrained triaxial tests were

performed on both dense and loose samples with a salinity of 30 ppt. The specimens were prepared by rapidly freezing the samples and then slowly warming the samples to and subsequently shearing them at -3 ºC. The scope of this study is limited to the PWP response, and the analysis of mechanical behavior of partially frozen sand will be covered in a subsequent publication.

3.2 Material and methods

3.2.1 Material

The stored sand used in Chapter 2 was inadequate for the rest of the tests, so it was replaced with a similar sand (Fig. 3-1). The grain sizes are between 0.15 mm and 0.85 mm (D_{50} = 0.28 mm), and the specific gravity is 2.64, which is the similar material reported as Soil A by Hivon and Sego (1995). A salinity of 30 ppt (30 g/L) was selected in this study to represent high salinity pore fluid as found at some arctic coastal communities (Hivon and Sego 1993).

3.2.2 Test apparatus

A modified temperature and strain rate controlled triaxial cell apparatus was used (Fig. 3-2), which was originally developed for measuring internal PWP of soil (Liang et al. 2022). Three PeekSil tubes embedded at different heights within the specimen are connected to fiber optic pressure sensors to measure the internal PWP and to confirm the continuity in the water phase of the specimen. Continuity is confirmed by comparing the internal PWP to measured PWP using a conventional pressure transducer at the base of the specimen. To ensure that uniform

temperature throughout the specimen is achieved, the temperature is monitored using three thermistors located on the top, middle and bottom of the specimen's surface (membrane). Cell temperature is controlled by circulating water-glycol mixture (1:1) through two cold baths: cold bath A is connected to a spiral copper coil inside the cell and cold bath B is attached to the cooling plate at the base of the cell. The base cooling plate is also used to circulate liquid nitrogen for rapid freezing during the preparation of the test specimen. The triaxial cell is filled with a 3:7 solution of water-glycol, and the cell is double insulated using the fiberglass wrapped on the surface and a foam box surrounding the cell.

3.2.3 Test procedures

Large cylindrical specimens of 100 mm in diameter and 196 mm in height were prepared, saturated and then consolidated to targeted effective stress using the procedures described by Liang et al. (2022). After consolidation, the PWP coefficient (pre-shearing B value) of the unfrozen samples was checked by increasing cell pressure and measuring corresponding increases in PWP.

For partially frozen tests, the triaxial apparatus was set up in a walk-in freezer where the temperature was maintained at about 2 ºC to ensure the sample temperature is as close to the target temperature of -3 ºC as possible while preventing damage to electronic equipment. As illustrated in Figure 3-3, the rapid freezing and subsequent warming of the specimens were conducted in the three stages:

I. After consolidation, the specimen was frozen unidirectionally by circulating liquid

nitrogen through the base cooling plate for about 7 hours. This minimized salinity migration while assuring uniformity within the specimen (Hivon and Sego 1995). Then, the cold bath B with refrigerating fluid (water-glycol) at the temperature of -25 ºC was attached to the cooling plate and circulated for an additional 12 h. The top drainage (back pressure) line was kept open, while the back pressure (400 kPa) and cell pressure remained constant. About 60 ml of water was expelled during freezing, which was close to the estimated value of 64 ml corresponding to 9 % of total pore volume.

II. Cold bath A with a temperature of -11 ºC was connected to a spiral copper coil to maintain uniform temperature of the specimen around -11 ºC, normally for 8 hours. To prevent the uncontrolled thawing at the bottom of the specimen, the circulation of water-glycol through the base plate remained but was changed to a temperature (-15 ºC) lower than cold bath B because of the energy loss during thermal transfer between the base plate and the bottom of the specimen. The top drainage line was found blocked during this stage.

III. The specimen then was warmed uniformly to -3 ºC by raising the temperature of cold bath A to -3 ºC over a period of approximately 36 to 42 hours. To clear the drainage line of ice, the back pressure line was switched to the bottom and the temperature of cold bath B was raised to 1 ºC for several hours. Once the drainage line thawed, the temperature of cold bath B was lowered to -2.5 ºC to keep the drainage line thawed and the temperature gradient throughout the specimen

minimized. A maximum of 0.001 ºC /mm gradient was observed while the temperature stabilized. During this stage, around 33 ml was recorded to refill (re-saturate) the specimen (Fig. 3-3) and the gravimetric unfrozen water content (UWC) was estimated at 16 %. Meanwhile, PWP measured using the FRPs and the transducer gradually increased and approached the back pressure (Fig. 3-4a).

Continuity in the water phase within partially frozen specimens at -3 ºC was evaluated by increasing the back pressure in 30 kPa increments independent of the applied cell pressure and measuring the corresponding increase in PWP measured by the base transducer and the FRPs (Kia, 2012). A continuous water phase was confirmed when all the sensors showed the same pore pressure and reflected the back pressure (Fig. 3-4b). Then the PWP coefficient (pre-shearing B value) of partially frozen specimens was determined prior to shearing. Finally, all the specimens were sheared at a constant strain rate of 1% /min.

A summary of the testing program is shown in Table 3-1, including two unfrozen specimens, three partially frozen, loose and dense specimens. In this chapter, the terms D, L, PL, and PD refer to unfrozen dense, unfrozen loose, partially frozen loose and partially frozen dense specimens, respectively. The unfrozen specimens were used as references to assist with interpreting the behavior of the partially frozen specimens. The first two partially frozen, loose samples utilized the same heavy mineral oil as used in the unfrozen samples for the piezometer fluid of the FRPs, but an apparent hysteresis existed in PWP measurement due to the high viscosity of the heavy mineral oil at -3 ºC. Thereafter the piezometer fluid was replaced with

light mineral oil for all subsequent tests.

3.3 Results

3.3.1 Calibration

Prior to the partially frozen tests, all the PWP sensors were calibrated in a water-glycol (3:7) filled triaxial cell by adjusting cell pressure at a temperature of -3 ºC. The response corresponded to that observed by Liang et al (2022) in an unfrozen test, the FRPs showed a faster response above 100 kPa during loading and a slower response during unloading below 150 kPa compared to the basal transducer (Fig. 3-5).

3.3.2 B value tests

The initial (before consolidation) and pre-shearing B values are shown in Table 3-2. For unfrozen loose and dense specimens, a decrease in B value from 0.97 to 0.92 and 0.98 to 0.94 were recorded after consolidation, respectively. A similar phenomenon was also reported by Kia (2012) when he investigated the effects of pre-consolidation on PWP response. The pre-shearing B values of the partially frozen specimens were measured after the continuity in the water phase was validated. Note that the pre-shearing B value is a function of the initial value where higher initial values lead to higher pre-shearing values. This indicates that the test temperature has limited influence on B value, particularly for partially frozen, loose specimens. However, Lyu et al. (2021b) found a significant decrease in B value in frozen saline clay. More detail about the B value will be discussed later.

3.3.3 PWP measurements in unfrozen samples

Firstly, two unfrozen samples (L-1 and D-1) were tested under effective confining pressure of 100 kPa to check the measuring system as well as establish a baseline. A typical contractive behavior of loose sand and a dilative behavior of dense sand were observed, where the excess PWP developed until close to the applied cell pressure or the PWP continuously dropped to below zero, respectively (Fig. 3-6). All the FRPs showed a similar response as the base transducer throughout the tests, although different suction levels were measured in dense sample by the FRPs. The different suction is relevant to local voids around the tip of the tube and to the surface tension of mineral oil and water (Liang et al. 2022). Overall, the continuity of PWP measurements between the FRPs and the base transducer were observed in unfrozen samples.

3.3.4 PWP measurements in partially frozen samples

Figure 3-7 presents the stress and PWP response of three partially frozen, loose samples under different effective confining pressures. All samples showed a ductile response compared to strain softening behavior observed in the unfrozen loose sample. For the sample PL-1 (Fig. 3-7a), only FRP-10 cm recorded a continuous decrease in PWP until the end of the test, while FRP-8 cm and 12 cm reported a constant PWP after 3 % and 4 % strain. Similarly, PWP measured by FRP-8 cm and 10 cm in the sample PL-2 (Fig. 3-7b) presented a noticeable slower response compared to the base transducer and remained unchanged after 4 % of strain. The FRP-12 cm was likely blocked shortly after the test started. Recall, PL-1 and PL-2 were tested

with the heavy mineral oil, but PL-1 did not have PWP measured using the base transducer. These erratic measurements from the FRPs were also observed by Kia (2012) and attributed to the local ice blockage in the pores associated with the measuring tubes, but he neglected the effect of high viscosity of heavy mineral oil at subzero temperature, which would significantly reduce the hydraulic conductivity of piezometer fluid. For this reason, a light mineral oil was used in sample PL-3 (Fig. 3-7c), and the performance of FRPs greatly improved. The PWP response of FRP-8 cm matched with the base transducer, which indicated the continuity in the water phase throughout the test and hence validated the effectiveness of PWP measurement in partially frozen, loose sand. Besides, almost all the erratic measurements appeared after 2 % of strain and worsened as the tests continued. This would be associated with blockage of the tube. The tubes were compressed following axial deformation of soil, thus small particles (ice crystal or mineral grains) were likely blocking the tip of the tube with increased strain. For further analysis, only the continuity of PWP measurement was selected, such as FRP-10 cm of PL-1, transducer of PL-2, and FRP-8 cm or transducer of PL-3.

The stress and PWP response of partially frozen, dense samples are shown in Figure 3-8. Continuity in the water phase was confirmed by near identical measurements between the embedded FRPs and the base transducer for sample PD-3 (Fig. 3-8c). The base pressure line containing saline water froze during the PD-2 test, so it showed an inaccurate response after 3 % strain (Fig. 3-8b). In sample PD-1 (Fig. 3-8a), FRP-10 cm behaved poorly in the pre-shearing continuity test and then showed erratic measurement at an early stage. The reason for different suction recorded by FRPs were mentioned previously. With the consistent PWP

measurements between FRPs and base transducer, the effectiveness of PWP measurements in partially frozen, dense sand was also validated at -3 ºC.

3.4 Discussion

Due to different sample preparation methods, only de-aired saline water was flushed in dense samples during pre-saturation, rather than flushing carbon dioxide followed with de-aired saline water to replace the pore air used in loose samples. Hence, some air could remain in the pores and the dense samples were not 100% saturated. In addition, previously dissolved air was driven out from pore fluid and coalesced with existing air to form larger air bubbles after freezing, resulting in a lower degree of saturation in partially frozen, dense samples. This could explain why B values of samples PD-2 and PD-3 reduced to 0.7 from initial values of 0.91 and 0.93. In frozen saline clay, considerably lower B values were determined by Lyu et al. (2021a), potential due to the difference in bulk stiffness of ice and soil skeleton. However, continuity in the water phase was not examined before the B value tests, so their measured B values were questionable. Kia (2012) also reported lower B values in the partially frozen state than that in the unfrozen state because of the resistance of pore ice. However, the effect of high viscosity of heavy mineral oil and of separated air bubbles on the B value tests were not considered. Since the pore ice is more compressible relative to the pore water than the soil skeleton, and more fragile ice needles grow in saline sand (Arenson and Sego 2006), the authors hypothesize that the pore ice does not affect the B value at a given saturation level. This is supported by observations of B values in samples with the high initial degree of saturation (Table 3-2).

The partially frozen, loose samples show the dilative behavior as the PWP continuously decreases to below zero (e.g., FRP-10 cm of PL-1) due to the presence of ice, which is significantly different from the contractive behavior of the unfrozen loose sand under undrained loading. In other words, the ice needles grown on the soil grains contribute the sample behaving at a "denser" state. The decrease in PWP was also presented in ice-rich samples (extremely loose) by Arenson and Springman (2005), and the cracking of bonds and breaking of pore ice were considered to cause expansion in pore volume. After the test, no shear plane was observed in the partially frozen, loose samples (Fig. 3-9), therefore the shear-induced dilation could only occur in the pore ice of the partially frozen, loose sand. In contrast, an apparent shear plane formed in the partially frozen, dense sample (Fig. 7b), implying that the shear-induced dilation was caused by the soil skeleton.

3.5 Conclusion

This paper presents a new testing method to examine continuity in the water phase and measure PWP in partially frozen sand under consolidated, undrained triaxial condition. To minimize the effect of temperature on the conductivity of piezometer fluid, the light mineral oil is recommended to use in the FRPs. Continuity in the water phase within the sample at a subfreezing temperature is confirmed by the consistent PWP measurements between the FRPs and the base transducer, and therefore the base transducer measured PWP is validated to be representative of the entire sample. With the continuous water phase, the B value of partially frozen sand is mainly governed by the initial degree of saturation and not affected by the pore

ice. However, the pore ice has a significant impact on the behavior of loose sand because it will contribute to the sand behaving in a "denser" state. The decreases in PWP of partially frozen, loose and dense sand are mainly attributed to the shear-induced dilation of the pore ice and the soil skeleton respectively. Given continuity in the water phase, the measured PWP can be used to conduct effective stress analysis on the mechanical behavior of partially frozen soil in future work.

3.6 Tables

Table 3-1 Summary of the testing program

State	Test ID	Initial Height (cm)	Initial Void Ratio	Initial Water Content (%)	Confining Pressure (kPa)	T (°C)	Piezometer Fluid of FRPs
Unfrozen	L-1	19.59	0.834	32	100	23	heavy mineral oil
	D-1	19.62	0.599	23	100	23	heavy mineral oil
Partially Frozen	PL-1	19.60	0.835	32	100	-3	heavy mineral oil
	PL-2	19.60	0.834	32	200	-3	heavy mineral oil
	PL-3	19.61	0.835	32	400	-3	light mineral oil
	PD-1	19.58	0.596	23	100	-3	light mineral oil
	PD-2	19.61	0.599	23	200	-3	light mineral oil
	PD-3	19.55	0.594	22	400	-3	light mineral oil

Note: L, loose; D, dense; PL, partially frozen loose; PD, partially frozen dense.

Table 3-2 Summary of initial and pre-shearing B values

Test ID	Initial B value	Pre-shearing B value	Ratio of pre-shearing to initial B value
L-1	0.97	0.92	0.95
D-1	0.98	0.94	0.96
PL-1	0.98	0.95	0.97
PL-2	0.99	0.93	0.94
PL-3	1	0.88	0.88
PD-1	0.99	0.88	0.89
PD-2	0.91	0.7	0.77
PD-3	0.93	0.7	0.75

3.7 Figures

FIG 3-1 Comparison of grain size distribution of sand

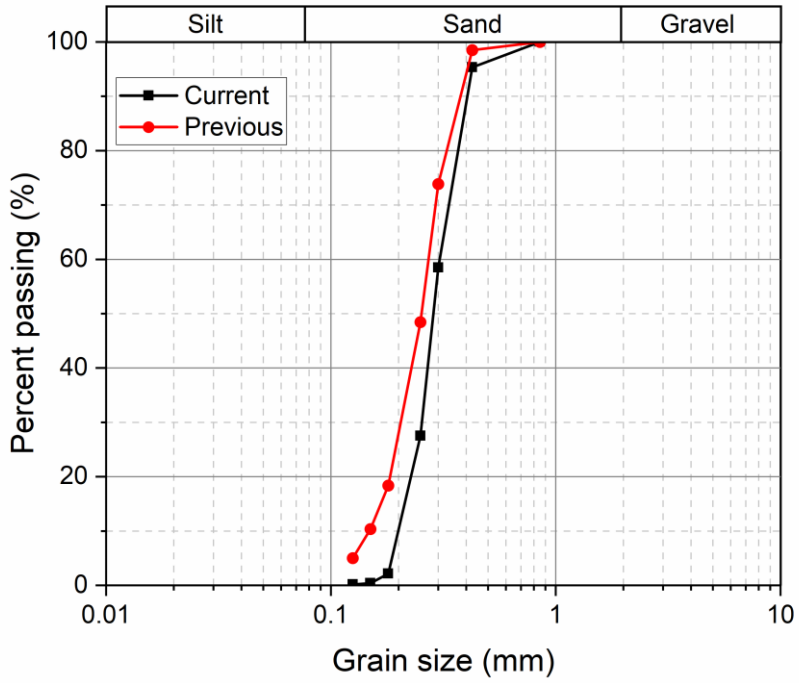

FIG 3-2 Illustration of testing apparatus. (a) schematic of apparatus (modified from Liang et al. 2022) and (b) photograph of apparatus

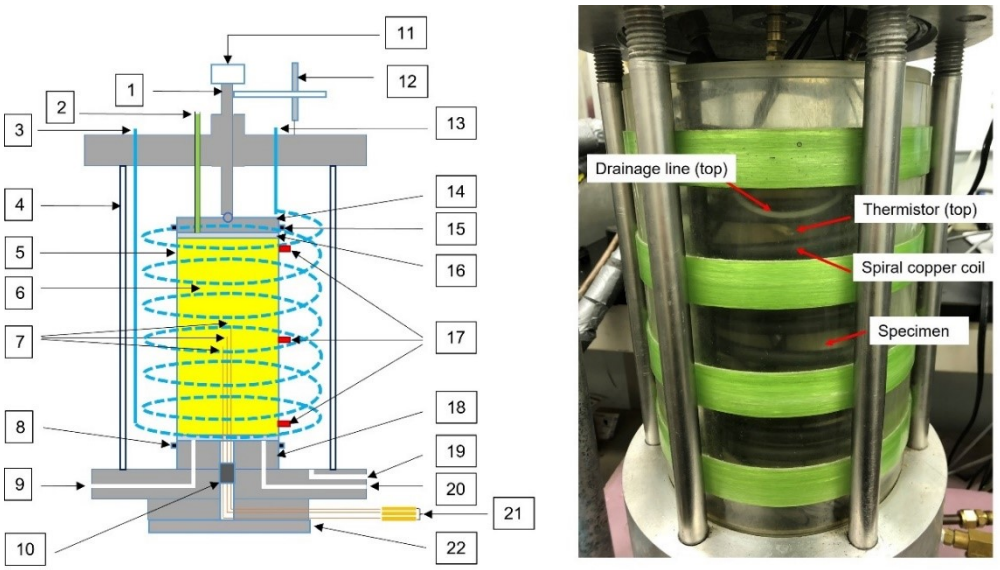

(a) (b)

1. Load ram
2. Back pressure (Top drain)
3. Inflow of glycol
4. Perspex cell
5. Membrane
6. Specimen
7. PeekSil tubes (12cm, 10cm, 8cm)
8. O-ring
9. Backpressure (Bottom drain)
10. Multiconductor feedthrough
11. Load cell
12. LP
13. Outflow of glycol
14. Top cap
15. O-ring
16. Porous stone + Filter paper
17. Thermistors
18. Pedestal
19. Cell pressure
20. Pore pressure transducer
21. Three FRPs
22. Cooling plate

FIG 3-3 Temperature and volume change during rapid freezing and subsequent warming: PL-2

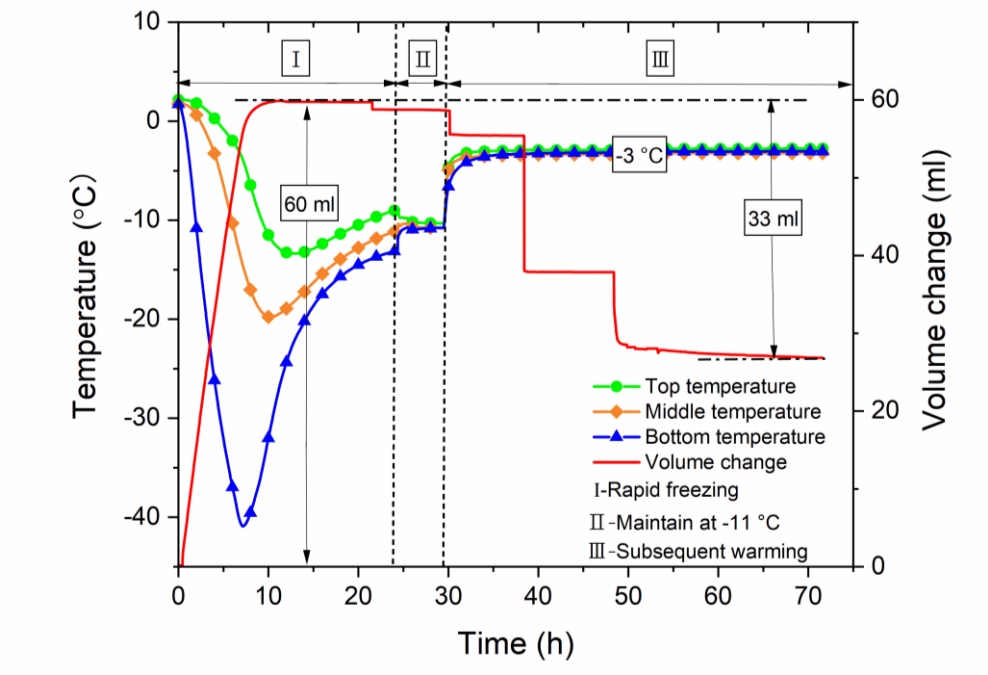

FIG 3-4 PWP response before shearing. (a) subsequent warming during stage III at -3 °C: PD-2 and (b) confirmation of continuity in the water phase: PL-2

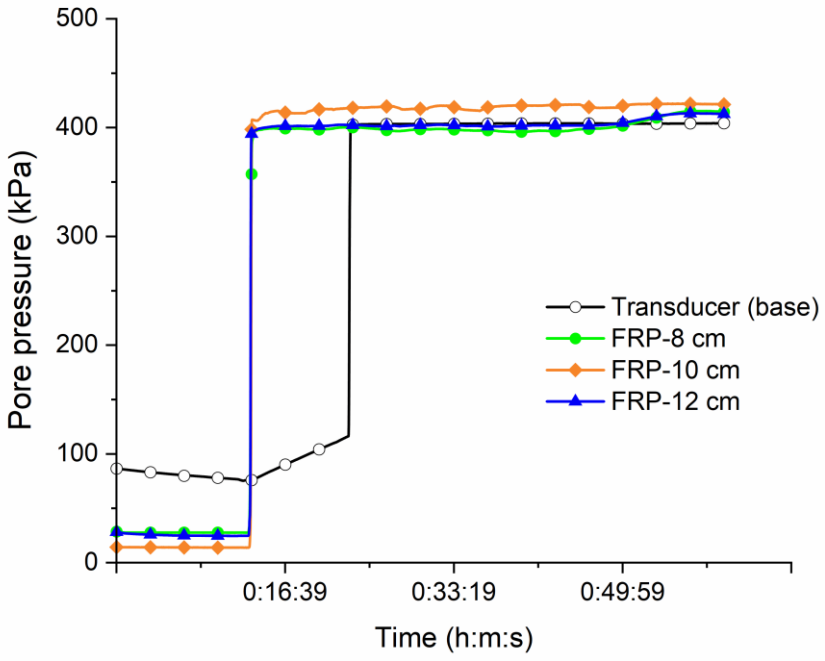

(a)

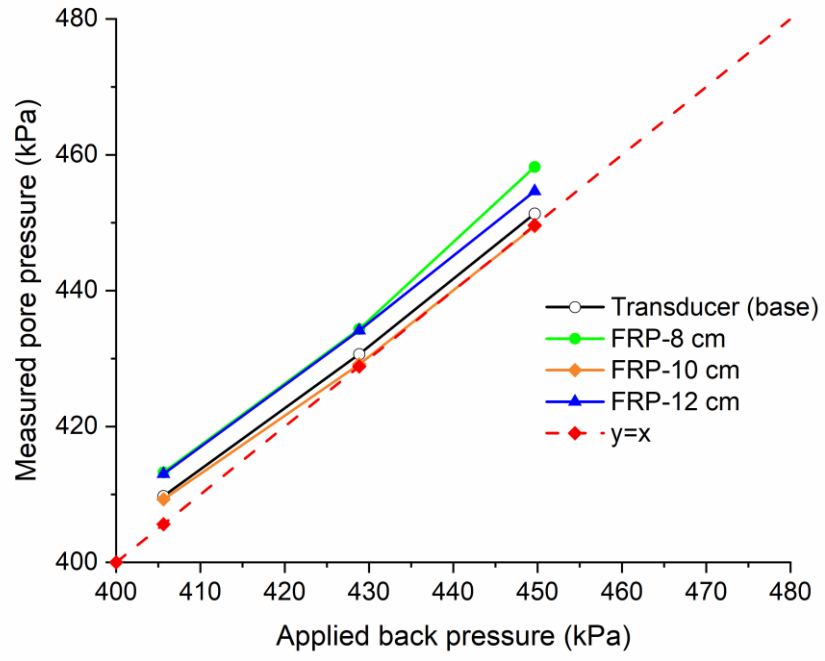

(b)

FIG 3-5 Results of calibration at -3 ℃

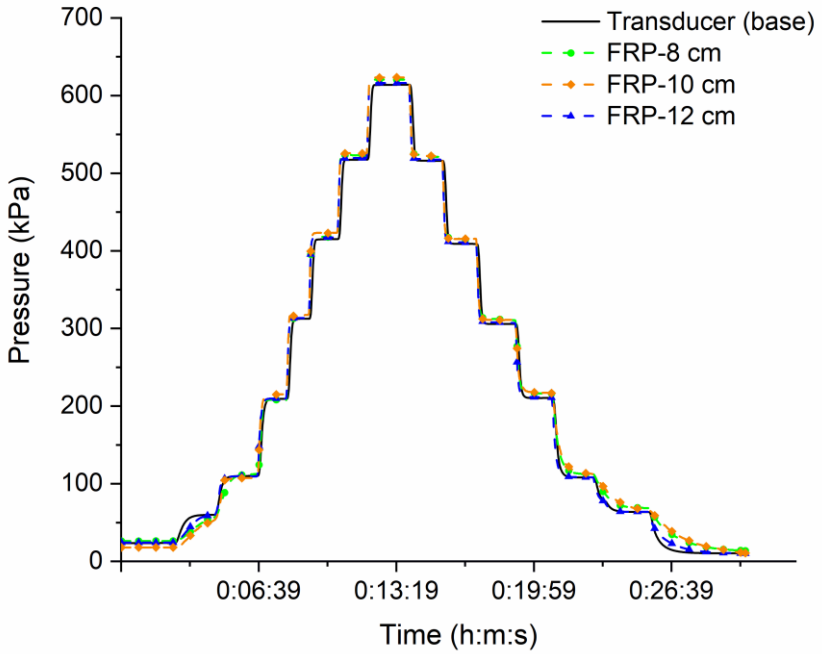

FIG 3-6 PWP measurements in unfrozen samples. (a) L-1 and (b) D-1

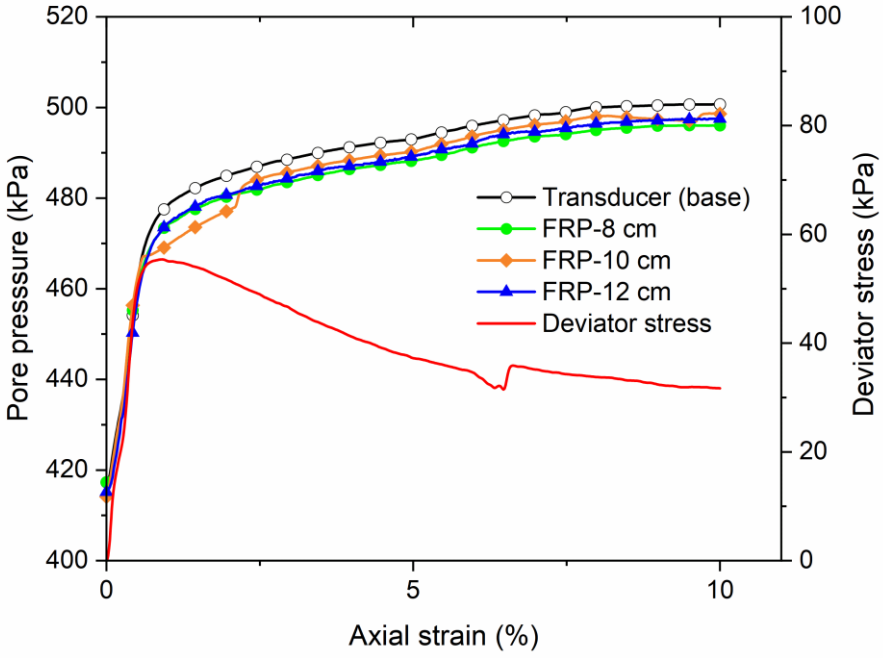

(a)

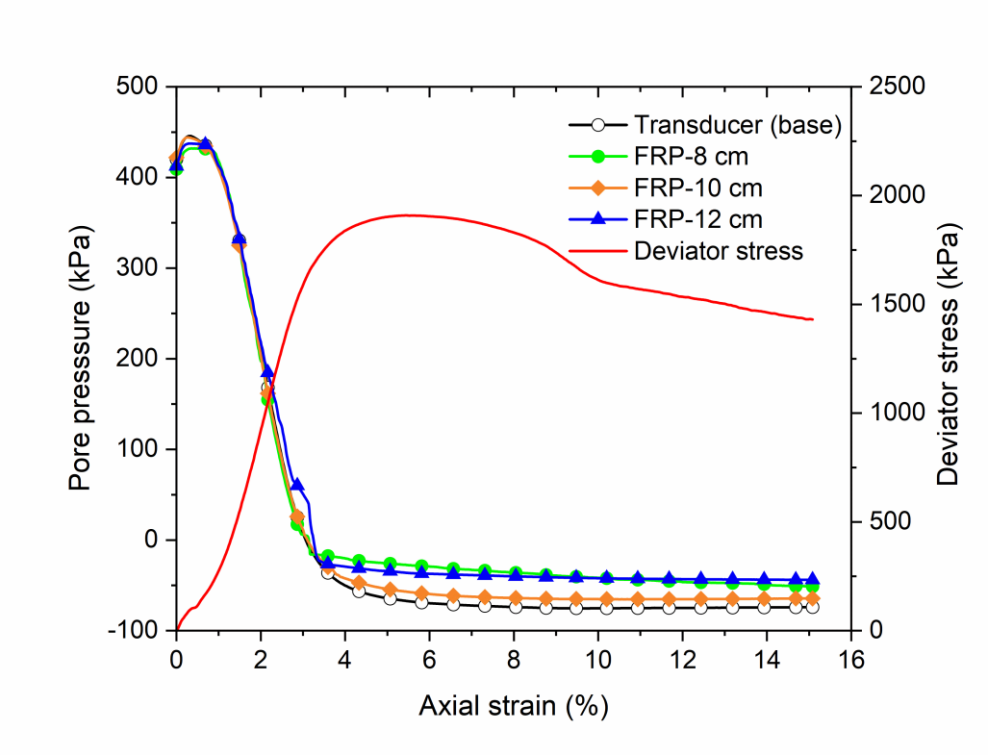

(b)

FIG 3-7 PWP measurements in partially frozen loose samples. (a) PL-1, (b) PL-2, (c) PL-3

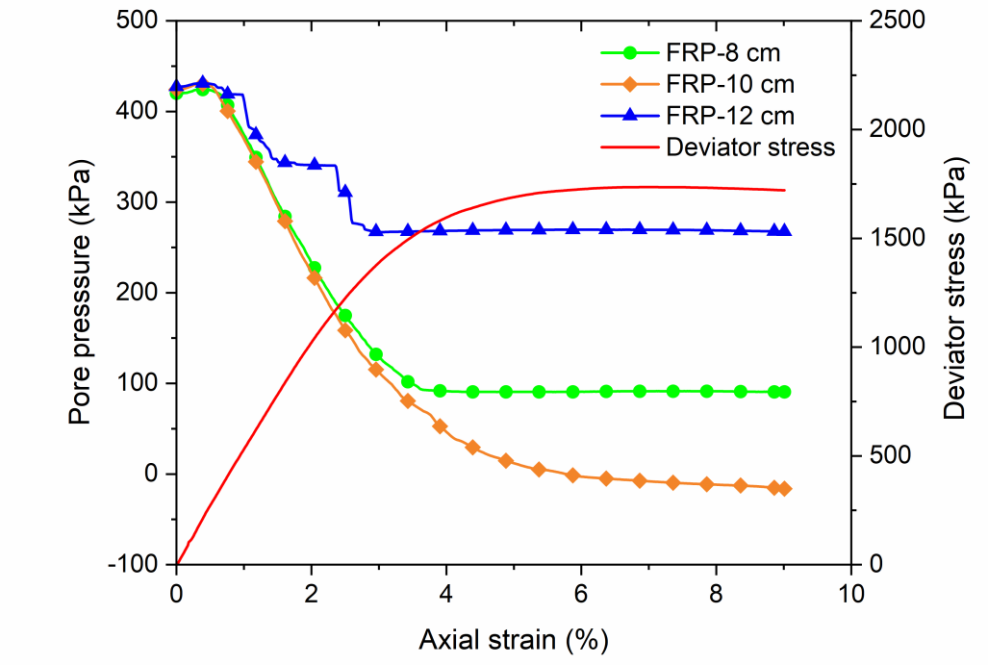

(a)

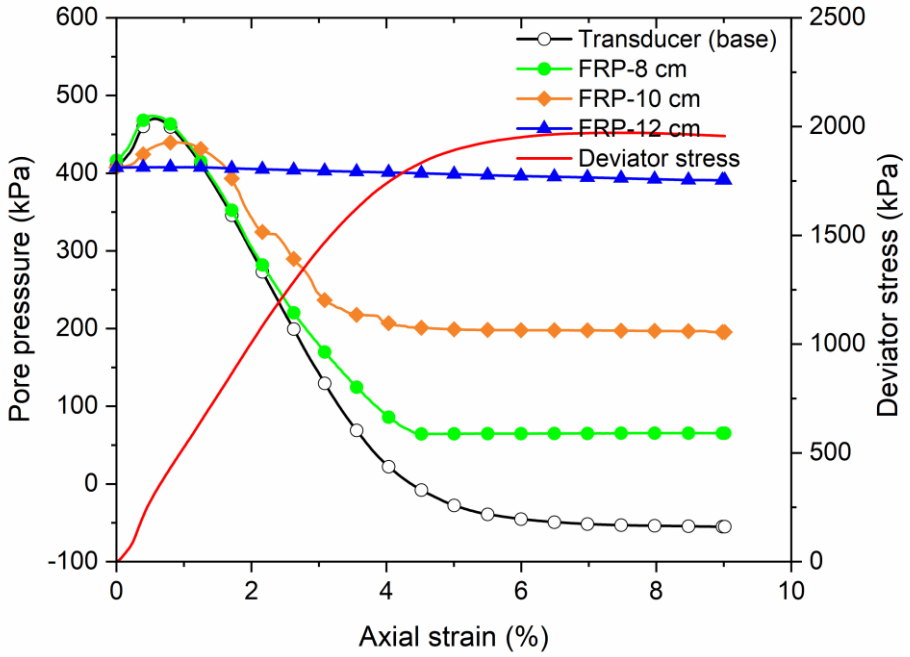
Transducer (base)
FRP-8 cm
FRP-10 cm
FRP-12 cm
Deviator stress
Pore pressure (kPa)
Deviator stress (kPa)
Axial strain (%)
600
500
400
300
200
100
0
-100
2500
2000
1500
1000
500
0
0
2
4
6
8
10

(b)

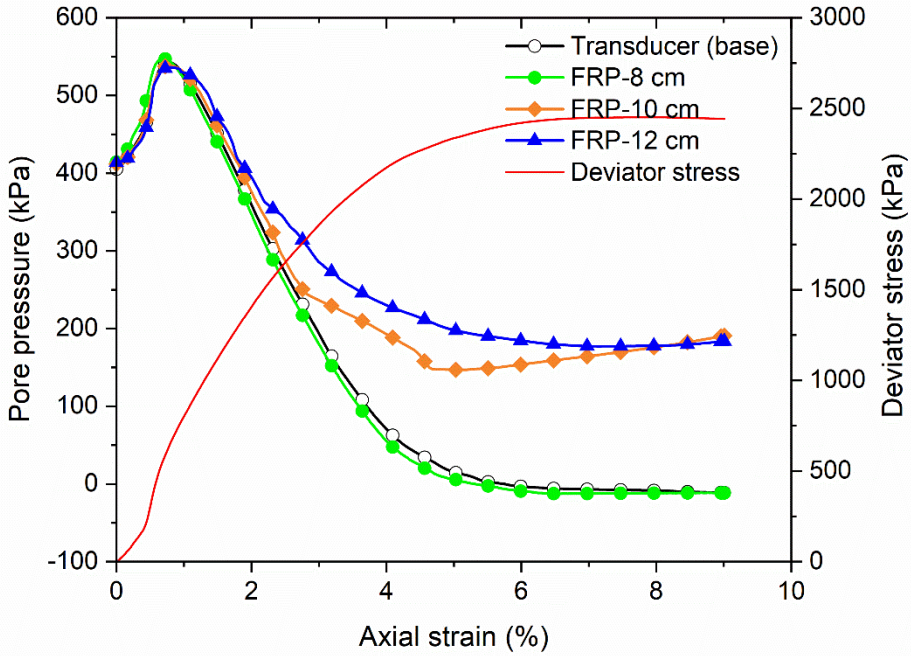
Transducer (base)
FRP-8 cm
FRP-10 cm
FRP-12 cm
Deviator stress
Pore pressure (kPa)
Deviator stress (kPa)
Axial strain (%)
600
500
400
300
200
100
0
-100
3000
2500
2000
1500
1000
500
0
0
2
4
6
8
10

(c)

FIG 3-8 PWP measurements in partially frozen dense samples. (a) PD-1, (b) PD-2, (c) PD-3

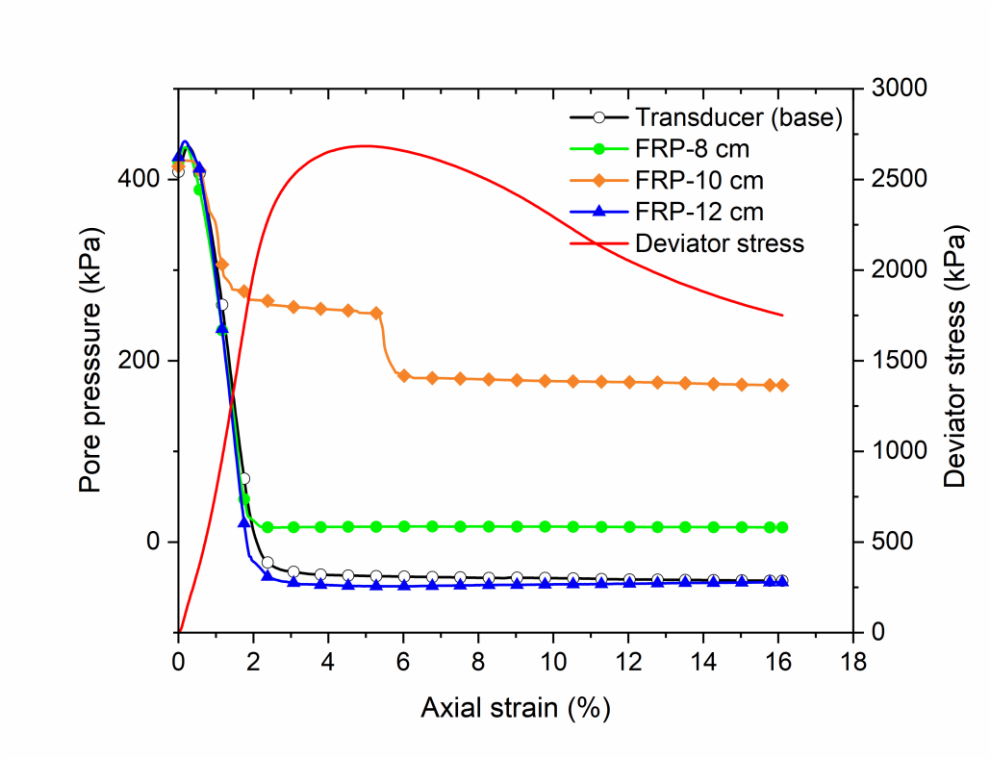

(a)

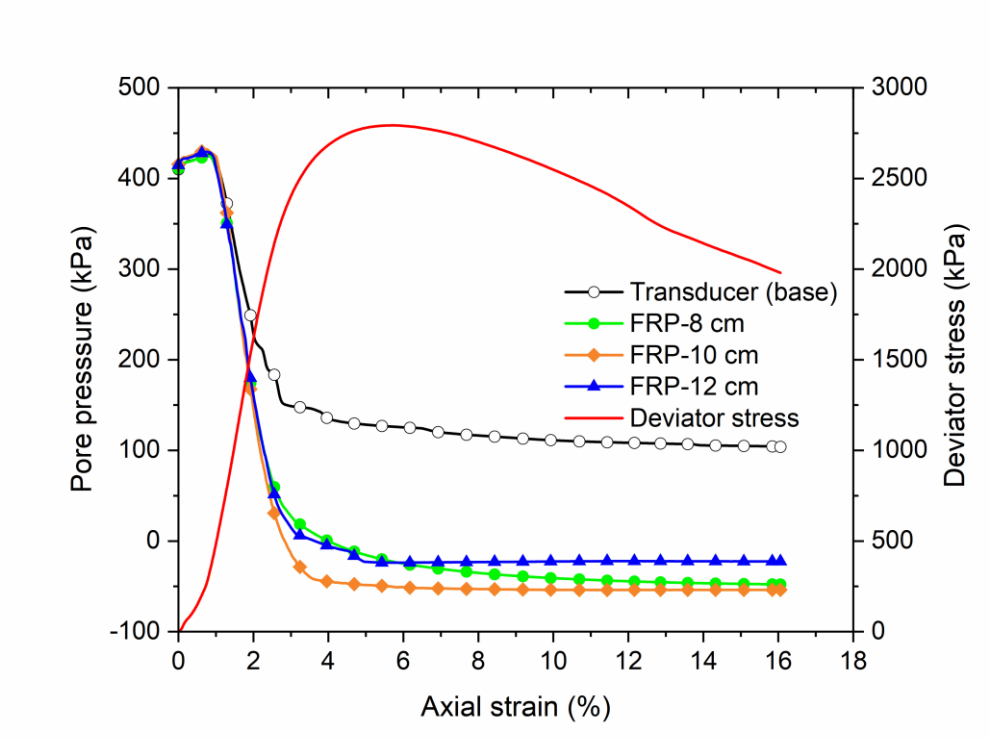

(b)

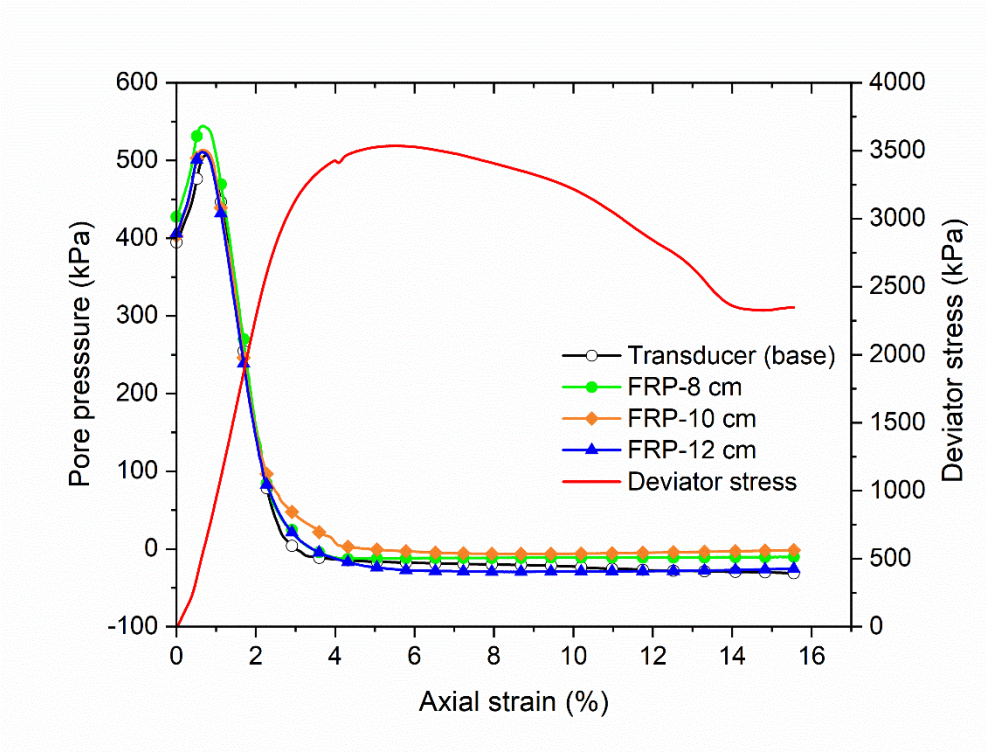

(c)

FIG 3-9 Images of samples after test. (a) PL-1, (b) PD-1

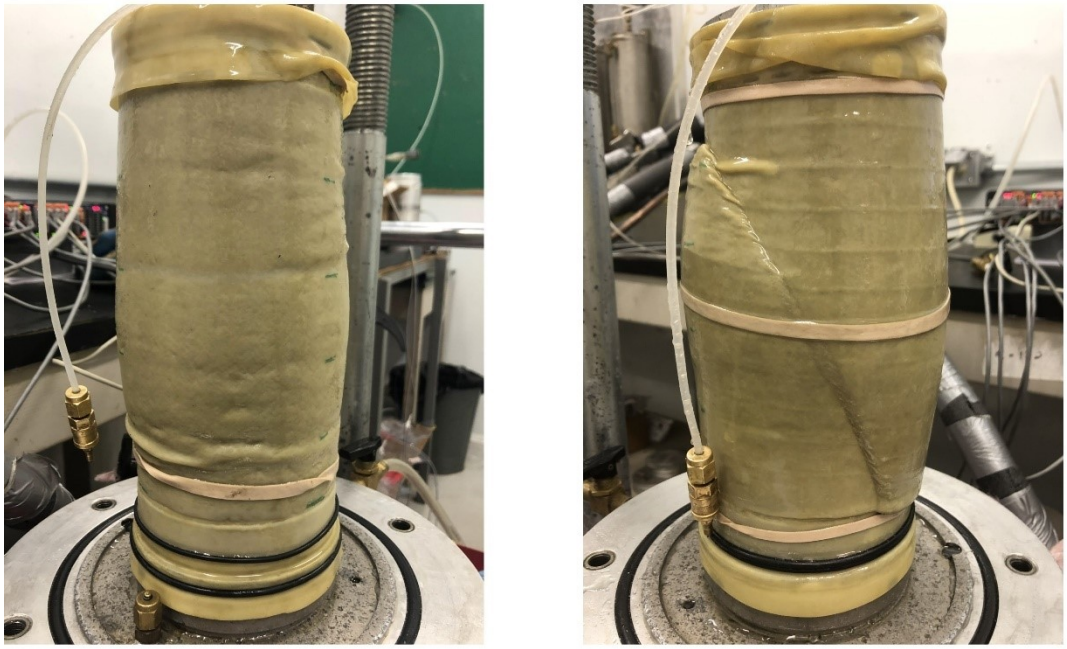

(a) (b)

3.8 References

Anderson, D.M., and Morgenstern, N.R. 1973. Physics, chemistry, and mechanics of frozen ground : a review. In 2nd International Conference on Permafrost. National Academy of Science, Washington, D.C., Yakutsk, USSR. pp. 257-288.

Arenson, L.U., and Springman, S.M. 2005. Triaxial constant stress and constant strain rate testson ice-rich permafrost samples. Canadian Geotechnical Journal, 42(2): 412-430.

Arenson, L.U., and Sego, D.C. 2006. The effect of salinity on the freezing of coarse-grained sands. Canadian Geotechnical Journal, 43(3): 325-337.

Barden, L. 1965. Consolidation of compacted and unsaturated clays. Géotechnique, 15(3): 267-286.

Eigenbrod, K.D., Knutsson, S., and Sheng, D. 1996. Pore-Water Pressures in Freezing and Thawing Fine-Grained Soils. Journal of Cold Regions Engineering, 10(2): 77-92.

Harris, C., and Davies, M.C.R.1998. Pressures recorded during laboratory freezing and thawing of a natural silt-rich soil. In Seventh International Conference on Permafrost, Yellowknife, NWT, Canada, pp. 23-27.

Hivon, E., and Sego, D. 1993. Distribution of saline permafrost in the Northwest Territories, Canada. Canadian Geotechnical Journal, 30(3): 506-514.

Hivon, E., and Sego, D. 1995. Strength of frozen saline soils. Canadian Geotechnical Journal, 32(2): 336-354.

Kia, M. 2012. Measuring Pore-water Pressure in Partially Frozen Soils. Ph.D. thesis, Faculty of Graduate Studies and Research, University of Alberta, Edmonton, AB.

Konrad, J.M. 1989. Pore water pressure at an ice lens: Its measurement and interpretation. ColdRegions Science and Technology, 16(1): 63-74.

Ladanyi, B., and Morel, J.-F. 1990. Effect of internal confinement on compression strength of frozen sand. Canadian Geotechnical Journal, 27(1): 8-18.

Lian-hai, Z., Wei, M.A., and Cheng-song, Y. 2015. Pore water pressure measurement for soil subjected to freeze-thaw cycles. Rock and Soil Mechanics, 36(7): 1856-1864.

Liang Y, Beier N, and Sego DC. 2022. New method for internal pore-water pressure

measurements. Geotechnical Testing Journal, 45(2): 490-502.

Lyu, C., Grimstad, G., and Nishimura, S. 2021a. Pore pressure coefficient in frozen soils (Published online). Géotechnique: 1-10.

Lyu, C., Nishimura, S., Amiri, S.A.G., Zhu, F., Eiksund, G.R., and Grimstad, G. 2021b. Pore-water pressure development in a frozen saline clay under isotropic loading and undrained shearing. Acta Geotechnica, 16(12): 3831-3847.

Penner, E. 1959. Pressures developed in a porous granular system as a result of ice segregation.Highway Research Board Special Report, (40): 191-199.

Sheeran, D.E., and Yong, R.N. 1975. Water and salt distribution in freezing soils. Proceedings, 1st Conference on Soil-Water Problems in Cold Regions, Calgary, Alta. pp. 58-69

Tsarapov, M. 2007. Use of pore pressure to determine strength characteristics of thawing soils. Soil Mechanics and Foundation Engineering, 44(4): 132-136.

Williams, P.J. 1966. Pore Pressures at a Penetrating Frost line and their prediction. Géotechnique,16(3): 187-208.

Zhang, L., Ma, W., Yang, C., and Yuan, C. 2014. Investigation of the pore water pressures of coarse-grained sandy soil during open-system step-freezing and thawing tests. Engineering Geology, 181: 233-248.

4. Strength of Partially Frozen Sand Under Triaxial Compression

Abstract: To investigate the effect of the pore matrix (i.e., ice and unfrozen water) on the strength of partially frozen sand, a series of consolidated undrained triaxial tests with internal pore water pressure measurements were performed. Both dense and loose saline sand samples were prepared by rapidly freezing the samples and then slowly warming the samples to, and subsequently shearing at the temperature of -3 °C. Test results indicate the temperature only affects the effective cohesion, not the effective friction angle of sand. The pore ice stress was estimated using Ladanyi and Morel's (1990) postulate on the internal stresses within frozen soil; the stress (hydrostatic) change in pore ice was reflected by an equal change in pore water pressure in the partially frozen loose sand. Based on Ladanyi and Morel's (1990) concept of internal confinement in frozen sand, a Mohr–Coulomb model that uses effective failure and residual friction angles from unfrozen sand to estimate the strength of partially frozen sand is presented. The proposed model reflects how the pore matrix contributes to the strength of partially frozen sand. For loose sand, the peak strength is enhanced by the internal confinement and cohesion resulting from the pore water (suction) and pore ice, respectively. For dense sand, only pore ice affects the peak strength by incorporating the internal confinement and cohesion.

Keywords: pore matrix (ice and unfrozen water), partially frozen soil, shear strength, effective stress, pore ice stress

4.1 Introduction

Climate change is a major challenge facing coastal and northern communities in Canada's North. A growing body of reports provides evidence that well-functioning infrastructure in permafrost regions are starting to fail due to the thawing of permafrost, and the current engineering designs utilized in cold permafrost regions are less robust in warm permafrost regions, where the soil is at a partially frozen state due to the coexistence of unfrozen water and ice in the pores (Holubec 2008; Laxton and Coates 2010; Allard et al. 2012; Swanson et al. 2021). The maintenance of aging infrastructure in warm permafrost regions and designs for new soil structures to withstand climate change require a better understanding of the mechanical properties of these partially frozen soils. Therefore, investigating the effect of internal stresses resulting from unfrozen water and adjacent pore ice on the strength of partially frozen soil is essential.

To study the strength of partially frozen sand, it is necessary to briefly review the mechanisms that contribute to the strength of frozen sand. Frozen sand consists of four different constituents: solid mineral grains, ice, unfrozen water, and air. At cold temperatures (below -5 ℃), the majority of non-saline pore exists as ice, and the saturated frozen sand can be simplified as only sand and ice. Based on the extensive literature and experimental data, Ting et al. (1983) concluded the mechanics of saturated frozen sand is mainly controlled by the following four physical mechanisms: (1) ice strength; (2) soil strength, including frictional component, dilatancy effects, and particle interference; (3) mechanical interactions between the ice and soil through dilatancy hardening; and (4) structural hindrance. Although the main sources of

strength for frozen sand are clear, the inability to directly measure the value of individual components under loading makes it impossible to assess their respective contributions (Ladanyi and Morel 1990).

In coarse-graded frozen soil, a significant adhesion strength exists between the ice and soil skeleton as the ice crystals are considered to have directly grown from the solid particles (Sheeran and Yong 1975; Ting et al. 1983). Since ice can sustain both hydrostatic and deviator stresses, the mechanical behavior of frozen soil is strongly affected by the pore ice. For loose or ice-rich samples in which the volume concentration of sand is less than about 42 %, the mechanical behavior and measured strength were similar to polycrystalline ice because the solid particles are barely in contact (Goughnour and Andersiand 1968). The behavior of polycrystalline ice is greatly dependent on the strain rate: it shows a ductile response at lower strain rates but transitions into a brittle material as strain rate increases (Mellor 1979). This transition marked by strain rate and overall ice strength is governed by stress state, temperature, and grain-size (Kalifa et al. 1992). When the sand becomes denser, structural hindrance and dilatancy hardening come into effect. To evaluate the effect of internal confinement generated in the pore ice due to dilatancy hardening on the overall strength of the frozen dense sand, Ladanyi and Morel (1990) proposed the following equation:

[4-1] $q_{FS} = (\sigma_{3cell} + T_i)\left(K'_p - 1\right) + q_i$

Where

q_{FS} is the peak strength of frozen sand;

σ_{3cell} is the cell pressure;

T_i is the tension stress provided by pore ice due to dilatancy hardening;

K'_p is the passive earth pressure coefficient and is calculated as follows

[4-2] $K'_p = \tan^2(45 + \emptyset'/2)$ where $\emptyset'$ is the effective friction angle; and

q_i is the shear strength of polycrystalline ice.

The effective friction angle can be determined from unfrozen, dense samples under drained or undrained conditions, as the pore ice does not affect the friction angle of frozen sand (Alkire and Andersland 1973; Sayles 1974).

However, it is difficult to accurately assess the tension and shear strength of pore ice without knowing the stress state within the pores and directly measuring the value of pore ice stress. Consequently, identifying the strength contributed by soil grains is also unrealistic because the ice strength and related effects (hindrance and dilatancy) cannot be distinguished from the stress carried by the soil skeleton. For this reason, Ladanyi and Morel (1990) assumed that the soil skeleton would carry the same amount of stress in both frozen and unfrozen states when the frozen and unfrozen sand specimens share the same strain history.

For partially frozen sand, unfrozen water would be another major factor influencing the mechanical properties of soil, if the temperature is not cold enough for ice to fill most of the pore space. The strength of frozen soil will decrease as the unfrozen water content increases with warming temperatures and salinity (Ogata et al. 1983; Stuckert and Mahar 1984; Pharr and Merwin 1985; Hivon and Sego 1995; Xu et al. 2017). On the other hand, when there is sufficient unfrozen water to form a continuous water phase within partially frozen soil, measuring pore-water pressure (PWP) and establishing the internal effective stress and its

impact on the mechanical behavior become necessary. However, limited research on this issue has been reported. Recently, Arenson and Springman (2005) measured PWP in ice-rich samples in triaxial tests; Lyu et al. (2021) investigated the PWP response in frozen saline clay under consolidated, undrained triaxial test (CIU) at different temperatures and strain rates. However, continuity in the internal water phase was not established by Arenson and Springman (2005) nor by Lyu et al. (2021), which is a prerequisite to obtain true PWP throughout the entire sample. Kia (2012) confirmed continuity in the internal water phase and then measured PWP using five filter-less rigid piezometers (FRPs) within the partially frozen sand; however, these tests were restricted to one-dimension with no lateral yield loading conditions.

This chapter reports a series of CIU triaxial tests on dense and loose sand with 30 ppt (30 g/L) pore fluid salinity. The specimens were prepared by rapidly freezing and then slowly warming them to, and subsequently shearing them at, -3 ^{o}C. The objective of this research is to establish effective stress within partially frozen sand and to investigate the individual effect of each component of the pore matrix (ice and unfrozen water) on the overall strength of partially frozen sand. With the continuity of PWP measurements, the effective stress path was established within the partially frozen samples. Based on Ladanyi and Morel's (1990) concept of internal confinement within frozen sand, a simple model for estimating the strength of partially frozen sand is presented. Also, the relationship between PWP and pore ice pressure and the mechanisms that control the strength of partially frozen sand are discussed.

4.2 Material and methods

4.2.1 Material

The tests were carried out using specimens 100 mm in diameter and 196 mm high comprised of a uniformly graded fine sand with a salinity of 30 ppt. This sample material is the same material as used in Chapter 3. The average volumetric unfrozen water content is estimated to be 24 % and 20 % in loose and dense specimens, respectively, at -3 ^{o}C, based on the monitored pore volume change during the tests. The tested loose and dense specimens have higher initial water contents and void ratios than 'Soil A' reported by Hivon and Sego (1995), so it is reasonable to have higher volumetric unfrozen water contents than Soil A at the same temperature.

4.2.2 Test apparatus

A new triaxial apparatus was developed by Liang et al. (2022b) to measure internal PWP within the soil while maintaining the thermal boundary conditions involved in a partially frozen test (Fig. 4-1). Further details regarding the apparatus can be found in Chapters 2 and 3.

4.2.3 Test procedures

The whole testing program included three unfrozen, dense and three unfrozen, loose specimens; five partially frozen, loose specimens; and three partially frozen, dense specimens (Table 4-1). In this paper, the terms D, L, PL, and PD refer to unfrozen dense, unfrozen loose, partially frozen loose and partially frozen dense specimens, respectively. Loose and dense specimens

were reconstituted by moist tamping and slurry deposition methods, respectively. Then the specimens were saturated and consolidated to the targeted effective stress using the procedures described by Liang et al. (2022a). Unfrozen tests were performed at room temperature (23 ºC). After consolidation, specimens were sheared under undrained conditions at the strain rate of 1 % per minute to determine the effective friction angle at failure.

The triaxial apparatus was placed in a cold room with the temperature set to approximately 2 ºC to carry out partially frozen tests. To provide enhanced temperature control, fiberglass insulation surrounded the cell, and a foam board insulated box encompassed the cell. Partially frozen samples were prepared in five stages following consolidation as described by Liang et al. (2022b). First, the specimen was frozen unidirectionally by circulating liquid nitrogen through the base cooling plate for about 7 h, followed by a circulation of the water-glycol mixture (-25 ºC) from the cold bath for 12 h, with free drainage at the top (back pressure line).

Then, the specimen was maintained around -11 ºC, using a cold bath (A) set at -11 ºC connected to the spiral copper coil and another cold bath (B) set at -15 ºC attached to the base cooling plate.

Next, the temperature of cold bath (A) was set to -3 ºC and maintained for approximately 36 h to 42 h to warm the specimen uniformly to -3 ºC and to stabilize the constant internal temperature. The top drainage line became frozen in the last stage, so the drainage line was switched to the bottom. Cold bath (B) was first raised to 1 ºC for several hours until the drainage line thawed, and then the bath was lowered to -2.5 ºC to keep the drainage line thawed and to

minimize the temperature gradient within the specimen. For these stages, the back pressure (400 kPa) and cell pressure remained constant following consolidation.

Continuity in the water phase was confirmed by increasing the back pressure independent of the applied cell pressure and by measuring the corresponding increase in pore pressure measured by the base transducer and the internal FRPs (Kia 2012). Finally, the specimen was sheared at a constant strain rate (1 %/min or 0.1 %/min) at a constant test temperature.

4.3 Results

4.3.1 Stress and PWP response of partially frozen samples

The stress and PWP responses of partially frozen, loose and dense sand are shown in Figure 4-2. There were some erratic measurements in the PWP associated with a blockage of the measuring tube during the tests, so only validated continuity of PWP measurements as reported by Liang et al. (2022b) were plotted for analysis. The behavior of the partially frozen, loose sand was ductile, and the peak strengths were similar to that of saline ice as reported by Melton and Schulson (1997). A continuous decrease of the PWP as exhibited in the partially frozen, loose sand indicated that dilatancy occurred within pore spaces. Since no shear plane was observed after failure, this shear-induced dilation was more likely caused by pore ice (Liang et al. 2022b). The stress and PWP curves of the partially frozen, loose samples at the lower strain rate (0.1 %/min), exhibited an apparent hysteresis and terminated at a lower stress and suction compared to the samples tested at a higher strain rate (1 %/min).

In contrast, the partially frozen, dense samples showed the same dilative response as the unfrozen, dense samples. In addition, an apparent shear plane presented in both the partially frozen and unfrozen states, suggesting that the behavior of the partially frozen, dense sand was still mainly controlled by the particles making up the soil skeleton and not the included pore ice.

4.3.2 Effective stress path of partially frozen samples

According to the definition, the effective stress is the difference between total stress and PWP, and it controls the deformation and strength of soil. In partially frozen soil, the ice-soil system is treated as a solid phase (Blanchard and Fremond 1985; Ghoreishian Amiri et al. 2016). With continuity of PWP measurements, the effective stress paths of partially frozen samples are plotted in Figure 4-3. The effective stress paths of the partially frozen, loose samples converged independent of confining pressures but showed different slopes for the different strain rates (Fig. 4-3a), which reflects the strain rate-dependency of pore ice. Despite a clear distinction in the range of pre- and post-peak stress, the effective stress paths of the partially frozen, loose and dense samples were very close during the initial stage (Fig. 4-3b), possibly because the initial behavior of the partially frozen, dense samples was also primarily dependent on the cementing of the pore ice. It is worth noting that both sets of effective stress paths converged on the same ultimate line, indicating they had the same large strain structure after failure. A comparison of the effective stress paths between the partially frozen, loose samples and the unfrozen, dense samples is also presented (Fig. 4-4). These two sets of effective stress paths

were nearly identical before the peak stress was reached at the same confining pressure. This indicates the pore ice in contact with the soil grain assembles the sample into a denser state behavior, similar to the unfrozen, dense sand.

4.3.3 Pore ice stress

As mentioned before, it is difficult to separately quantify the ice strength and related effects (hindrance and dilatancy) on the overall behavior, so the stress caused by pore ice is referred to as pore ice stress (PIS) in this paper. Whether the ice phase is continuous remains unknown; using this simple term, PIS may provide guidance to quantify the overall effect of pore ice. According to Ladanyi and Morel's (1990) postulate that the soil skeleton carries the same amount of stress in both frozen and unfrozen states when the frozen and unfrozen sand specimens share the same strain history, the stress tensor of pore ice is equal to the difference between the effective stress tensor of the partially frozen soil and unfrozen soil with the same initial void ratio. Then the deviator stress (q_i), mean stress (p_i), and minor principal stress ($\sigma_{3(i)}$) of pore ice can be expressed as

[4-3] $q_i = q_{pf} - q_{uf}$

[4-4] $p_i = p'_{pf} - p'_{uf}$

[4-5] $\sigma_{3(i)} = \sigma'_{3(pf)} - \sigma'_{3(uf)}$

Where the subscripts "pf" and "uf" denote the partially frozen state and unfrozen state at the same axial strain, respectively.

In this way, the stresses (q_i and $\sigma_{3(i)}$) and stress paths of pore ice for both the partially frozen, loose and dense samples are shown in Figs. 4-5 and 4-6, respectively. The deviator stress and stress path of the pore ice in the partially frozen, loose sand (Figs. 4-5a and 4-5c) exhibited approximately the same response as those of the ice-soil system (Figs. 4-2a and 4-3a), which implied that the behavior of the partially frozen, loose sand was mainly controlled by pore ice. The strain rate-dependency of the pore ice was also presented in these graphs. This behavior supports the effectiveness of determining PIS using Ladanyi and Morel's (1990) postulate in partially frozen, loose sand. The minor principal stress of the pore ice continuously increased until close to or slightly above the confining pressure, in the same manner as excess PWP development in unfrozen, loose samples (Fig. 4-5b), suggesting that the confining pressure applied on the sample was gradually taken by the pore ice. This also indicated that the pore ice was under a combination of compression and shear stresses in the loose sample. The negative deviator stress of pore ice at strains less than 0.75% was due to the incompatibility among the loading ram, loading platen, and sample at the beginning of the test, resulting in a nonuniform initial strain field.

In partially frozen, dense sand, the curve for the deviator stress of the pore ice was characterized by an initial linear region (up to 2 % of strain), followed by a relative constant region (until around 9 % strain) and a strain softening region, before a short upward slope, with the peak stress ranging from 730 kPa to 1100 kPa in three samples (Fig. 4-6a). The stress paths of the pore ice of all three samples showed the same response at the beginning and converged at the end of the test around 400 kPa, despite pulling back at different points (Fig. 4-6c). The minor

principal stress of the pore ice first increased up to 2 % of strain but then decreased sharply to a negative value (Fig. 4-6b). This means the tensile stress generated in the pore ice is similar to the suction measured from the pore water due to shear-induced dilation of the soil skeleton. Thus, the pore ice is under a combination of tensile and shear stresses after this initial failure in the dense sample.

4.3.4 Strength of partially frozen samples

The strengths of unfrozen sand and partially frozen sand are summarized in Figure 4-7. The peak strength is defined at the maximum deviator stress sustained by the sample, while the residual strength is determined at large strain at the end of the test. The peak and residual strengths of partially frozen, loose sand are close, so only the peak strength is used for comparison.

It can be observed that unfrozen and partially frozen, dense samples have similar slopes but different interceptions of failure lines (peak strength). Similarly, the failure line of partially frozen, loose samples has a similar slope to the ultimate line (residual strength) of unfrozen samples (dense and loose). This is because the strength of partially frozen, loose samples is predominated by the pore ice, and the soil skeleton is already at the residual state when the peak strength of sample is reached. In other words, the soil skeleton and pore ice do not simultaneously reach the peak state. For instance, the soil skeleton reaches the peak state at the very early stage, around 1 % of strain in the unfrozen test. Therefore, the temperature (or pore ice) only affects the effective cohesion, instead of the effective friction angle of partially frozen

sand, similar to what is found in frozen sand (Alkire and Andersland 1973; Xu et al. 2016; Xu et al. 2017). The stress of partially frozen, dense samples decreases slightly at the end of the tests, so the selected points may not accurately represent the residual strength, leading to the difference in the slope of ultimate line between the unfrozen and partially frozen, dense samples. Additionally, the residual strength of partially frozen, dense sand is approximately equal to the peak strength of partially frozen, loose sand under the same confining pressure. Peak strengths of the partially frozen, loose samples at the lower strain rate are on the ultimate line of the unfrozen samples, suggesting that the effect of the ice matrix decays and creates additional contacts between soil grains (Sayles 1974). Further, this provides insight to estimate the strength of a partially frozen soil based on the mechanical properties of an unfrozen soil.

4.3.5 Proposed model and verification

According to Ladanyi and Morel's (1990) concept of internal confinement in frozen sand and the experimental results above, a model is proposed for the peak strength of partially frozen sand based on the following assumptions.

(1) In a partially frozen, loose sand, the internal confinement resulting from tension or suction is solely generated via the pore water due to the dilation of pore ice as it is sheared.

(2) In a partially frozen, dense sand, the tension or suction caused by the dilation of the soil skeleton is generated and shared by the pore water and pore ice, but only the tensile stress sustained by the pore ice is considered as an additional internal confinement of the sand skeleton and is equal to the measured suction in the pore water at failure.

As mentioned in the foregoing, the effective failure angle of partially frozen, loose sand is similar to the effective residual angle of unfrozen samples; thus, the peak strength of partially frozen, loose sand at a strain rate of 1 %/min will be

[4-6] $\mathrm{q_{PLS}} = (\sigma_{3\mathrm{cell}} + T_{\mathrm{w}})\tan\beta' + c_L$

where

$\mathrm{q_{PLS}}$ is the peak strength of partially frozen, loose sand;

$\sigma_{3\mathrm{cell}}$ is the cell pressure;

$\mathrm{T_w}$ is the measured suction of the pore water;

β' is the angle of the ultimate line or the effective residual angle of unfrozen sand; and

c_{L} is the cohesion caused by pore ice, which is a function of temperature and strain rate and is determined from partially frozen, loose sand at peak strength or from partially frozen, dense sand at residual strength.

The residual strength of partially frozen, dense sand can also be predicted using Eq. 4-6, because it has almost the same value as the peak strength of the partially frozen, loose sand.

At or less than the 0.1 %/min strain rate, ice cohesion decreases due to creep, and c_{L} will approach zero; therefore, the peak strength of partially frozen, loose sand at a lower strain rate becomes

[4-7] $q_{PLS(low)} = (\sigma_{3cell} + T_w)\tan\beta'$

where

$q_{PLS(low)}$ is the peak strength of partially frozen, loose sand at a lower strain rate;

In the same way, the peak strength of partially frozen, dense sand is given by

[4-8] $q_{PDS} = (\sigma_{3cell} + T_i)\tan\alpha' + c_D$

where

q_{PDS} is the peak strength of partially frozen, dense sand;

T_i is the tensile stress of pore ice, which is equal to the measured suction of pore water;

α' is the angle of the failure line or the effective failure angle of unfrozen, dense sand; and

c_D is also the cohesion caused by pore ice but determined from partially frozen, dense sand at peak stress.

For this set of experimental data, the effective friction angle α', β', and cohesion (c_L, c_D) are 72.5°, 67.7° and 447 kPa and 855 kPa, respectively, at -3 °C (Fig. 4-7). Note that the values of c_D and c_L are related to the deviator stresses of the pore ice (Fig. 4-6a) at about 5 % and 14 % strain, which will be discussed later. The PWP at peak and residual strength is presented in Table 4-2. According to Figure 4-8, the proposed model reflects the measured strength of partially frozen sand. Therefore, the strength of partially frozen sand can be expressed using

the Mohr–Coulomb criterion, provided effective failure and residual angles are determined from unfrozen sand. Irrespective of the difference in PWP at peak or residual strength, conducting testing on a partially frozen, loose or dense sample along with PWP measurements allows an estimate of the cohesion associated with the pore ice and a prediction of strengths for other samples at different confining pressures.

The model could explain how the PWP (suction) affects the strength of partially frozen, loose sand by increasing the confining pressure, while the pore ice influences the effective cohesion at higher strain rates. It also shows how the pore ice affects the peak strength of partially frozen, dense sand by adding an internal confining pressure and contributing to the effective cohesion. Although the model is verified, it is limited to the current testing conditions, such as the temperature, stress level, and salinity. Further investigations are required to examine the model under other situations.

4.4 Discussion

4.4.1 Relationship between PWP and PIS ($\sigma_{3(i)}$)

When the sample is not under strain and load, the pore ice pressure is higher than PWP, and their difference remains constant under isothermal conditions, according to the Clausius–Clapeyron equation (Black 1995; Nishimura et al. 2009; Nishimura and Wang 2019). Whether it is also a fact under undrained shear conditions is unknown at present. Since the pore water cannot sustain the shear stress, only hydrostatic pressure $\sigma_{3(i)}$ and PWP are compared in Figs. 4-9 and 4-10.

In partially frozen, loose sand, the $\sigma_{3(i)}$ and PWP show opposite trends (Fig. 4-9a). At the beginning of the test, 400 kPa (back pressure) out of a total 500 kPa of confining pressure was carried by pore water, while the pore ice did not contribute to the confining pressure. As the test continued, the pore space as well as the pore ice contracted; therefore, the pore ice gradually carried more confining pressure. On the other hand, the pore ice also was subjected to shear stress; hence, the cracking and breaking of the pore ice occurred, resulting in the expansion of pore volume and decrease in PWP (Arenson and Springman 2005). By the end of the test, the applied confining pressure was completely taken by pore ice and transferred to the soil skeleton, which prevented the collapse of the sample. Clearly the difference of $\sigma_{3(i)}$ and PWP varied during the test until the post-peak region. The results depicted in Fig. 4-9b revealed that the stress change in the pore ice was reflected by an equal change in the pore water, as the ratio was around -1 after the initial disturbance. This also experimentally proves Ladanyi and Morel's (1990) postulate about internal stress distribution within a partially frozen soil.

In contrast, the $\sigma_{3(i)}$ of partially frozen, dense sand initially increased to 200 kPa at around 2 % strain and then decreased to almost the same negative value as the PWP (Fig. 4-10a). This was because the applied confining pressure increasingly acted on the soil skeleton in which the shear-induced dilation triggered tensile stress in the pore matrix. At the initial portion (0~2 %), only the pore water responded to the dilatancy effect, so the PWP decreased rapidly. In addition, the summation of $\sigma_{3(i)}$ and PWP at or after failure was close to that of the PWP measured in the unfrozen sample. Thus, this supports the assumption that the tension caused by the dilation of the soil skeleton is shared between the pore ice and pore water. In other words, the pore ice

and pore water of a partially frozen, dense sand are in a collaborative and not a competitive relationship found in a partially frozen, loose sand. Similar to the loose sample, the difference of $\sigma_{3(i)}$ and PWP varied until failure. However, the stress change in the pore ice was not reflected by an equal change in pore water, and the ratio was not constant (Fig. 4-10b). Thus Ladanyi and Morel's (1990) postulate that a stress change in one phase is reflected by an equal change in the other phase within the pore does not apply in partially frozen, dense sand.

4.4.2 Stress distribution and mechanism

To assist in understanding the influence of each soil phase on the measured strength, the stress distribution of the partially frozen, dense and loose samples at an effective confining pressure of 100 kPa are shown in Figs. 4-11 and 4-12. Compared with the soil skeleton, the pore ice has nearly total control over the behavior and strength of the loose sample (Fig. 4-11). The tested sample (PL-1) is characterized by 54 % volumetric sand contents, 23 % volumetric pore ice contents and 23 % volumetric pore water contents, irrespective of pressure melting and phase change at the current stress level. Since the sand concentration is over 40 % but less than 60 %, the structural hindrance between the pore ice and soil skeleton should also impact the measured strength (Goughnour and Andersiand 1968; Ting et al. 1983). Recall, the stress in the pore ice represents overall effects caused by the pore ice, so the deviator stress curve of the pore ice plotted here includes both ice strength and contribution from structural hindrance. The curve of the soil skeleton is taken from the unfrozen sample and refers to the strength of the soil skeleton only. More specifically, from Eq.4-6, the ice cohesion (c_L) represents the ice strength,

and the summation of the cell pressure and measured suction of the pore water ($\sigma_{3\text{cell}} + T_{\text{w}}$) indicates the total effective confining pressure acting on the soil skeleton through interactions between the ice and soil (structural hindrance), including the applied confining pressure and an internal confinement caused by dilation of the pore ice. It is concluded that there are four mechanisms involved in partially frozen, loose sand: (1) pore ice strength; (2) soil strength; (3) dilatancy of the pore ice; and (4) structural hindrance.

In partially frozen, dense sand, the stress distribution throughout the test can be divided into three regions. The response of the sand-ice system due to pore ice in region 1, and then to that of the soil skeleton in following regions 2 and 3 (Fig. 4-12), suggesting that the initial behavior of soil is mainly controlled by the pore ice, but thereafter, the behavior is governed by the soil skeleton. This is consistent with frozen, dense sand in which the ice matrix mainly controls the early elastic region and later the internal friction and dilatancy dominate the soil strength (Bragg and Andersland 1980; Parameswaran and Jones 1981; Bourbonnais and Ladanyi 1985; Sayles 1989; Andersen et al. 1995). The peak stress of the pore ice at around 2 % of strain corresponding to the maximum confining stress of pore ice (Fig. 4-10a) likely indicates the initial cracking of the ice matrix. After that, the deviator stress of the pore ice slowly decreases until 10 % of strain where the transverse shear band forms in the sample. So, the continuous reduction of stress carried by the pore ice in region 3 is due to additional cracking and breaking in the ice matrix associated with shear movement inside the shear band. The deviator stress of the pore ice at the peak strength of the soil (about 5 % strain) and at the end of the test represent the cohesive components, c_{D} and c_{L}, in Eqs. 4-8 and 4-6, respectively. Similar to the loose

sample, $(\sigma_{3cell} + T_i)$ is also the total effective confining pressure acting on the soil skeleton, but tensile stress (T_i) results from the dilation of the soil skeleton and is added on the soil skeleton via the structural hindrance. Therefore, pore ice strength, soil strength, dilatancy of soil skeleton, and structural hindrance are the four mechanisms contributing to the strength of partially frozen, dense sand.

4.5 Conclusion

This paper presents the results of a series of CIU triaxial tests on loose and dense sand at -3 ºC and 23 ºC to conduct effective stress approach within partially frozen sand and to investigate the effect of the pore matrix (unfrozen water and ice) on the strength of partially frozen sand. Using Ladanyi and Morel's (1990) postulate on the unique relationship between the stress and strain of the soil skeleton, the stress distribution between the soil skeleton, pore ice, and pore water in partially frozen sand were evaluated. In addition a modified model for estimating the strength of partially frozen sand was proposed and validated based on the concept of internal confinement within the frozen sand (Ladanyi and Morel 1990). The following main conclusions can be drawn from this study:

(1) The behavior of partially frozen, loose and dense sand is mainly controlled by the pore ice and soil skeleton, respectively. The strength of partially frozen sand is a function of the cohesion of the pore ice and the friction angle of the sand grains. This ice cohesion is temperature and strain rate dependent. With lowering the strain rate, the ice cohesion will decrease via creep in the ice, and the strength of partially frozen sand is eventually governed

by the friction angle of the sand grains determined from an unfrozen state.

(2) The pore ice is subjected to different stress states in partially frozen, loose and dense sand under undrained shear conditions: a combination of compressive and shear stress in the loose sample but a combined tensile and shear stress in the dense sample (after 2 % of strain). The stress (hydrostatic) change in the pore ice is reflected by an equal change in the pore water in the partially frozen, loose sand.

(3) The proposed model provides a bridge between unfrozen and partially frozen sand in a form of the Mohr–Coulomb criterion. For partially frozen, dense sand, the peak stress is strengthened by the internal confinement and cohesion contributed by the pore ice. However, the internal confinement that enhances the strength of partially frozen, loose sand is generated from pore water suction.

(4) In addition to pore ice strength, soil strength, and structural hindrance, the dilatancy of the pore ice and the dilatancy of the soil skeleton also contribute to the mechanics of partially frozen, loose and dense sand, respectively.

4.6 Tables

Table 4-1 Summary of the testing program

Test ID	Initial Void Ratio	Stain Rate (%/min)	Confining Pressure (kPa)	T (°C)
D-1	0.599	1	100	23
D-2	0.599	1	200	23
D-3	0.597	1	400	23
L-1	0.834	1	100	23
L-2	0.834	1	200	23
L-3	0.832	1	400	23
PL-1	0.835	1	100	-3
PL-2	0.834	1	200	-3
PL-3	0.835	1	400	-3
PL-4	0.834	0.1	100	-3
PL-5	0.835	0.1	400	-3
PD-1	0.596	1	100	-3
PD-2	0.599	1	200	-3
PD-3	0.594	1	400	-3

Note: D, unfrozen dense; L, unfrozen loose; PL, partially frozen loose; PD, partially frozen dense.

Table 4-2 Summary of the measured and predicted strengths

Test ID	PWP at Peak Strength (kPa)	Measured Peak Strength (kPa)	Predicted Peak Strength (kPa)	PWP at Residual Strength (kPa)	Measured Residual Strength (kPa)	Predicted Residual Strength (kPa)
PL-1	-8	1735	1734	-	-	-
PL-2	-53	1970	2088	-	-	-
PL-3	-8	2451	2473	-	-	-
PL-4	-5	1345	1278	-	-	-
PL-5	-12	2079	2035	-	-	-
PD-1	-37	2684	2623	-43	1753	1821
PD-2	-51	2793	2982	-54	1984	2092
PD-3	-17	3536	3522	-30	2346	2530

Note: PL, partially frozen loose; PD, partially frozen dense.

4.7 Figures

FIG 4-1 Schematic of apparatus (after Liang et al. 2022a & b)

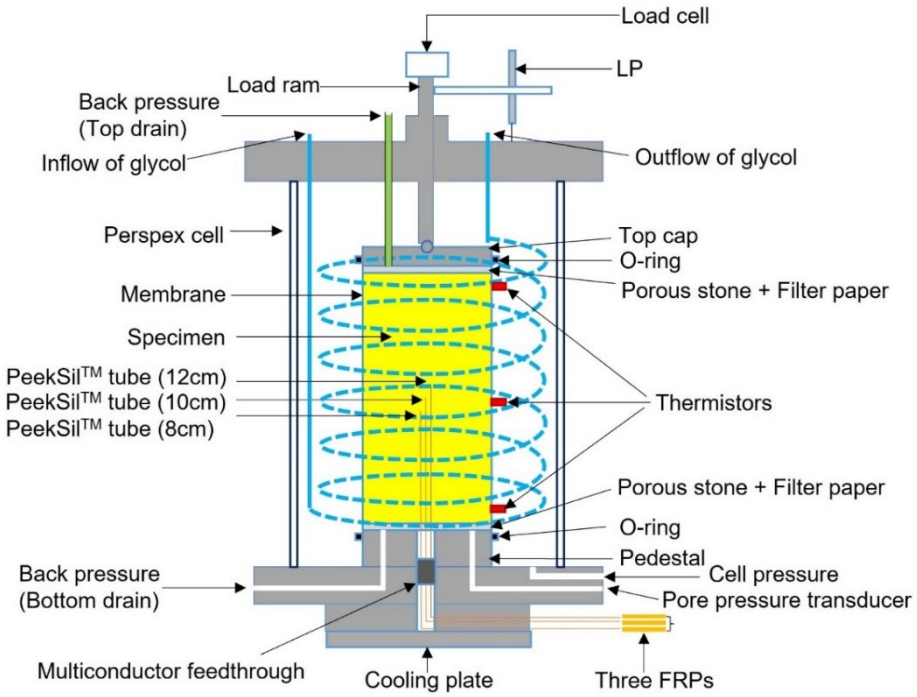

FIG 4-2 Stress and PWP response of partially frozen sand. (a) stress and (b) PWP (Note: PL, partially frozen loose; PD, partially frozen dense)

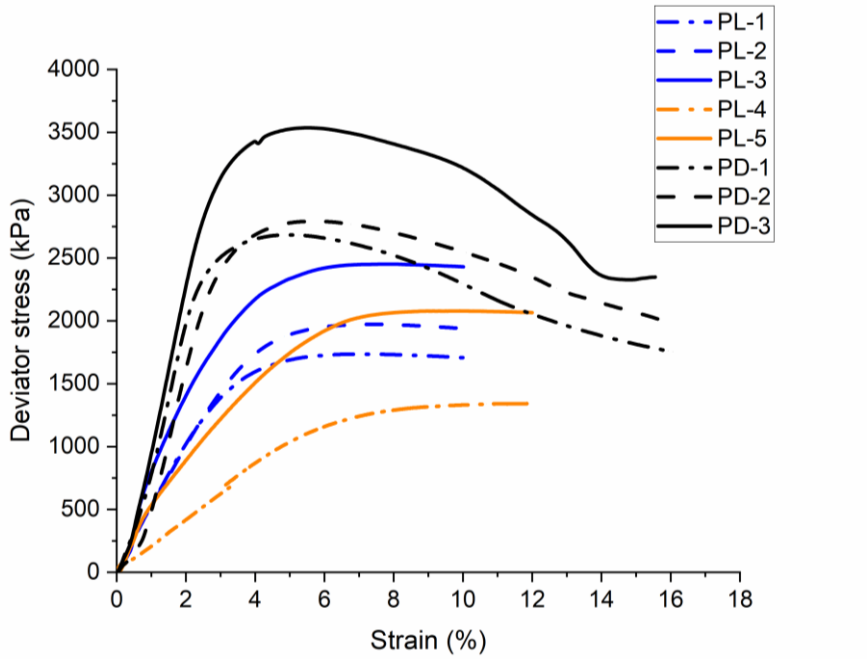

(a)

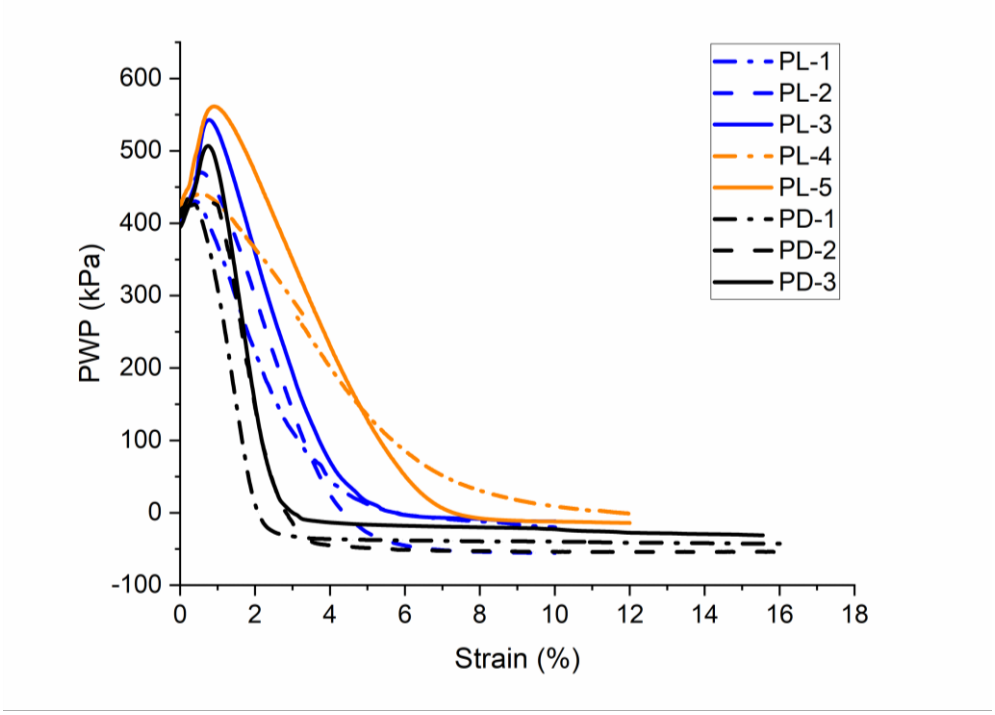

(b)

FIG 4-3 Effective stress path of partially frozen sand. (a) partially frozen loose sand under different strain rates (1% & 0.1%/min) and (b) comparison of partially frozen loose and dense sand

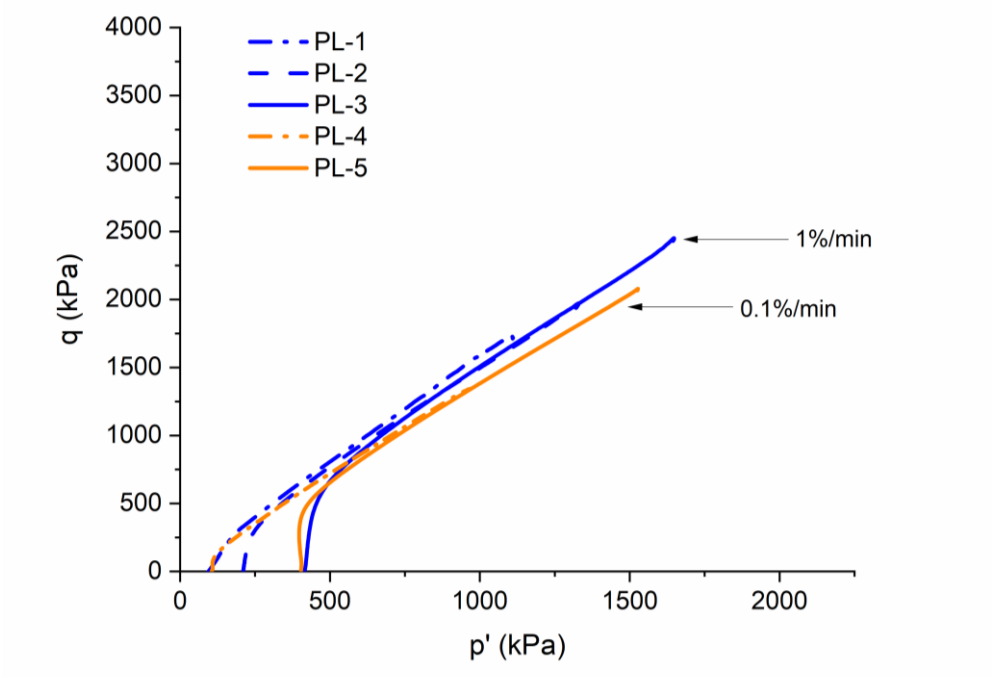

(a)

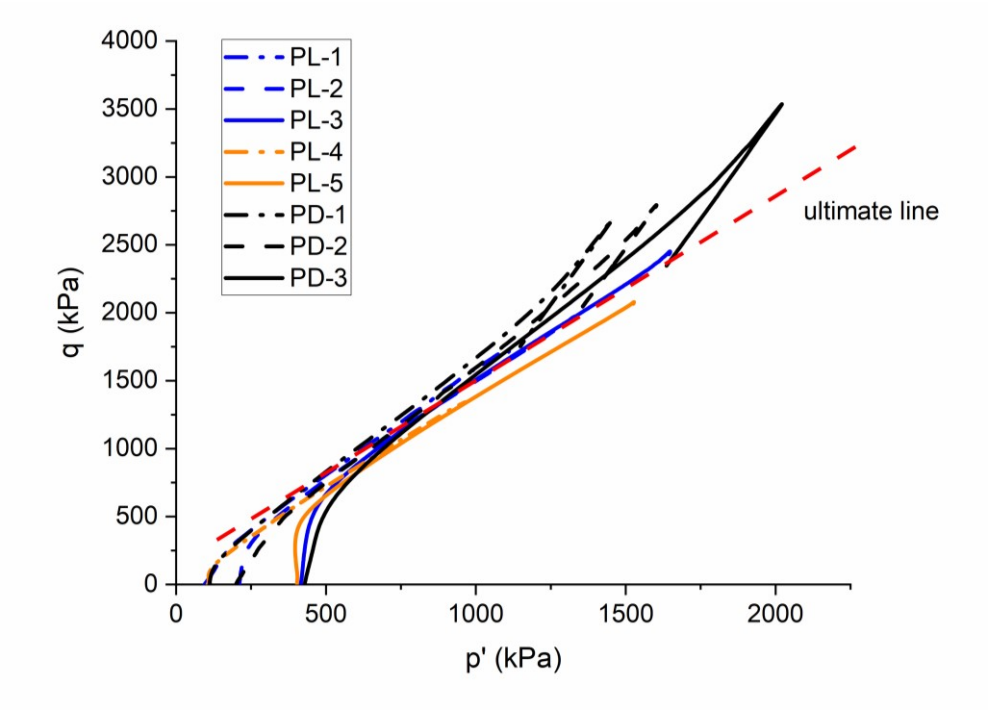

(b)

FIG 4-4 Comparison of stress paths between partially frozen loose and unfrozen dense sand (1%/min)

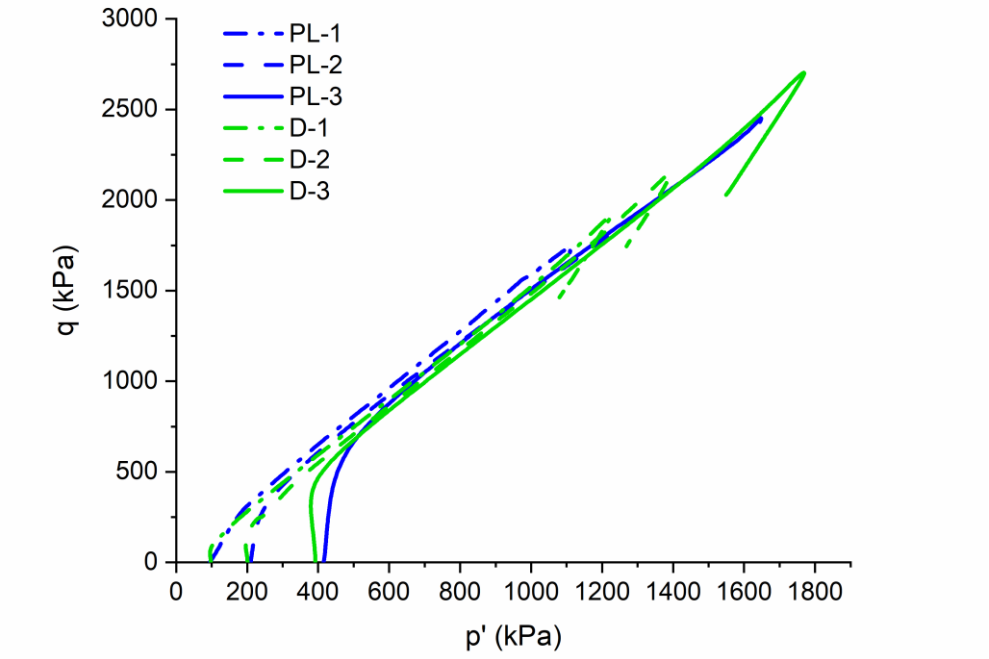

FIG 4-5 Pore ice stress of partially frozen loose sand. (a) deviator stress, (b) minor principal stress, (c) stress path

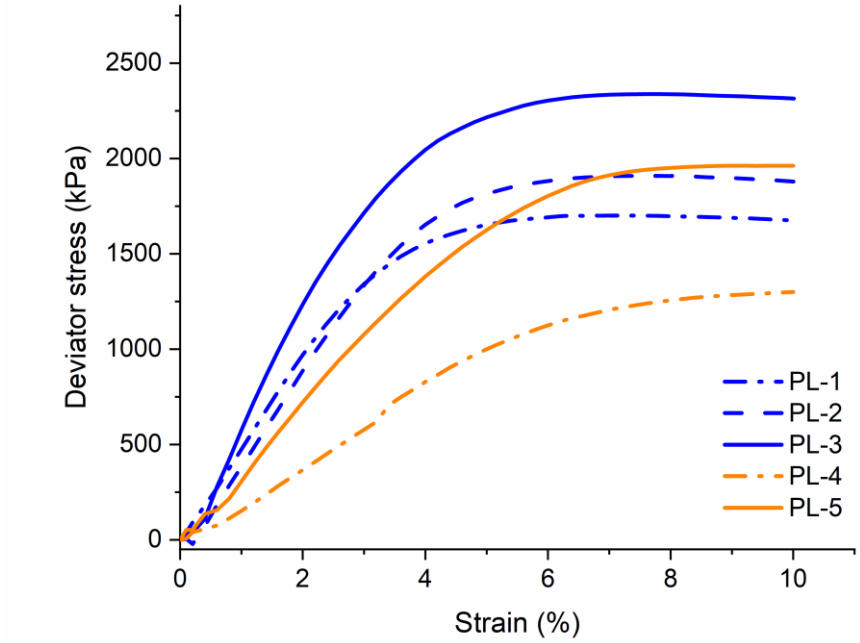

(a)

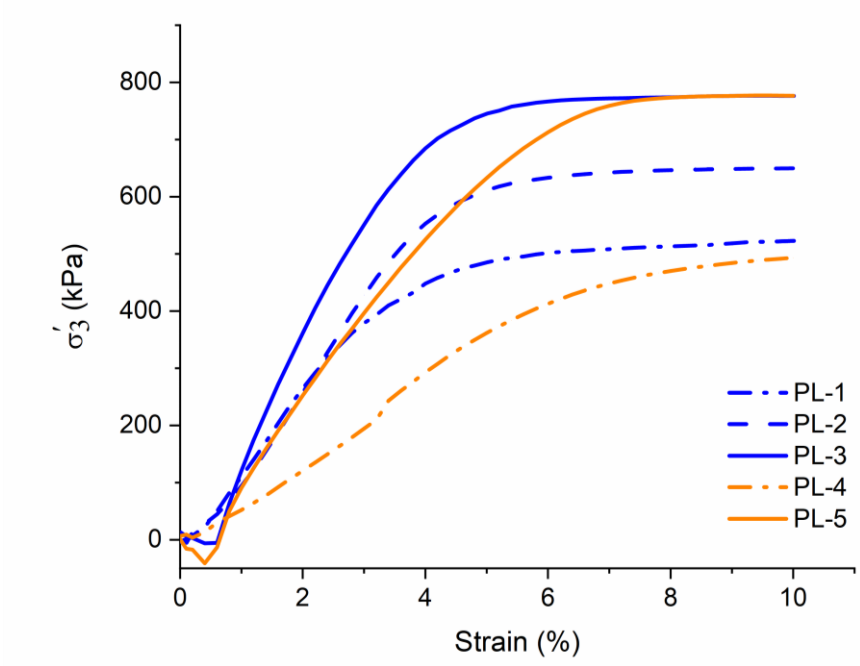

(b)

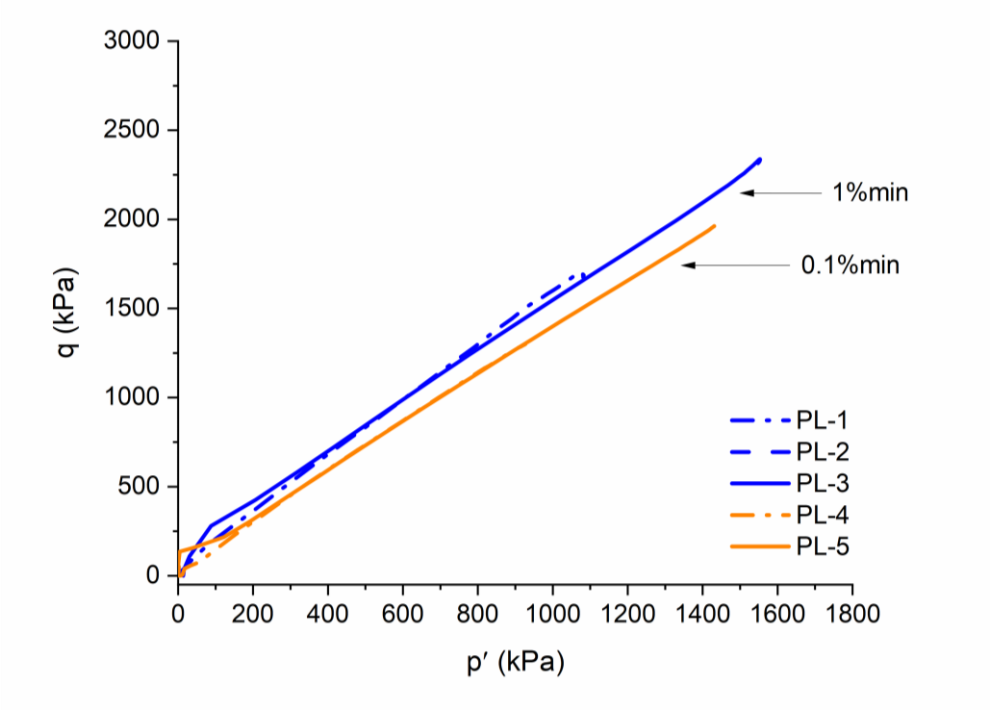

(c)

FIG 4-6 Pore ice stress of partially frozen dense sand. (a) deviator stress, (b) minor principal stress, (c) stress path

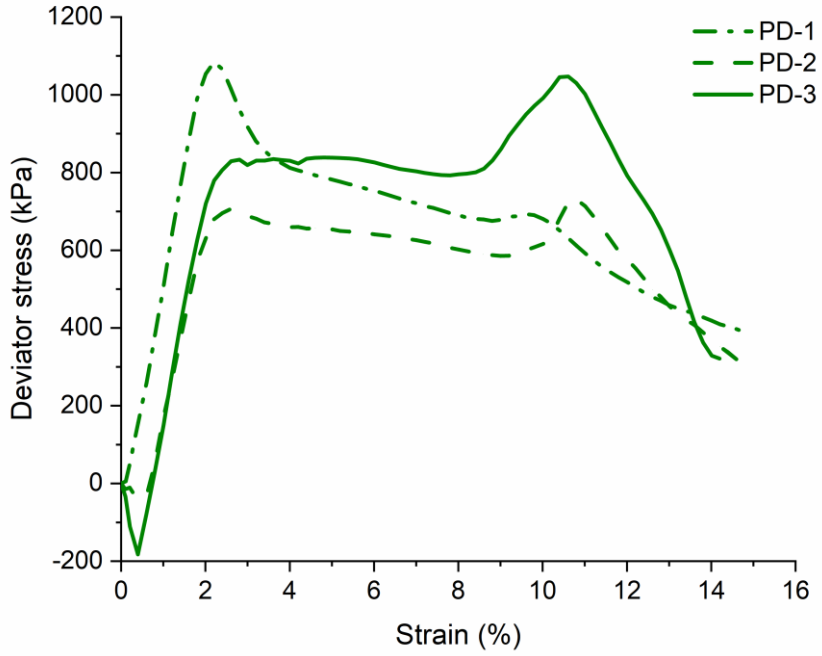

(a)

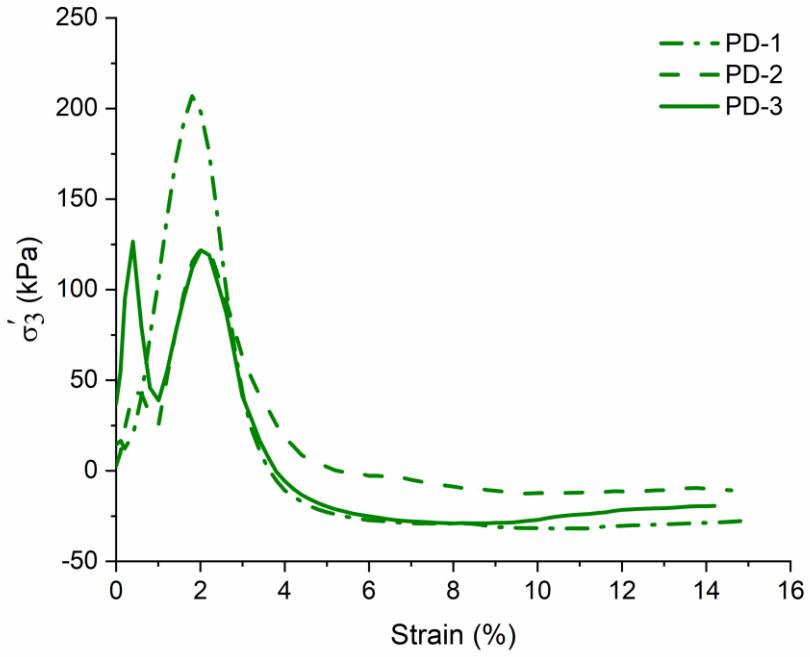
PD-1
PD-2
PD-3
σ'3 (kPa)
Strain (%)
250
200
150
100
50
0
-50
0
2
4
6
8
10
12
14
16

(b)

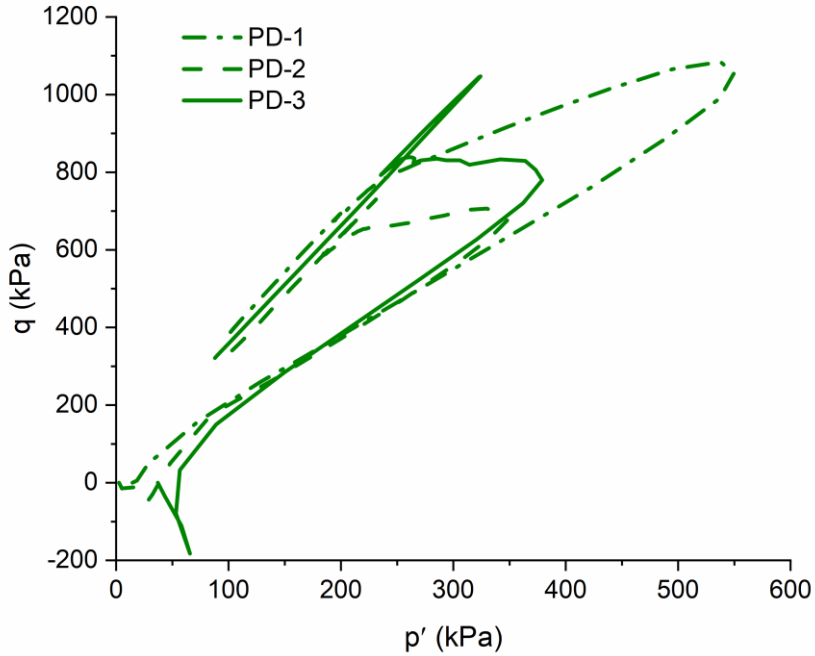
PD-1
PD-2
PD-3
q (kPa)
p′ (kPa)
1200
1000
800
600
400
200
0
-200
0
100
200
300
400
500
600

(c)

FIG 4-7 Strength of partially frozen and unfrozen sand

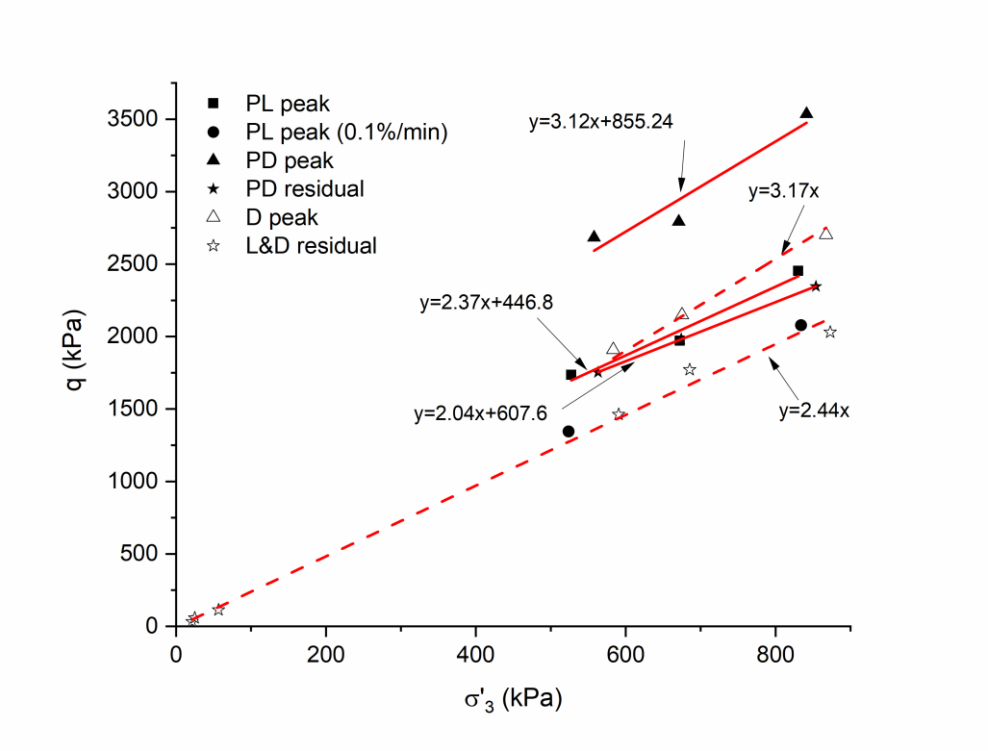

FIG 4-8 Verification of model

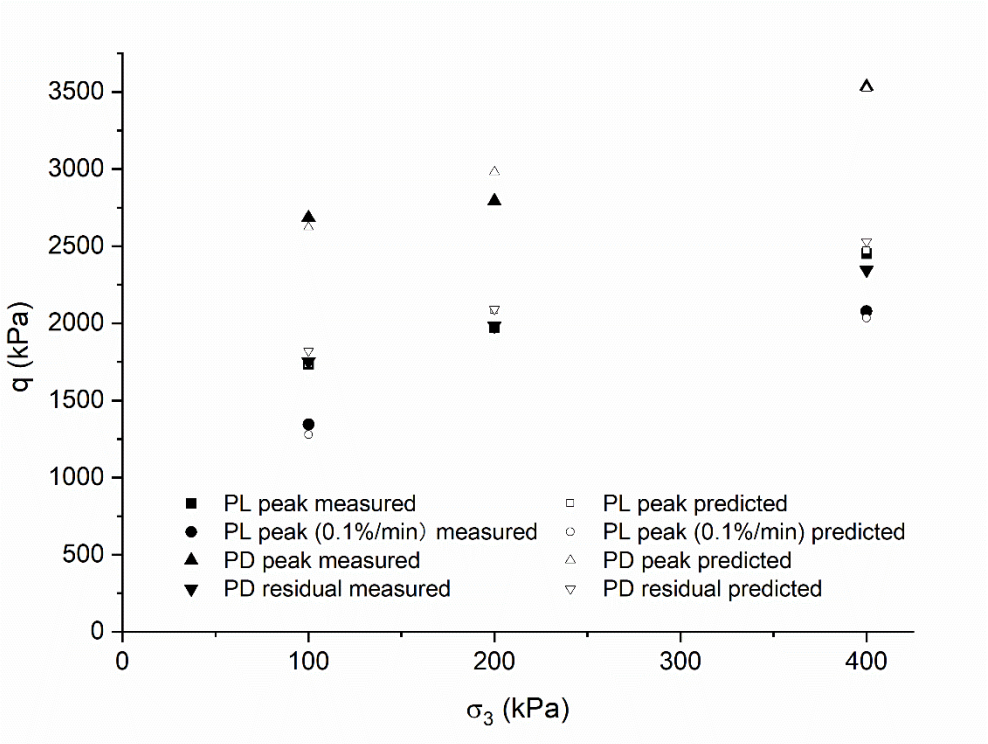

FIG 4-9 Relationship between PWP and PIS in partially frozen loose sand (PL-1). (a) PWP vs $\sigma_{3(i)}$ and (b) ΔPWP vs $\Delta\sigma_{3(i)}$

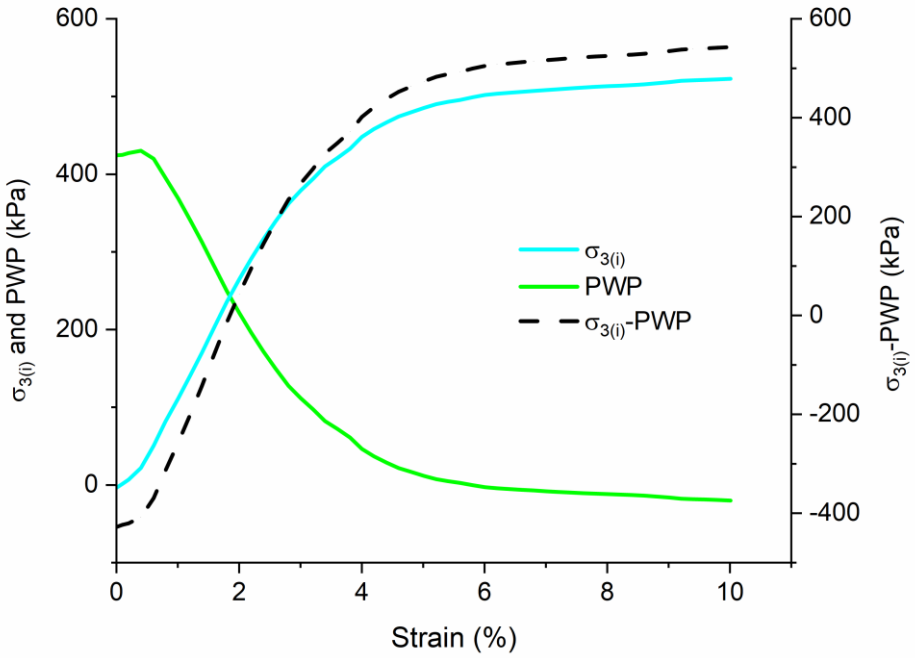

(a)

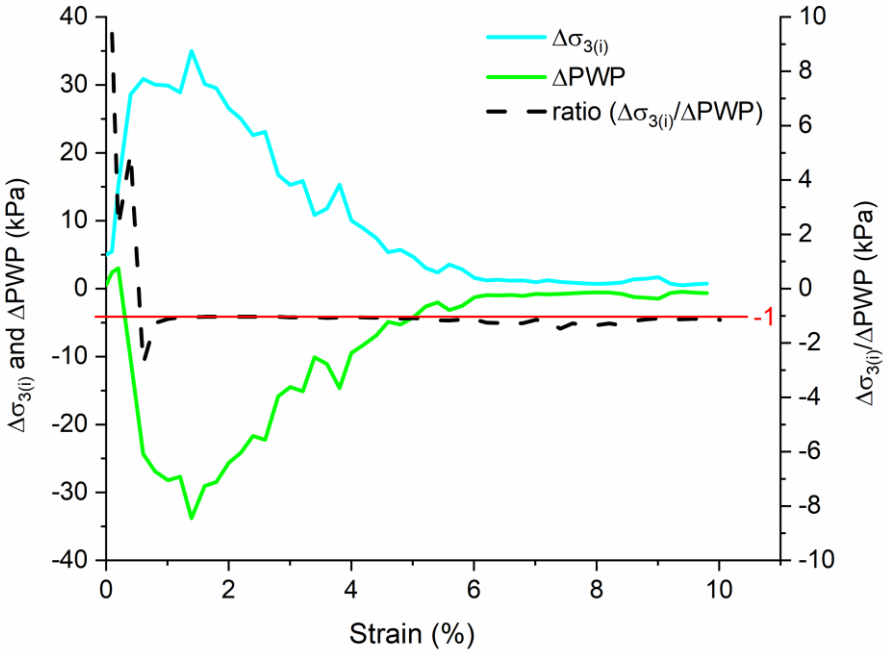

(b)

FIG 4-10 Relationship between PWP and PIS in partially frozen dense sand (PD-1). (a) PWP vs $\sigma_{3(i)}$ and (b) ΔPWP vs $\Delta\sigma_{3(i)}$

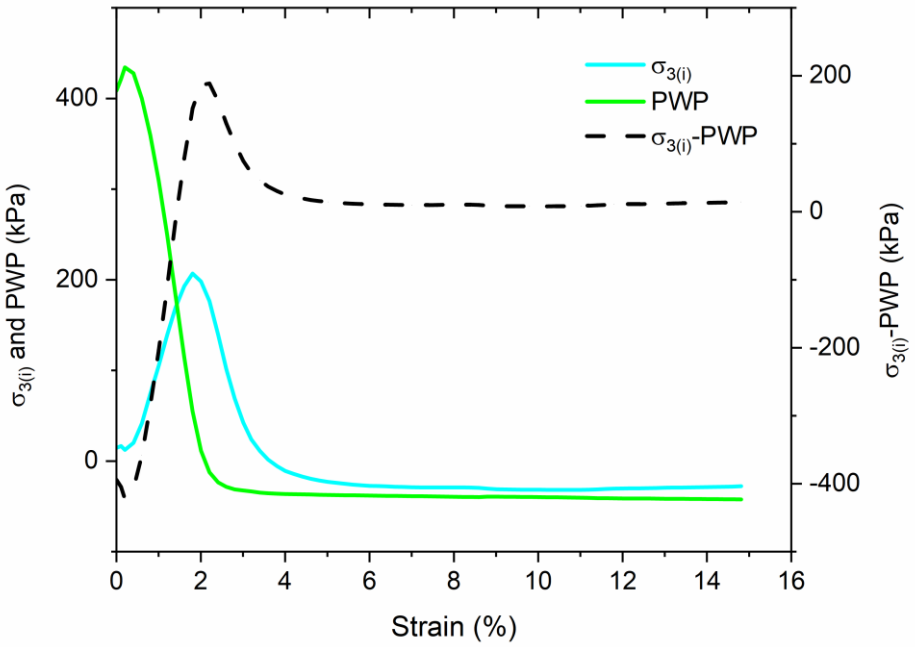

(a)

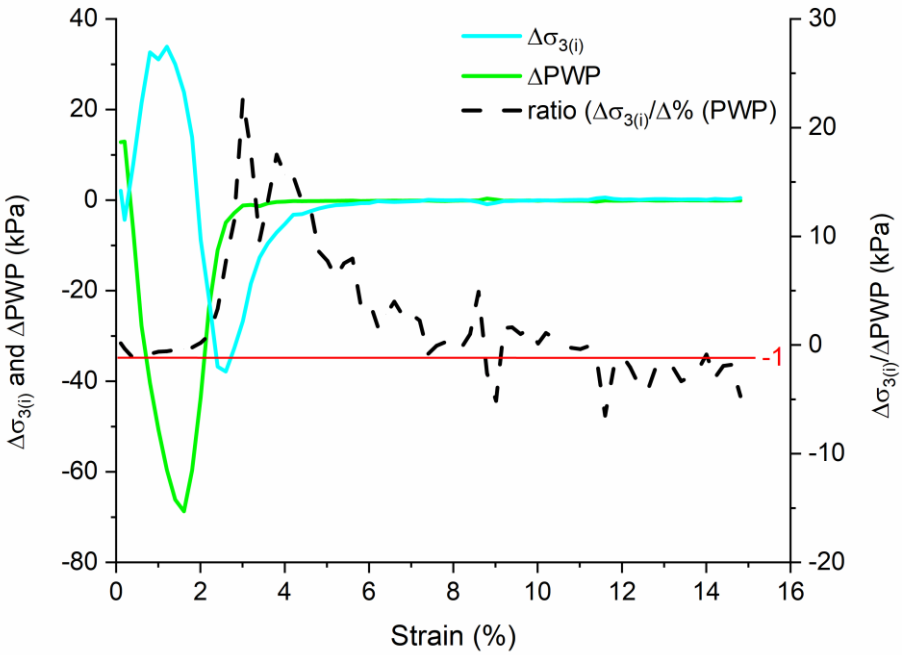

(b)

FIG 4-11 Stress distribution in partially frozen loose sand (PL-1)

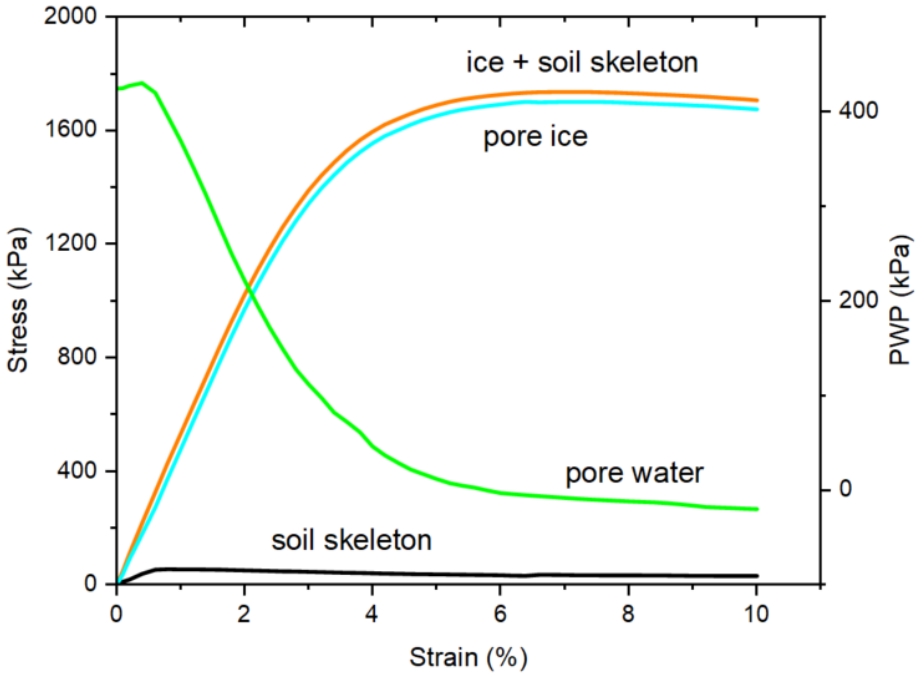

FIG 4-12 Stress distribution in partially frozen dense sand (PD-1)
(Note: c_L, cohesion caused by pore ice from eq.6; c_D, cohesion caused by pore ice from eq.8)

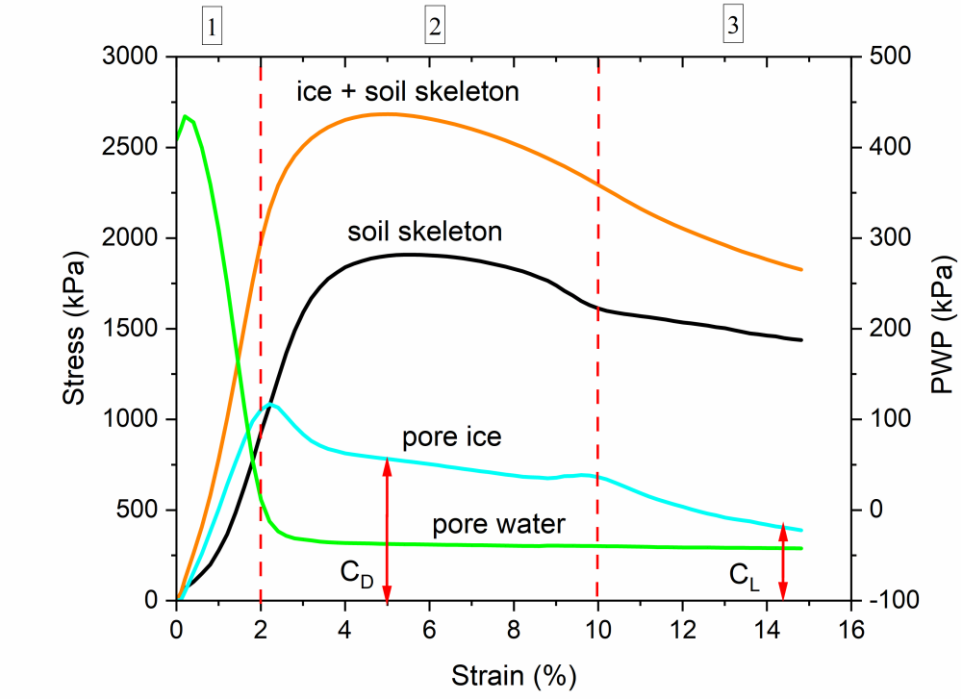

4.8 References

Alkire, B.D., and Andersland, O.B. 1973. The effect of confining pressure on the mechanical properties of sand–ice materials. Journal of Glaciology, 12(66): 469-481.

Allard, M., Lemay, M., Barrette, C., L'Hérault, E., Sarrazin, D., Bell, T., and Doré, G. 2012. Permafrost and climate change in Nunavik and Nunatsiavut: Importance for municipal and transportation infrastructures. Nunavik and Nunatsiavut: From science to policy. An Integrated Regional Impact Study (IRIS) of climate change and modernization, ArcticNet Inc, Quebec City, Que. pp. 171–197.

Andersen, G.R., Swan, C.W., Ladd, C.C., and Germaine, J.T. 1995. Small-strain behavior of frozen sand in triaxial compression. Canadian Geotechnical Journal, 32(3): 428-451.

Arenson, L.U., and Springman, S.M. 2005. Triaxial constant stress and constant strain rate tests on ice-rich permafrost samples. Canadian Geotechnical Journal, 42(2): 412-430.

Black, P.B. 1995. Applications of the Clapeyron equation to water and ice in porous media. Cold Regions Research and Engineering Laboratory, U. S. Army Corps of Engineers, Hanover, NH, USA, Report 95-6.

Blanchard, D. and Fremond, M. 1985. Soil frost heaving and thaw settlement. In Proceedings of the 4th International Symposium on Ground Freezing, Boca Raton, FL, pp. 209–216.

Bourbonnais, J., and Ladanyi, B. 1985. The mechanical behaviour of frozen sand down to cryogenic temperatures. In Proceedings of 4th International Symposium on Ground Freezing, Boca Raton, FL, pp, pp. 235-244.

Bragg, R.A., and Andersland, O. 1980. Strain rate, temperature, and sample size effects on compression and tensile properties of frozen sand. Proceedings, 2nd International Symposium on Ground Freezing, Trondheim, Norway. University of Trondheim, Norwegian Institute of Technology, pp. 34- 47.

Ghoreishian Amiri, S., Grimstad, G., Kadivar, M., and Nordal, S. 2016. Constitutive model for rate-independent behavior of saturated frozen soils. Canadian Geotechnical Journal, 53(10): 1646-1657.

Goughnour, R.R., and Andersland, O. 1968. Mechanical properties of a sand-ice system. Journal of the Soil Mechanics and Foundations Division, 94(4): 923-950.

Hivon, E., and Sego, D. 1993. Distribution of saline permafrost in the Northwest Territories,

Canada. Canadian Geotechnical Journal, 30(3): 506-514.

Hivon, E., and Sego, D. 1995. Strength of frozen saline soils. Canadian Geotechnical Journal, 32(2): 336-354.

Holubec, I. 2008. Flat loop thermosyphon foundations in warm permafrost. Government of the Northwest Territories Asset Management Division of Public Works and Services and the Climate Change Vulnerability Assessment of the Canadian Council of Professional Engineers.

Kalifa, P., Ouillon, G., and Duval, P. 1992. Microcracking and the failure of polycrystalline ice under triaxial compression. Journal of Glaciology, 38(128): 65-76.

Kia, M. 2012. Measuring Pore-water Pressure in Partially Frozen Soils. Ph.D. thesis, Faculty of Graduate Studies and Research, University of Alberta, Edmonton, AB.

Ladanyi, B., and Morel, J.-F. 1990. Effect of internal confinement on compression strength of frozen sand. Canadian Geotechnical Journal, 27(1): 8-18.

Laxton, S., and Coates, J. 2010. Geophysical and borehole investigations of permafrost conditions associated with compromised infrastructure in Dawson and Ross River, Yukon. Yukon Exploration and Geology. Yukon Geological Survey, pp. 135-148

Liang Y, Beier N, and Sego DC. 2022a. New method for internal pore-water pressure measurements. Geotechnical Testing Journal, 45(2): 490-502.

Liang Y, Beier N, and Sego DC. 2022b. Continuity of pore-water pressure measurements in partially frozen sand. (Manuscript submitted for publication)

Lyu, C., Nishimura, S., Amiri, S.A.G., Zhu, F., Eiksund, G.R., and Grimstad, G. 2021. Pore-water pressure development in a frozen saline clay under isotropic loading and undrained shearing. Acta Geotechnica, 16(12): 3831-3847.

Mellor, M. 1980. Mechanical properties of polycrystalline ice. In Physics and Mechanics of Ice, International Union of Theoretical and Applied Mechanics, Copenhagen, Springer Verlag, Berlin, pp. 217-245.

Melton, J.S., and Schulson, E.M. The ductile deformation of columnar (S2) saline ice under triaxial compression. In The Seventh International Offshore and Polar Engineering Conference. 1997. OnePetro.

Nishimura, S., and Wang, J. 2019. A simple framework for describing strength of saturated

frozen soils as multi-phase coupled system. Géotechnique, 69(8): 659-671.

Nishimura, S., Gens, A., Olivella, S., and Jardine, R. 2009. THM-coupled finite element analysis of frozen soil: formulation and application. Géotechnique, 59(3): 159-171.

Ogata, N., Yasuda, M., and Kataoka, T. 1983. Effects of salt concentration on strength and creep behavior of artificially frozen soils. Cold Regions Science and Technology, 8(2): 139-153.

Parameswaran, V., and Jones, S. 1981. Triaxial testing of frozen sand. Journal of Glaciology, 27(95): 147-155.

Pharr, G., and Merwin, J. 1985. Effects of brine content on the strength of frozen Ottawa sand. Cold Regions Science and Technology, 11(3): 205-212.

Sayles, F. 1989. State of the art, mechanical properties of frozen soil. In Proceedings of 5th International Symposium on Ground Freezing, Nottingham, England. A.A. Balkema, Rotterdam, pp. 143-165.

Sayles, F.H. 1974. Triaxial constant strain rate tests and triaxial creep tests on frozen Ottawa sand. Corps of Engineers, US Army Cold Regions Research and Engineering Laboratory. Technical Report 253.

Sheeran, D.E., and Yong, R.N. 1975. Water and salt distribution in freezing soils. Proceedings, 1st Conference on Soil-Water Problems in Cold Regions, Calgary, Alta. pp. 58-69.

Stuckert, B., and Mahar, L. 1984. Role of ice content in the strength of frozen saline coarse grained soils. In Proceedings, Cold Regions Engineering Specialty Conference, Edmonton, AB. Montreal: Canadian Society for Civil Engineering. pp. 579-587.

Swanson, D., Murphy, D., Temmer, J., and Scaletta, T. 2021. Advancing the Climate Resilience of Canadian Infrastructure: A Review of Literature to Inform the Way Forward. International Institute for Sustainable Development.

Ting, J.M., Torrence Martin, R., and Ladd, C.C. 1983. Mechanisms of strength for frozen sand. Journal of Geotechnical Engineering, 109(10): 1286-1302.

Xu, J., Liu, H., and Zhao, X. 2017. Study on the strength and deformation property of frozen silty sand with NaCl under tri-axial compression condition. Cold Regions Science and Technology, 137: 7-16.

Xu, X., Wang, Y., Bai, R., Fan, C., and Hua, S. 2016. Comparative studies on mechanical

behavior of frozen natural saline silty sand and frozen desalted silty sand. Cold Regions Science and Technology, 132: 81-88.

5. Determination of the Critical State Line in Partially Frozen Sand

Abstract: A new test method to determine critical state line (CSL) in partially frozen sand is presented to investigate the influence of temperature and strain rate on critical state parameters. A series of consolidated undrained and drained triaxial tests along with internal PWP measurements were conducted on both dense and loose specimens under different temperatures and strain rates. Similar to unfrozen sand, a unique CSL is established in both stress (q-p') and void ratio (e-p') space for the partially frozen sand at the temperature of -3 ºC. The results show that the critical state friction angle (φ'_{cs}) is not affected by temperature while the critical state cohesion (c'_{cs}) is a function of temperature, strain rate, and failure mode. The c'_{cs} increases with decreasing temperature from 23 ºC to -3 ºC and to -10 ºC, but decreases to zero when the strain rate is reduced to 0.1% /min from 1% /min. In e-p'space, the slope λ_d represents the dilatancy of partially frozen sand, which increases with decreasing temperature and rising strain rate associated with the contact area between the pore ice and sand grains. This study is expected to contribute to the formation of constitutive models for partially frozen soil and ultimately to enhanced engineering design in warm permafrost regions.

Keywords: partially frozen soil, critical state line (CSL), critical state parameters, temperature, strain rate.

5.1 Introduction

The concept of critical (or steady) state has been widely used to capture the fundamental behaviour of unfrozen soil and for the design of soil structures, such as the liquefaction evaluation (Roscoe et al. 1958; Schofield and Wroth1968; Wood 1991; Poulos et al. 1985; Jefferies and Been 2015). The construction of artificially islands in the Beaufort Sea also relied on the strength at steady state (Been et al. 1987; Jefferies et al. 1988; Been et al. 1991). In addition, the critical-state-based constitutive models were developed to represent important features of frozen soil involved in the freeze-thaw cycling and different loading conditions, for example, frost heave and thaw settlement (Nishimura and Wang 2019; Nishimura et al. 2009; Ghoreishian Amiri et al. 2016; Zhang and Michalowski 2015; Yu et al.2021). Recently, the concern with thawing of permafrost associated with climate change in warm permafrost regions was raised by Northern communities (Holubec 2008; Allard et al. 2012; Swanson et al. 2021). The “near surface” soils in those warm regions (ice-rich and/or saline) are at a partially frozen state with unfrozen water and ice coexisting in the internal pores. To understand the critical state behavior of partially frozen soil, the relationship between critical void ratio and mean effective stress, which is called the critical state line, needs to be established. Hence, a reliable method to determine the critical state line (CSL) of partially frozen soil is required.

Typically, the CSL of unfrozen sand is determined by a series of isotopically consolidated undrained (CIU) and consolidated drained (CID) triaxial tests carried out on loose and dense specimens respectively. However, the strain localization may occur at the shear zones of dense specimens under drained conditions, and the local void ratio within the shear band is different

from the measured global average sample void ratio. Desrues et al. (1996) found that the local void ratio rather than global average void ratio should be used to represent the void ratio at the critical state of the specimen. The local void ratio is not conveniently measured in a traditional triaxial test, therefore Jefferies and Been (2015) suggested using three loose specimens under CIU test at effective confining pressures of 100, 200, and 400 kPa and one loose specimen under CID test at the effective confining pressure of 400 kPa to provide a CSL for common geotechnical engineering problems.

The biggest challenge in determining the CSL of frozen soil is to obtain the effective stress due to the absence of reliable experimental techniques to measure the internal stresses (pore water pressure and pore ice pressure). Several models adopted the total stress to describe the mechanical behavior of frozen soils (Arenson and Springman 2005; Lai et al. 2008; Zhu et al. 2010; Yu et al. 2021), but the influence of pore matrix (ice and unfrozen water) content and pressure cannot be reflected by these models (Ghoreishian Amiri et al. 2016). To quantify the internal stresses, Li et al. (2002, 2008) distributed proportionally the pore pressure into air, water, and ice phases by volume. Nishimura et al. (2009) introduced a cryo-suction between the pore water pressure (PWP) and pore ice pressure according to the Clausius-Clapeyron equation, as the relationship of the two phases within the pore is similar to that in unfrozen unsaturated soil (Henry 2000; Thomas et al. 2009; Koopmans and Miller 1966). Zhang and Michalowski (2015) considered the ice phase as part of the solid phase and employed a volumetric ratio between the pore ice and solid particles in the model to simulate frost heave phenomenon. However, some assumptions involved in these models are questionable. The

Clausius–Clapeyron equation, which is valid under static conditions where the pressure and temperature remain constant, has not proved effective when soil is under shear, either undrained or drained (Li et al. 2001), so the calculated cryo-suction may not represent the true relationship between the ice and water pressure. Due to the lack of experimental data on the measurement of the internal stresses, the distribution of the pore ice or water pressure was often assumed (Yu et al. 2021). Besides, the pore ice may have different stress states from the other phases, not only because the ice can sustain shear stress, but also it has mechanical interaction with the soil skeleton through the dilatancy effect and structural hindrance (Ting et al. 1983).

Inspired by Ladanyi and Morel's (1990) postulate on the unique relationship between the effective stress path (ESP) and strain path in both frozen and unfrozen soil, Wang et al. (2017) attempted to map CSLs of the frozen clay specimens under different temperatures and strain rates by referring to the unfrozen specimens with the same strain history. The deviator stress q was measured from the frozen tests while the effective mean stress p' was taken from the unfrozen tests according to this postulate. The issue is that the q was a combination of the soil skeleton strength and the ice strength, but p' referred to the stress of the soil skeleton only, so the mapped effective stress paths and CSLs in q-p'space were not reliable.

It is known that the effective stress controls the deformation and strength of soil, and it is defined by the difference between total stress and PWP. The ice-soil system is therefore treated as a solid phase in partially frozen soil (Blanchard and Fremond 1985; Ghoreishian Amiri et al. 2016). Hence, the effective stress of partially frozen soil can be obtained if the PWP is measured provided continuity in the internal soil water phase. However, the lack of experimental

techniques to measure the PWP and to examine the continuity in the water phase restricts the establishment of CSL in partially frozen soil. Arenson and Springman (2005) measured PWP in the ice-rich samples and then Lyu et al. (2021) investigated PWP response in the frozen saline clay under different temperatures and strain rates. But the continuity in the internal water phase was not established by either Arenson and Springman (2005) or Lyu et al. (2021). To the authors' knowledge, only Kia (2012) and Liang et al. (2022b) confirmed continuity in the internal water phase by correctly measuring PWP via the Filter-less Rigid Piezometers (FRPs) within partially frozen sand.

The object of this manuscript is to apply a newly developed test method to determine CSL in partially frozen sand and to investigate the influence of temperature and strain rate on the critical state parameters. A series of CIU and CID triaxial tests along with internal PWP measurements were conducted on both dense and loose sand with a salinity of 30 ppt under different temperatures (23, -3, -5, and -10 ºC) and strain rates (1 and 0.1%/min). With the internal PWP measurements, the effective stress and CSL are therefore obtained in the partially frozen specimens. The factors that influence the critical state parameters are also discussed.

5.2 Material and methods

5.2.1 Material

The material and specimen dimension are the same as used in Chapter 3. Based on the monitored pore water volume change during the tests, the estimated unfrozen water content (UWC) under different temperatures is summarized in Table 5-1.

5.2.2 Test apparatus

The new triaxial apparatus was originally developed for measurement of internal PWP within the unfrozen soil by Liang et al. (2022a) and was later modified to extend its application into the partially frozen test, as shown in Fig. 5-1 (Liang et al. 2022b). Further details regarding the apparatus can be found in Chapters 2 and 3.

5.2.3 Test procedures

The whole testing program includes three series (Table 5-2): (i) unfrozen, (ii) partially frozen at a constant temperature of -3 ^{o}C and the strain rate of 1 %/min, and (iii) partially frozen (or frozen) at different temperatures (-5 and -10 ^{o}C) or strain rates (1 and 0.1 %/min). The unfrozen tests were used as references to assist with the establishment of the CSL in partially frozen specimens. Series (iii) was performed to investigate the effect of temperature and strain rate on the behavior and CSL of partially frozen sand.

The same procedures as described by Liang et al. (2022a) were used for sample preparation,

resaturation, and consolidation. Series (i) were performed at a room temperature of 23 ºC. After consolidation, specimens were tested under undrained or drained conditions at the same strain rate as Series (ii).

The Series (ii) were conducted in a cold room with temperature set to approximately 2 ºC. The procedures for rapid freezing, subsequent warming, and shearing of specimens at the temperature of -3 ºC are as described by Liang et al. (2022b).

In series (iii), the specimens tested at the temperatures of -5 and -10 ºC followed similar steps as above but no PWP measurement in the specimen at -10 ºC during shear. The drainage (back pressure) line was frozen, and the continuity in the water phase was not confirmed by the base transducer and the internal FRPs at -10 ºC, therefore the specimen FL-1 was considered frozen without a continuous water phase. For lower strain rate tests, the strain rate was 0.1 %/min.

5.2.4 Void ratio calculation

The determination of the initial void ratio was based on the initial dimension of the sample. The height was measured by comparing the reading of a vertical displacement gauge for the sample with a reference of the known height placed on the base of the triaxial apparatus (Sasitharan et al. 1993). The average diameter of the sample was calculated by using the volume of the membrane-lined cavity over the height of the sample. The volume of the cavity was obtained using the mass of water filled in the cavity, as suggested by Vaid and Sivathayalan (1997). The final void ratio was derived from the average water content after the test by freezing the whole sample. Alternatively, the final water content can be obtained by calculating

the final volume of pore water as follows (modified from Jefferies and Been 2015)

[5-1] $V_f = V_0 - \Delta V_c$

where

V_f is the final volume of pore water;

V_0 is the initial volume of pore water, assuming that the sample is fully saturated; and

ΔV_c is the volume change during the consolidation, which is recorded by a volume change device.

When shear drained, the final volume of pore water is given by

[5-2] $V_f = V_0 - \Delta V_c - \Delta V_s$

Where ΔV_s is the volume change during the shear.

In an unfrozen loose sample, the measured final water content by freezing the sample was consistent with the calculated final water content by eq. 5-1 or 5-2, while the measured final water content was larger than the calculated value in an unfrozen dense sample. The suctions were developed at large strains, so extra water from the pressure line and/ or pedestal was possibly drawn back to the dense sample. This was also the case with the partially frozen, loose and dense samples where the suction was observed. Besides, the voids were filled with ice and unfrozen water after the test, so the final void ratio would be underestimated by measuring the final water content.

During the rapid freezing, about 9 % of the total pore volume of water was expelled, indicating that the fabric of the specimen remained unchanged. Also, thaw strain was not observed in the subsequent warming. Therefore, it was assumed that the void ratio was not altered during the

freezing and warming processes, and hence the final water content (void ratio) can be determined by eq. 5-1 or 5-2 for the partially frozen specimens.

5.3 Results

5.3.1 Behavior of unfrozen sand

Typical results of the unfrozen loose and dense specimens are shown in Figure 5-2. The loose specimen with effective confining pressure of 400 kPa exhibits strain softening in the undrained condition (L-3) but contractive behavior in the drained condition (L-4), while the dense specimen shows dilative behavior under the undrained condition (D-3). All the FRPs show the same PWP response as the base transducer throughout the test and hence only PWP measured by the base transducer is displayed in figures. Apparently, the critical state is reached at the end of the tests where the specimens continuously deform under constant stress and void ratio (Roscoe et al. 1958), except the drained test of the loose specimen L-4. The deviator stress of the specimen L-4 slightly increases even after 10 % strain, but it is very close to the critical state at the end of the test.

5.3.2 Effective stress path and CSL of unfrozen sand

According to the stress-strain response of the unfrozen specimens, the ESPs are presented in Fig. 5-3. Since the ESPs are moving towards the critical state, both dense and loose specimens share the same ultimate line. The values at the end of tests are used to plot the CSL in q-p' space, so a unique CSL of the unfrozen specimens (Fig. 5-4a) is established by the following

equation

[5-3] $q = Mp'$

where

q is the deviator stress;

M is the slope of critical state line in q-p' plane, 1.33; and

p' is effective mean stress.

Further, the CSL in e-p' space (Fig. 5-4b) is determined using four loose specimens under undrained or drained loading (Jefferies and Been 2015), and is given by

[5-4] $e = \Gamma - \lambda ln p'$

where

e is the void ratio;

Γ is the intercept of critical state line in e-p' plane, 0.872; and

λ is the critical state parameter of unfrozen, slope of critical state line in e-p' plane, 0.014.

5.3.3 Behavior of partially frozen sand (-3 ºC)

Figure 5-5 shows the stress-strain and PWP response of partially frozen, dense and loose samples at temperature of -3 ºC. There are some erratic PWP measurements via the FRPs and the base transducer caused by blockage of the measuring tubes, or the pressure line, so only valid PWP measurements which indicate the continuity in the water phase within the samples as reported by Liang et al. (2022b) are displayed in Fig. 5-5b. The partially frozen, loose

samples exhibit ductile behavior, which is similar to the behavior of saline ice (Melton and Schulson 1997), while the partially frozen, dense samples behave in a dilative manner like the unfrozen dense samples (Fig. 5-5a). The PWP response indicates both partially frozen, loose and dense samples tend to dilate during shear (Fig. 5-5b). In the drained test (PL-4), the back pressure line was open and hence the PWP was affected not only by the dilatancy of the sample but also by the back pressure (400 kPa). The competition of these two factors caused the undulate response in PWP, corresponding to the fluctuating deviator stress after 4 % strain. Although the stress of a partially frozen, dense sample decreases slightly at the end of the test, the PWP is constant, and the stress change is possibly because of the non-uniformities of the sample after failure. Therefore, the conditions at the end of the tests are considered as the critical state in both partially frozen, dense and loose tests.

5.3.4 Effective stress path and CSL of partially frozen sand (-3 °C)

The ESPs of partially frozen samples are shown in Figure 5-6. Obviously, the ESPs of partially frozen, loose samples converge at the larger strain and the ESPs of partially frozen, dense samples terminate on the same line. Fig. 5-6c compares the ESPs between the partially frozen, loose and dense samples. In a similar trend observed in unfrozen samples, all the ESPs share the same ultimate line, suggesting there is also a unique CSL between the partially frozen, loose and dense samples in q-p′ space. As a result, the unique CSL in q-p' space (Fig. 5-7a) is expressed as

[5-5] $q = Mp' + c_{cs}{}'$

where c'_{cs} is the critical state cohesion resulting from the pore ice, 266.4 kPa and M is 1.29.

Since no shear band was observed in the partially frozen, loose tests, the CSL in e-p' space was determined using three partially frozen, loose samples under undrained conditions, excluding the drained test. The reason for conducting a drained test in the unfrozen, loose sand is that it shows contractive behavior to expand the range of CSL. However, the partially frozen, loose sand exhibits dilatant tendency under the drained condition without expanding the range of CSL. Moreover, the fluctuations in the stress response and the pore volume change due to the suction of water from the pressure line affect the determination of the critical stress and void ratio. Therefore, it is suggested to carry-out undrained tests only to determine CSL in partially frozen sand.

The critical state parameter λ is related to the compressibility of soil because the unfrozen, loose specimen shows contractive behavior. However, the results imply that both partially frozen, dense and loose specimens tend to dilate and hence the CSL in e-p' diagram should be interpreted in an opposite direction (upward). That is, the slope of CSL represents dilatancy of partially frozen sand, and therefore the critical state parameter λ_d is used for clarity. The critical state parameters Γ and λ_d are 1.075 and 0.036, at -3 °C, respectively (Fig. 5-7b).

According to the function of CSL, the critical void ratios within the shear band of partially frozen and unfrozen, dense specimens are obtained by back calculation (Table 5-3). The critical void ratios of partially frozen and unfrozen specimens are about 0.23 and 0.18 higher than the average final void ratios of the specimens, respectively. This implies that the partially frozen,

dense specimens show more dilation than the unfrozen dense specimens due to the presence of pore ice. Besides, the critical void ratio of a partially frozen, dense specimen is almost the same as that of a partially frozen, loose specimen under the same confining pressure.

5.3.5 Effect of temperature and strain rate on behavior of partially frozen sand

Figure 5-8 compares the behavior of partially frozen, loose specimens under different strain rates. The specimens PL-1 and PL-3 were sheared at 1 %/min while PL-5 and PL-6 were at 0.1 %/min. Compared with specimens tested at 1 %/min, the specimens under the lower strain rate show a lower deviator stress but end up with an equal suction at larger strain. It is noted that the PWP of specimens under the lower strain rate remains constant to larger strains, so the critical state is reached at the end of the tests.

The comparison of behavior of partially frozen, loose samples under different temperatures is shown in Fig. 5-9. With the decrease in temperature, the stress increases, and the PWP drops faster. Also, the specimen behaves more brittle at a colder temperature. The double peak stress is observed in the specimen at the temperature of -10 ^{o}C, which often occurs under the lower temperature and confining pressure. The first peak is associated with the rupture of ice bonding, and thereafter the internal friction and dilatancy govern the soil strength development (Bragg and Andersland 1980; Andersen et al. 1995). The black lines in Figs. 5-9a and 5-9b indicate the unfrozen and partially frozen, dense specimens (-3 ^{o}C) under the same confining pressure as the partially frozen, loose specimens.

In addition, the specimens failed in different modes with the decrease in temperature. The

failure mode changes from a slight barrelling type at -3 °C to the shear plane type (-5 °C) and then to the strong barrelling type at -10 °C (Fig. 5-10). This is mainly associated with ice content and the adhesion between the pore ice and the soil skeleton. As the temperature decreases, the behavior of the partially frozen, loose specimen resembles the dense specimen, particular at -5 °C where the partially frozen, loose specimen exhibits nearly identical stress response in post-peak region and the same shear plane failure mode as the partially frozen, dense specimen at -3 °C (Fig. 5-9a). For consistency, the conditions at the end of the test (-5 and -10 °C) are also considered as representative of their critical state.

5.3.6 Effect of temperature and strain rate on effective stress path and CSL of partially frozen sand

The ESPs of specimens with a strain rate of 0.1 %/min also converge at the end of the test but have a lower slope than that of the specimens under a higher strain rate, reflecting the strain rate-dependency of the pore ice within partially frozen sand (Fig. 5-11a). On the other hand, the set of ESPs under the lower strain rate share the same ultimate line with that of the unfrozen specimens (Fig. 5-11b). The ESP becomes steeper as the temperature decreases. Since the specimen under temperature of -10 °C is considered frozen without the continuous water phase, the stress path represents the total stress path.

In q-p' space, the critical state points of the specimens under the lower strain rate are not in line with the CSL from the higher strain rate but lie on the CSL of the unfrozen specimens (Fig. 5-12). This means the specimens under the lower strain rate have the same critical state friction

angle (φ'_{cs}) as the unfrozen specimens, and the cohesion resulting from the pore ice decreases via creep (Sayles 1974). The CSL of the partially frozen specimens at -3 ºC is almost parallel to the CSL of the unfrozen specimens, suggesting the temperature only affects the critical state cohesion (c'_{cs}) not the critical state friction angle (φ'_{cs}). Hypothetically, the CSL of frozen specimens at -10 ºC should also have the same φ'_{cs}, and then the c'_{cs} can be obtained using the critical state point of the specimen FL-1, which is 815.6 kPa. The dash line represents the projected CSL of the frozen specimens at -10 ºC. However, the critical state point of the specimen at -5 ºC is close to the CSL at -3 ºC, so the effect of temperature on the critical state cohesion needs further discussion.

The CSL becomes steeper with the decreasing temperature and increasing strain rate, reflecting the higher dilatancy of partially frozen specimens at the lower temperature and higher strain rate (Fig. 5-13). The CSLs of specimens at different strain rates are very close but there is a noticeable difference between the CSLs of unfrozen and partially frozen specimens (-3 ºC), so the temperature has a more profound effect on the CSL in e-p' space than the strain rate. Since the CSLs of unfrozen and partially frozen specimens (-3 ºC) have different slopes, it is expected to have an intersection point at the critical void ratio of 0.744 and p' of 9,800 kPa. In other words, ice content decreases with increase in density of specimen, and hence the effect of ice on the CSL will be minimal beyond this point. As a result, the specimen dilates to this critical void ratio irrespective of the test temperature. If this is also true at -10 ºC, the CSL of the frozen specimens at -10 ºC can be mapped with the intersection point and the critical state point of the specimen FL-1, which is also marked by a dash line. The critical state parameters are

summarized in Table 5-4. Note that the shear plane was observed in the specimen at -5 °C but the average final void ratio was used in this case, so the actual critical state point should locate above its current position.

5.4 Discussion

5.4.1 Factors influencing the critical state parameters of partially frozen sand

The critical state parameters (M, Γ, and λ) are governed by the intrinsic properties of a material. For example, grain shape, particle size distribution, and fine content have significant impact on the critical state parameters of the unfrozen cohesionless soil (Jia et al. 2021). The great difference in component between frozen and unfrozen soil is the presence of ice matrix, and hence the factors that affect the properties of ice will influence the critical state parameters of partially frozen sand, such as temperature and strain rate (Figs. 5-12 and 5-13). Additionally, the dilatancy of partially frozen, loose sand is attributed to the pore ice which bonds the sand grains and converts the specimen into a denser state behavior. At the lower strain rate, the ice bonding gradually decreases as more contacts between the sand grains are created via creep (Sayles 1974), and hence specimens become less dilative, therefore the CSL will approach to that of the unfrozen specimens in the q-p′ plot but has a lower λ_d than the specimens under the higher strain rate.

The ice cohesion is generally strengthened by decreasing temperature, but on the other hand, it will decrease rapidly when the specimen exhibits brittle failure at colder temperatures. This explains why the c'_{cs} increases as the temperature decreases from 23 °C to -3 °C and to -10 °C,

but c'_{cs} at -5 °C is close to that at -3 °C. The ice content is also influenced by temperature, but it seems the ice content does not affect the critical state parameters for a given temperature because the partially frozen, dense and loose specimens share the same CSL. However, the volume or mass ratio of ice to unfrozen water content is constant under isothermal conditions, but it increases with decreasing temperature, and the larger ratio indicates the higher contact ratio between the ice and sand grains, resulting in a more dilatant arrangement of the grains and ice bonding. This is the reason why the λ_d increases with the decrease in temperature (Table 5-4). Hence, the failure mode and volume or mass ratio of ice to unfrozen water content should be taken into consideration when evaluating the effect of temperature on critical state parameters of partially frozen sand.

The behavior of loose sand is also a function of temperature, or of its position in the state diagram with respect to the CSL (Fig. 5-14). For example, the point A is at the contractive state when the sample is unfrozen but turns into a dilative state if the sample is partially frozen at a subfreezing temperature. As for dense sand (point B), the temperature has no effect on its side on the diagram.

Although only one salinity was tested in this study, it is expected the critical state parameters will change with different salinities. It has been reported that the unfrozen water content, structure of ice matrix, strength, and ice cohesion at failure are related to salinity (Hivon and Sego 1995; Arenson and Sego 2006; xu et al. 2016), so the salinity may affect the λ_d and c'_{cs}, and it needs further study.

5.4.2 The implication of establishing CSL in partially frozen sand

As mentioned previously, the current constitutive models of partially frozen soil based on the critical state theory either adopted total stress principle or assumed the distribution of the internal stresses to incorporate effective stress principle, which would lead to errors in prediction of behavior of partially frozen soil and in assessment of the safety of a soil structure. The method to determine CSL provided in this study can contribute to calibrating and improving the effectiveness of these models. In addition, this method is also significant in engineering practice. For example, the critical state friction angle (φ'_{cs}) is often used to analyze the slope stability in granular soils. Our finding indicates that the φ'_{cs} is not affected by the temperature and strain rate. Further, if the slope is under the slow loading (creep) condition, the critical state cohesion c'_{cs} will decrease and eventually approach zero. The established relationship between the partially frozen and unfrozen states at the critical state can be applied to evaluate the steady (critical) state strength of partially frozen sand in the design of sand fill structures in warm permafrost regions.

5.5 Conclusion

This paper presents a new testing method to determine CSL in partially frozen sand. A series of CID and CIU triaxial tests along with internal PWP measurement were conducted on both dense and loose sand under different temperatures and strain rates. Based on these tests, a unique CSL is established in stress (q-p') and void ratio (e-p') space for the partially frozen sand at a temperature of -3 °C as well as for the unfrozen sand. It is suggested to only perform

CIU tests to determine CSL in e-p' diagram.

In q-p' space, the temperature only affects the critical state cohesion (c'_{cs}) not the critical state friction angle (φ'_{cs}). The critical state friction angle is solely controlled by the intrinsic properties of sand grains, while the critical state cohesion is mainly associated with the pore ice and is governed by the temperature, strain rate and failure mode, particularly the brittle failure. Accordingly, the c'_{cs} increases with decreasing temperature from 23 °C to -3 °C and -10 °C, but c'_{cs} at -5 °C is close to that at -3 °C.

Both partially frozen, dense and loose specimens tend to dilate under undrained and drained conditions, and therefore the slope of CSL in e-p' space represents dilatancy of partially frozen sand, which is expressed by the critical state parameter λ_d. The λ_d increases with decrease in temperature as more ice is in contact with sand grains, leading to a denser state. However, lowering the strain rate will reduce the ice bonding and generate more sand grains contacts due to creep, resulting in a lower c'_{cs} and λ_d.

This study has contributed to the understanding of and quantification of critical state parameters of partially frozen sand, which can also benefit the construction of constitutive models for simulating behavior of partially frozen soil and the engineering design in warm permafrost regions. However, due to the limited data and testing conditions, whether the conclusions can generally be applicable to different soil and conditions remains to be examined.

5.6 Tables

Table 5-1 Estimated unfrozen water content of specimens

Temperature (°C)	Specimen	Average volumetric of water contents (%)	Average gravimetric of water contents (%)	Average volume ratio of water to ice (%)
-3	Dense	20	12	1:1
	Loose	24	16	1:1
-5	Loose	11.5	8	1:3
-10	Loose	-	-	-

Note: Loose sample at -10 °C is considered as frozen without the continuous water phase.

Table 5-2 Summary of the testing program

Series	Test ID	Initial void ratio	Initial water content (%)	Stain rate (%/min)	Confining pressure (kPa)	Drainage condition	Temperature (°C)
i	L-1	0.834	32	1	100	undrain	23
	L-2	0.834	32	1	200	undrain	23
	L-3	0.832	31	1	400	undrain	23
	L-4	0.833	32	1	400	drain	23
	D-1	0.599	23	1	100	undrain	23
	D-2	0.599	23	1	200	undrain	23
	D-3	0.597	23	1	400	undrain	23
ii	PL-1	0.835	32	1	100	undrain	-3
	PL-2	0.834	32	1	200	undrain	-3
	PL-3	0.835	32	1	400	undrain	-3
	PL-4	0.834	32	1	400	drain	-3
	PD-1	0.596	23	1	100	undrain	-3
	PD-2	0.599	23	1	200	undrain	-3
	PD-3	0.594	22	1	400	undrain	-3
iii	PL-5	0.834	32	0.1	100	undrain	-3
	PL-6	0.835	32	0.1	400	undrain	-3
	PL-7	0.834	32	1	100	undrain	-5
	FL-1	0.834	32	1	100	undrain	-10

Note: D, dense; L, loose; PL, partially frozen loose; PD, partially frozen dense; FL, frozen loose.

Table 5-3 Summary of final void ratio

Temperature (°C)	Specimen	Average final void ratio	Critical void ratio (back calculation)	Difference
23	D-1	0.596	0.775	0.179
	D-2	0.592	0.772	0.180
	D-3	0.587	0.770	0.183
-3	PD-1	0.596	0.821	0.225
	PD-2	0.594	0.816	0.222
	PD-3	0.581	0.808	0.228

Note: Average final void ratio is obtained from eq. 5-1 or 5-2; Critical void ratio is calculated from established equations of CSLs in e-p' plane.

Table 5-4 Summary of critical state parameters

Temperature (°C)	Strain rate (%/min)	φ'_{cs} (°)	M	c'_{cs} (kPa)	Γ	λ
23	1	53	1.33	0	0.872	0.014
-3	1	52	1.29	266.4	1.075	0.036
-3	0.1	53	1.33	0	1.011	0.027
-10	1	52	1.29	815.6	1.13	0.042

Note: φ'_{cs}, critical state friction angle; M, slope of CSL in q-p' plane; c'_{cs}, critical state cohesion; Γ, intercept of CSL in e-p' plane; λ, slope of CSL in e-p' plane.

5.7 Figures

FIG 5-1 Schematic of apparatus (modified from Liang et al. 2022a)

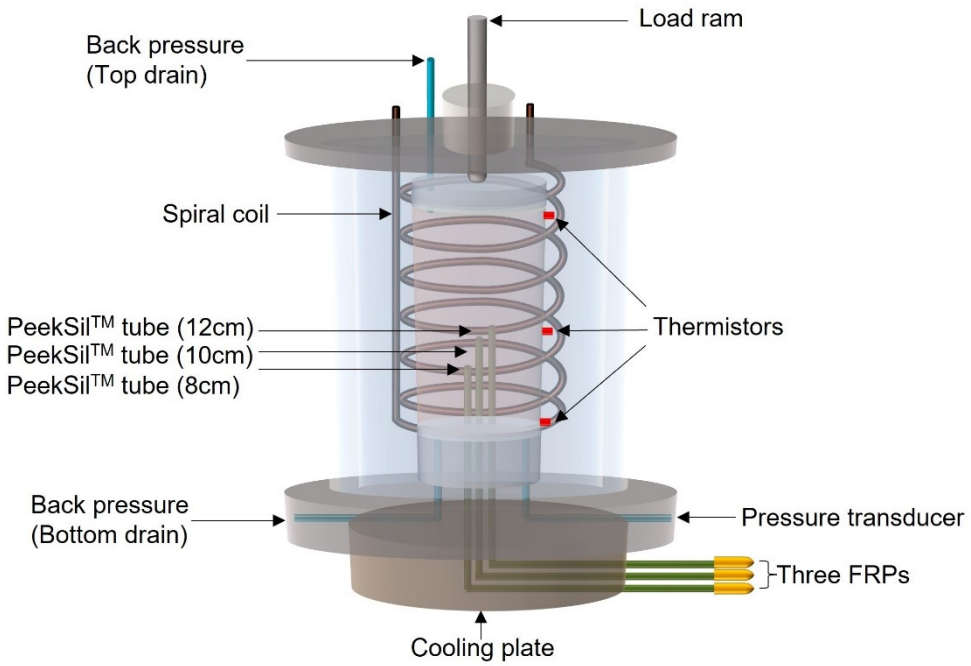

FIG 5-2 Stress and PWP response of unfrozen specimens under effective confining pressure of 400 kPa. (a) loose and (b) dense
(Note: L, unfrozen loose; D, unfrozen dense)

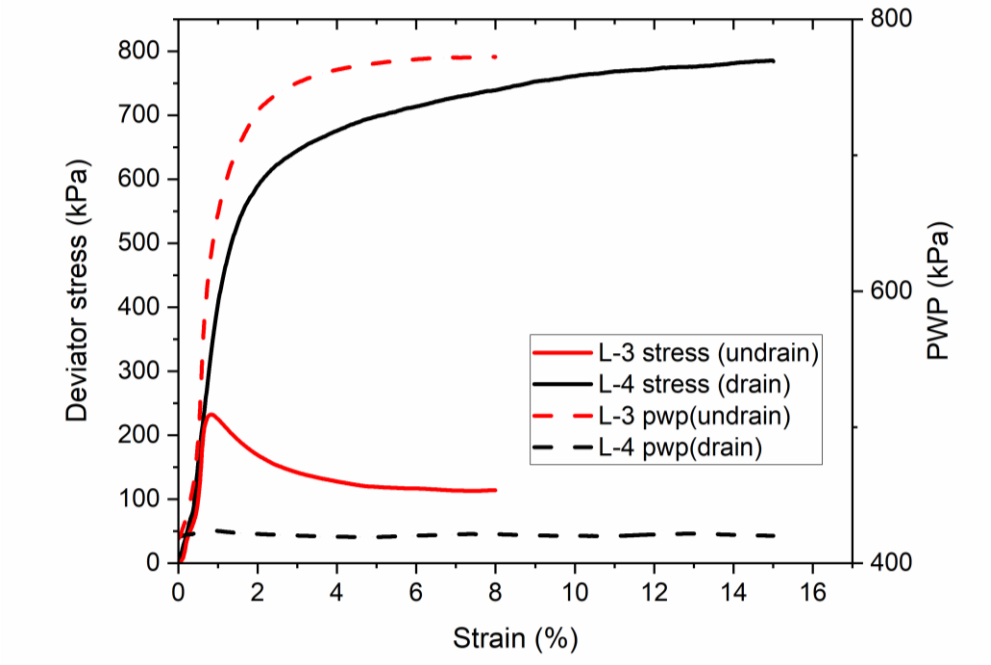

(a)

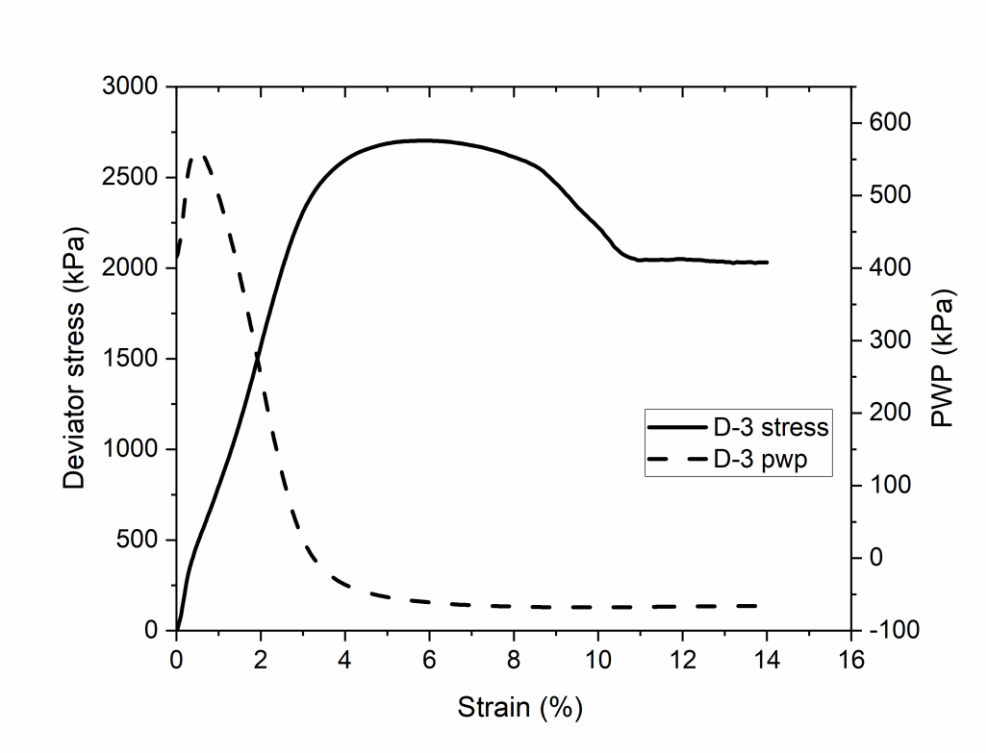

(b)

FIG 5-3 Effective stress path of unfrozen specimens

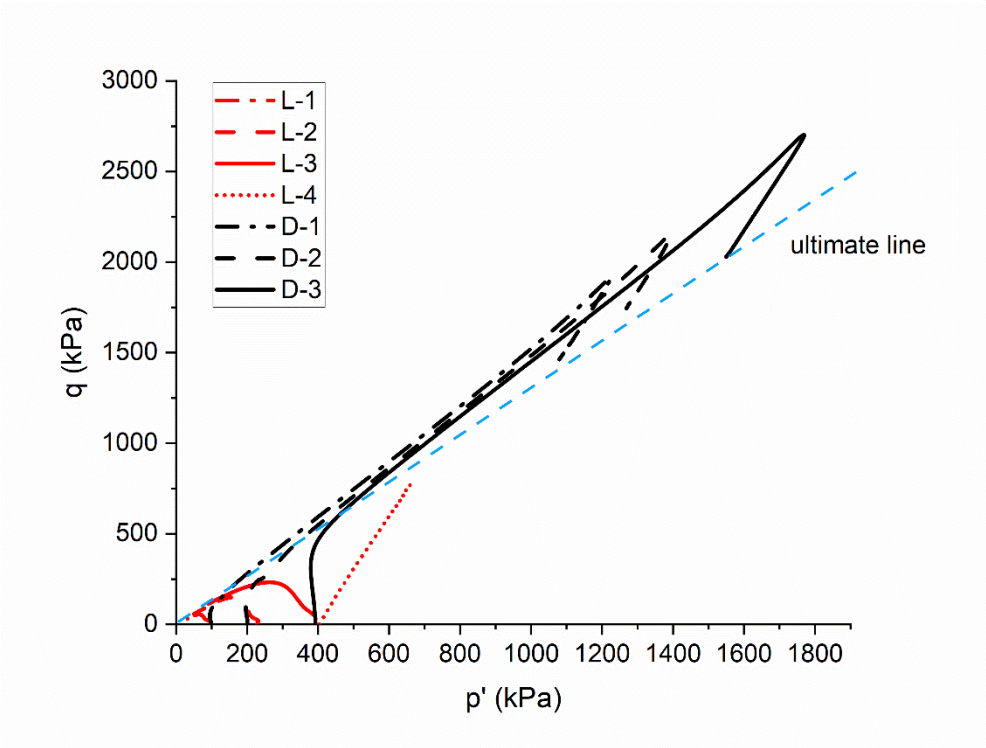

FIG 5-4 Critical state line of unfrozen specimens. (a) q-p' space and (b) e-p' space

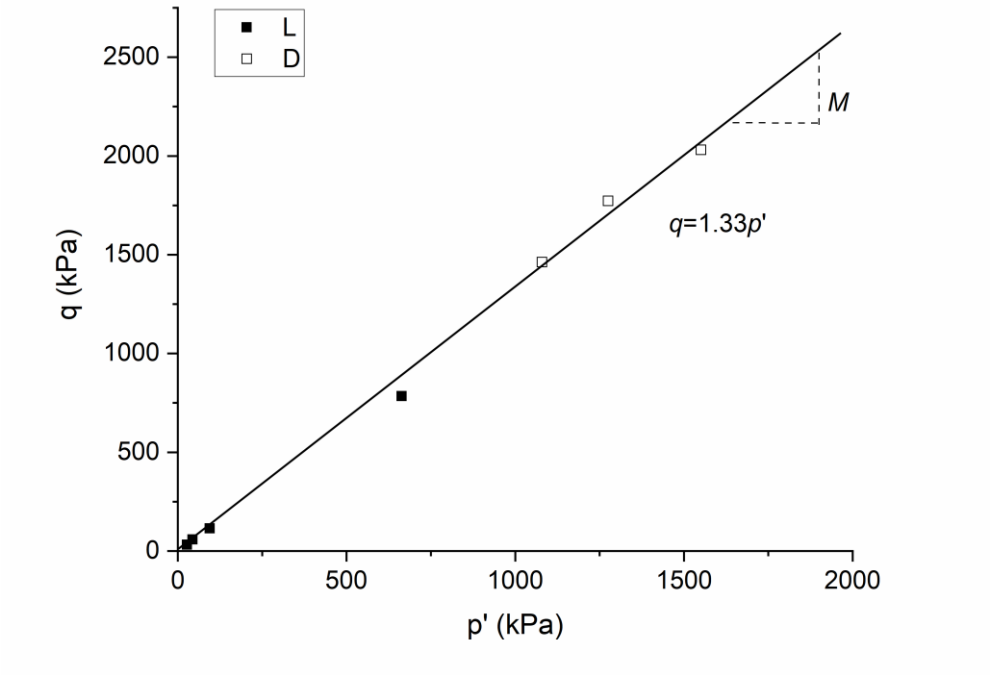

(a)

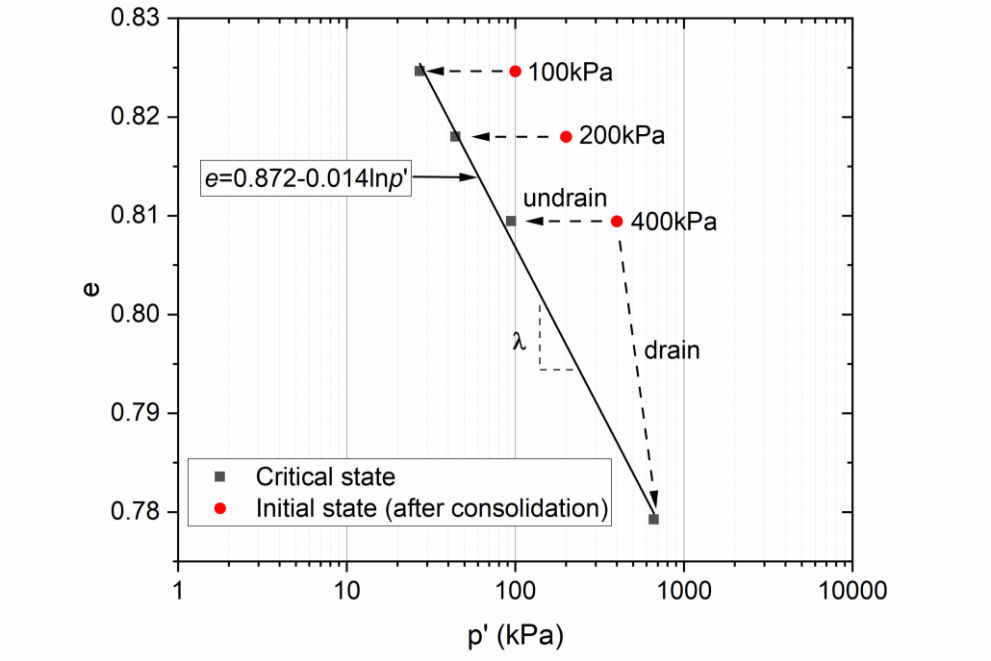

(b)

FIG 5-5 Stress and PWP response of partially frozen specimens (-3 ºC). (a) stress and (b) PWP
(Note: PL, partially frozen loose; PD, partially frozen dense)

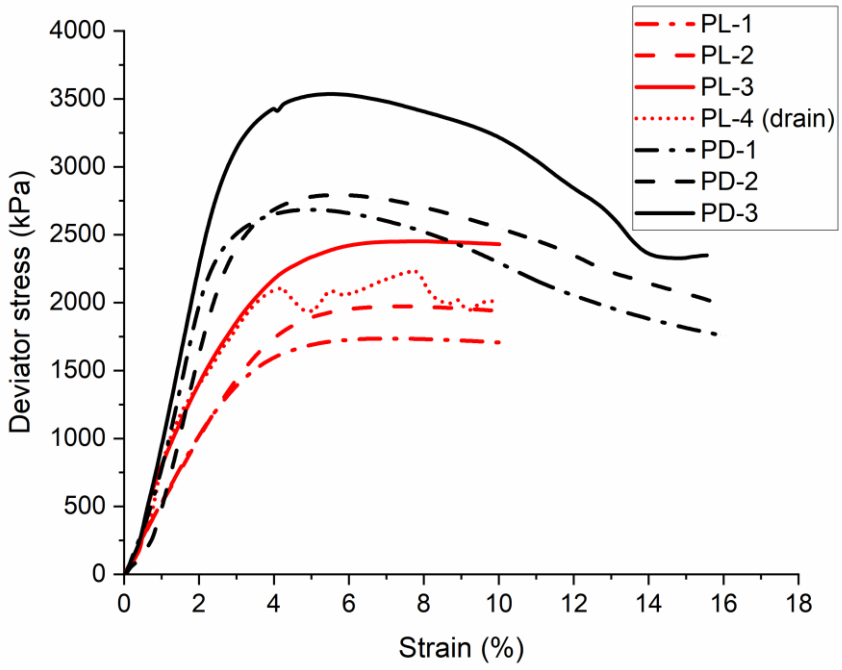

(a)

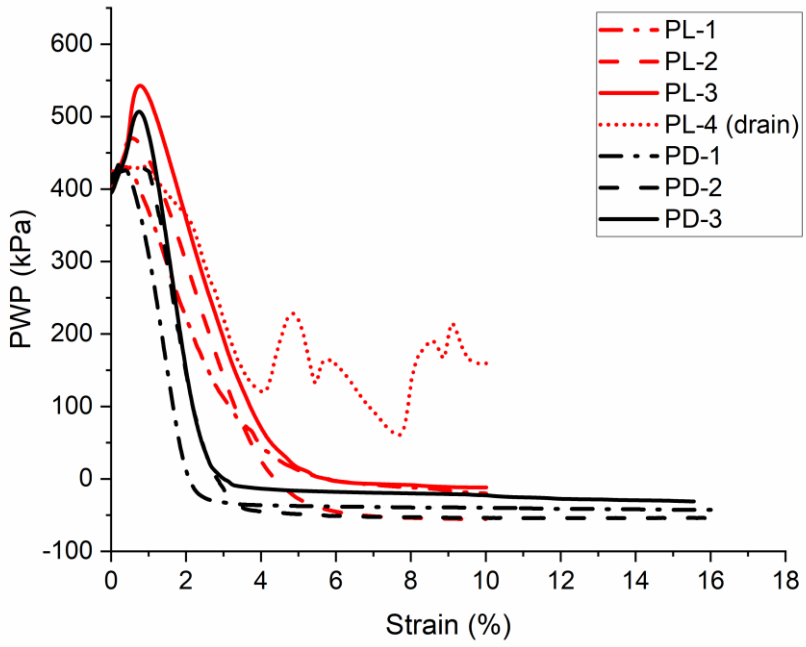

(b)

FIG 5-6 Effective stress paths of partially frozen specimens (-3 ºC). (a) loose (b) dense (c) comparison of loose and dense

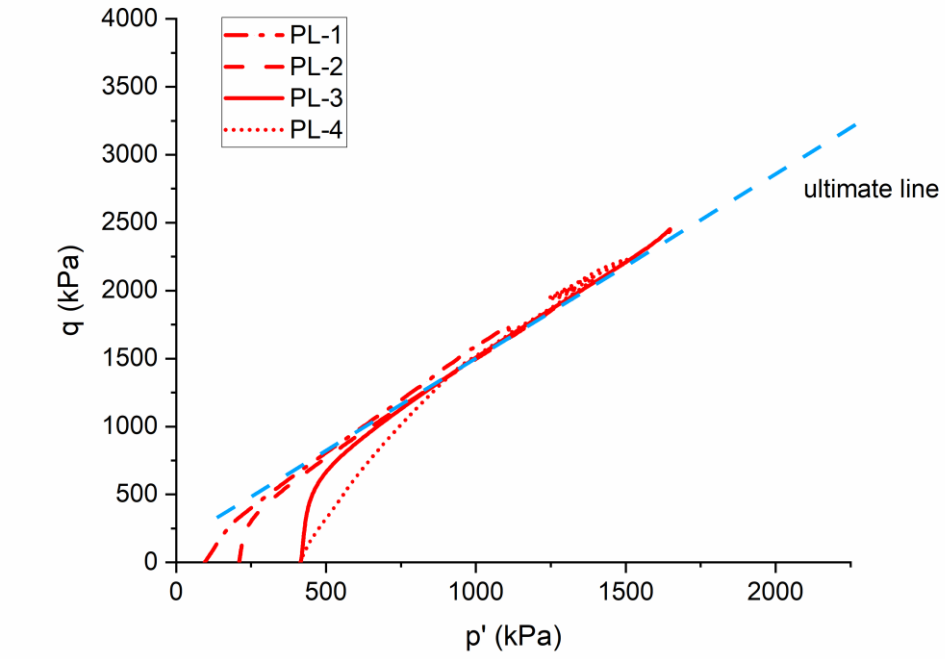

(a)

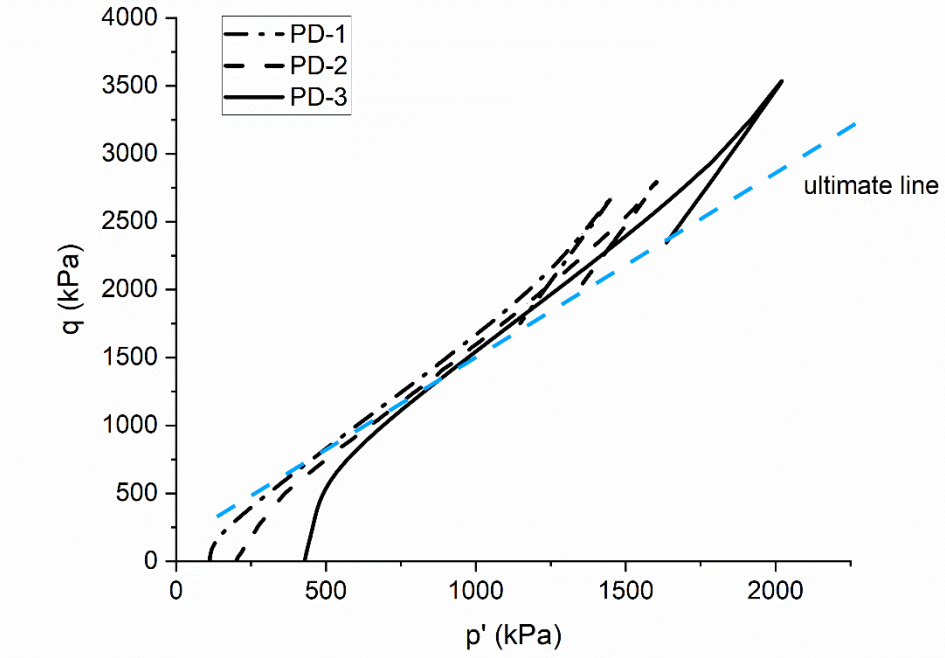

(b)

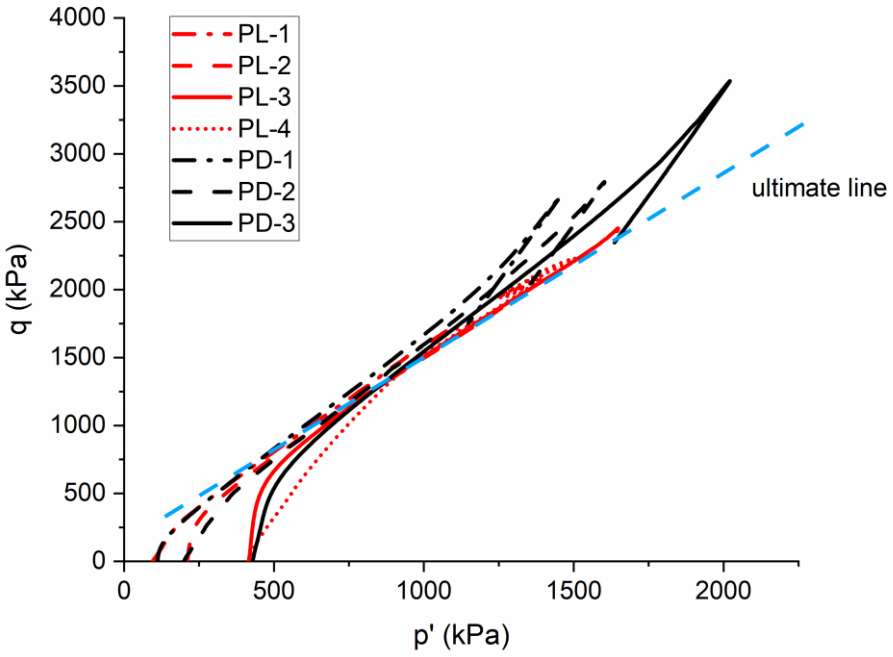

(c)

FIG 5-7 Critical state line of partially frozen specimens (-3 ºC). (a) q-p' space and (b) e-p' space

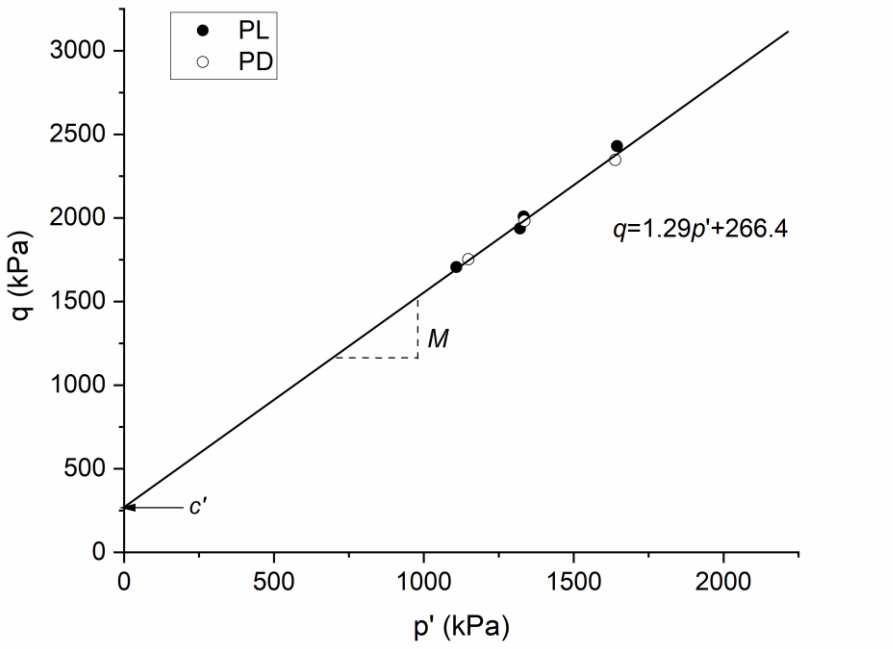

(a)

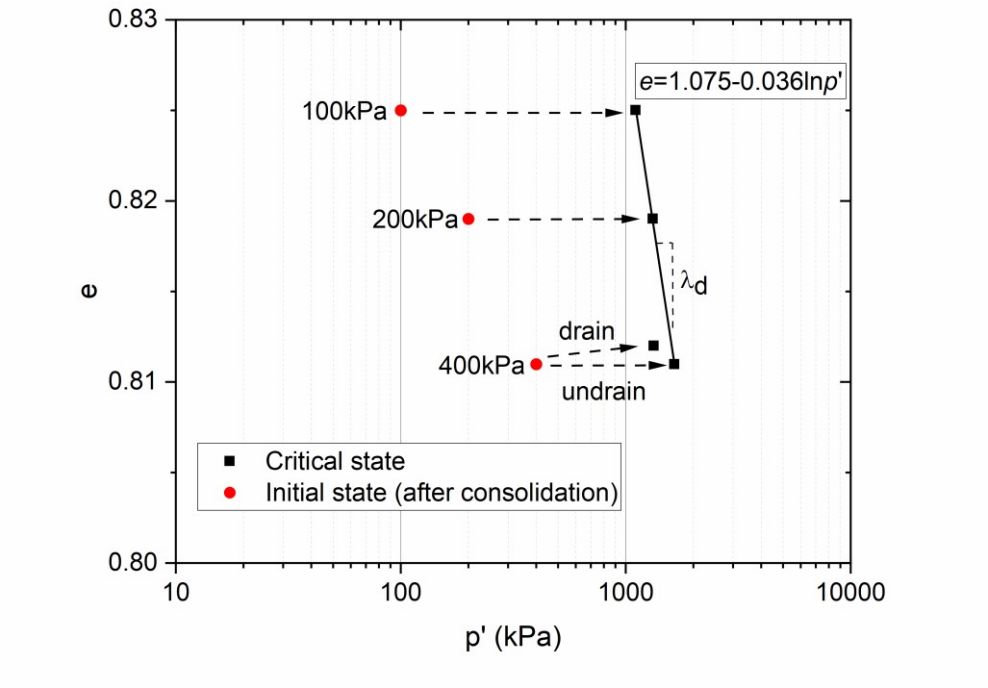

(b)

FIG 5-8 Behavior of partially frozen loose specimens under different strain rates. (a) stress and (b) PWP

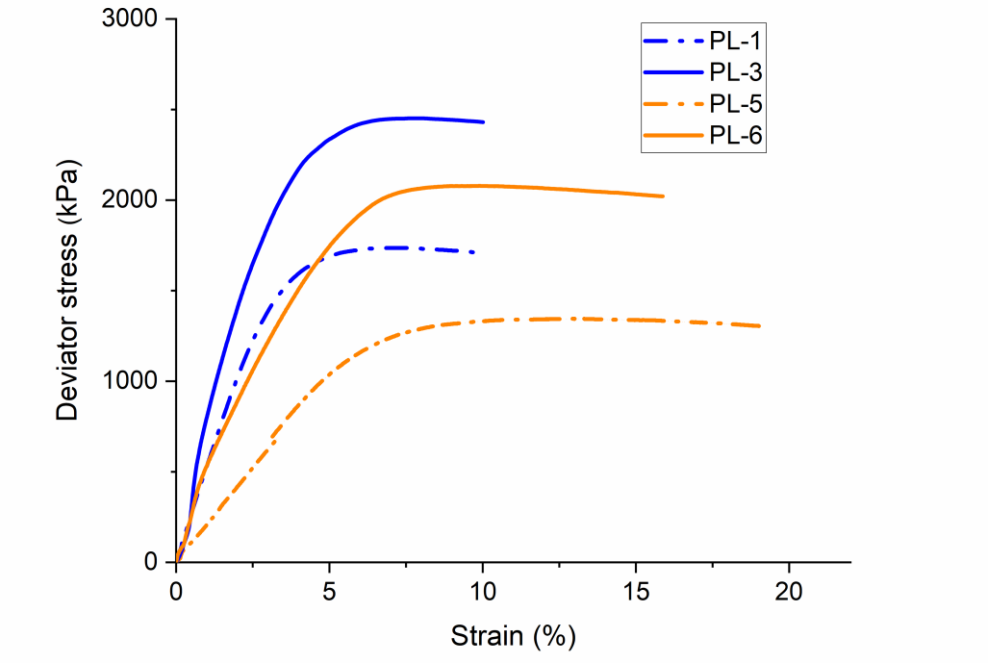

(a)

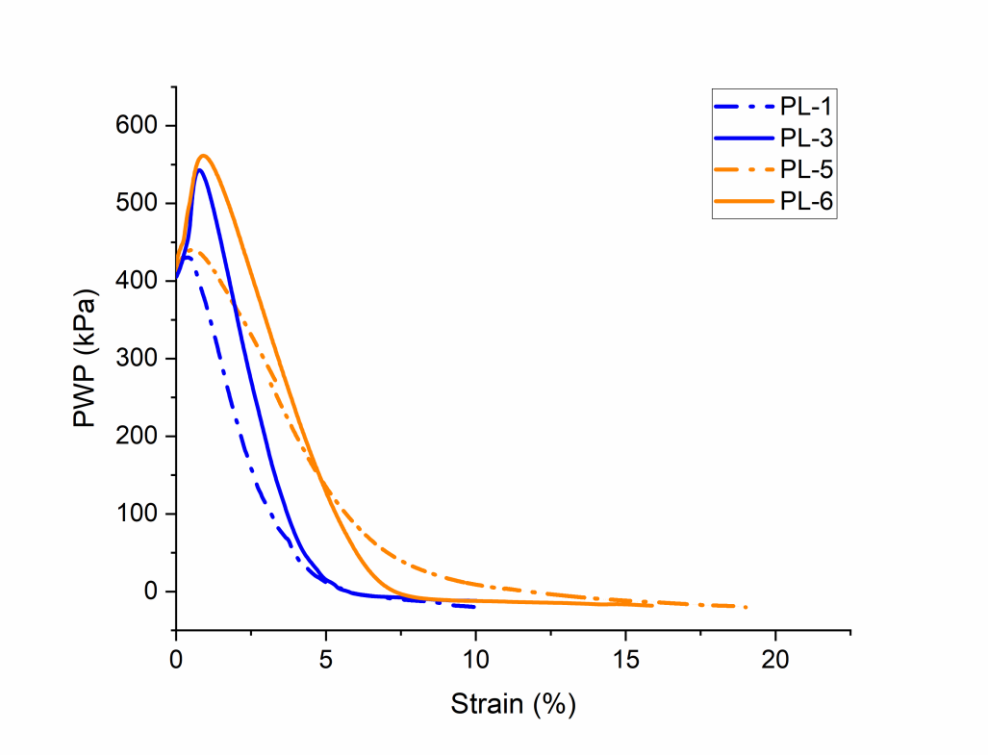

(b)

FIG 5-9 Behavior of partially frozen loose specimens under different temperatures. (a) stress and (b) PWP

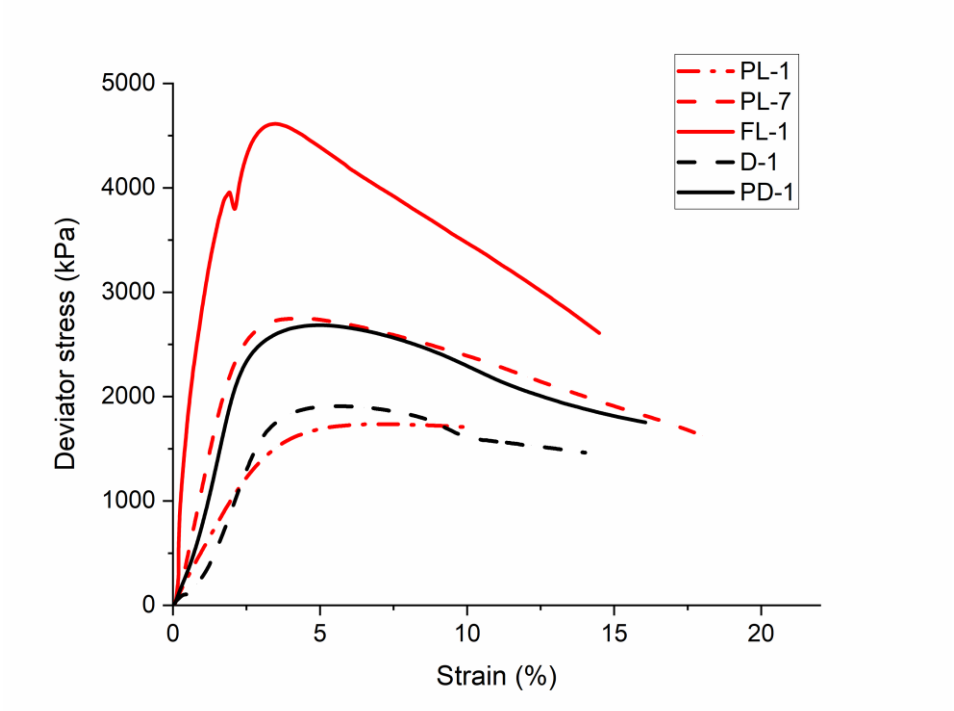

(a)

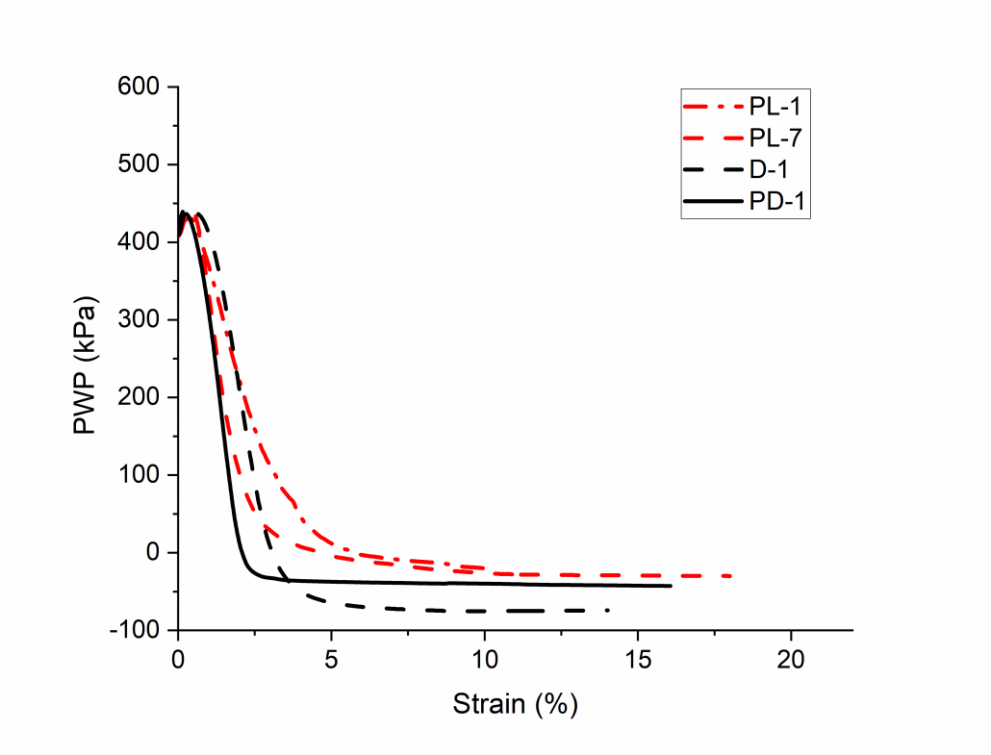

(b)

FIG 5-10 Images of samples after test. (a) PL-1, (b) PL-7, (c) FL-1.

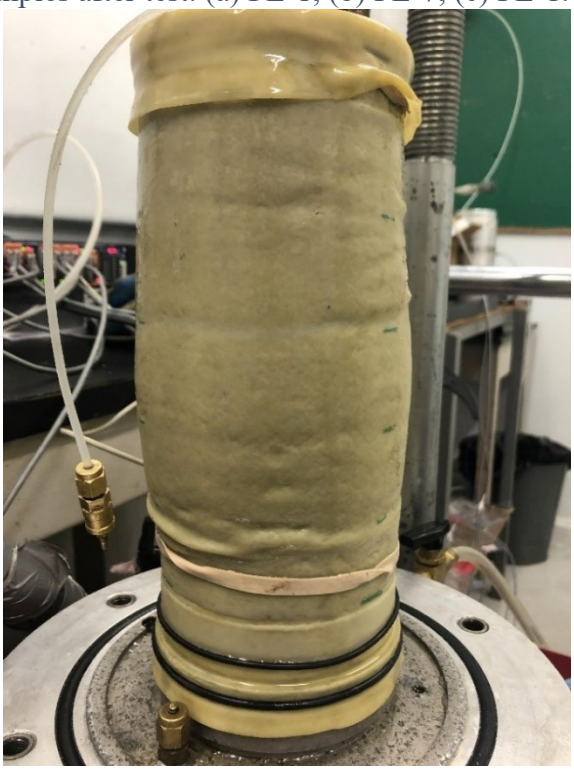

(a)

(b)

(c)

FIG 5-11 Stress paths of partially frozen loose specimens under different stain rates and temperatures. (a) partially frozen loose and (b) comparison with unfrozen dense

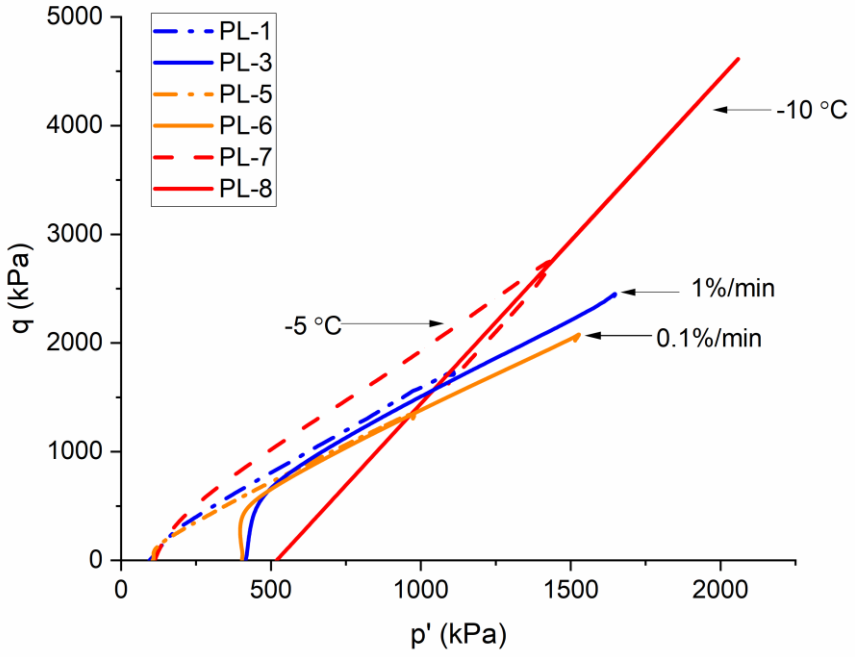

(a)

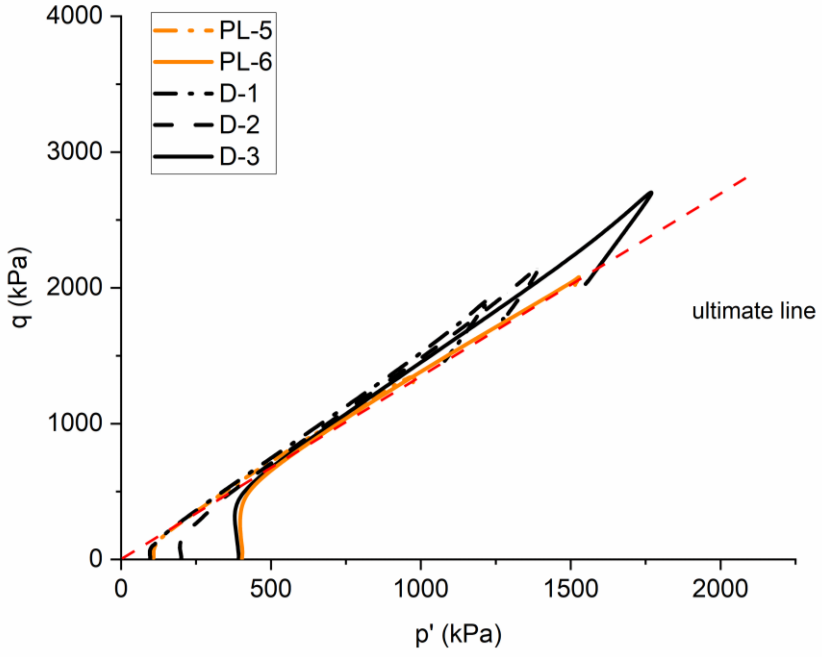

(b)

FIG 5-12 Effect of strain rate and temperature on critical state line in q-p' space

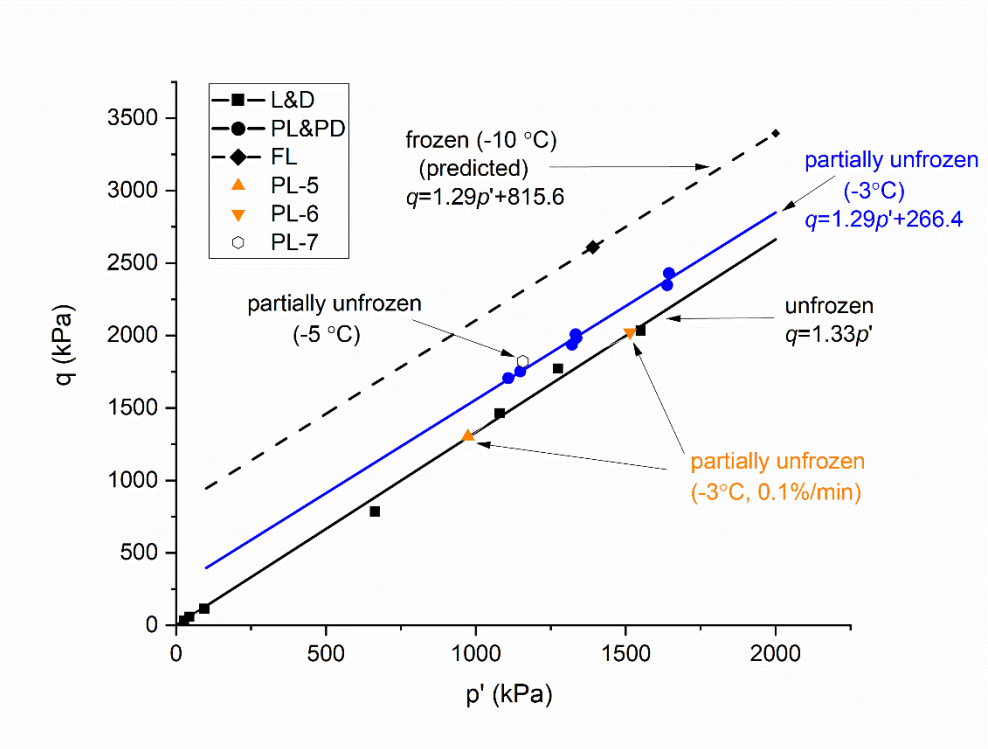

FIG 5-13 Effect of strain rate and temperature on critical state line in e-p' space

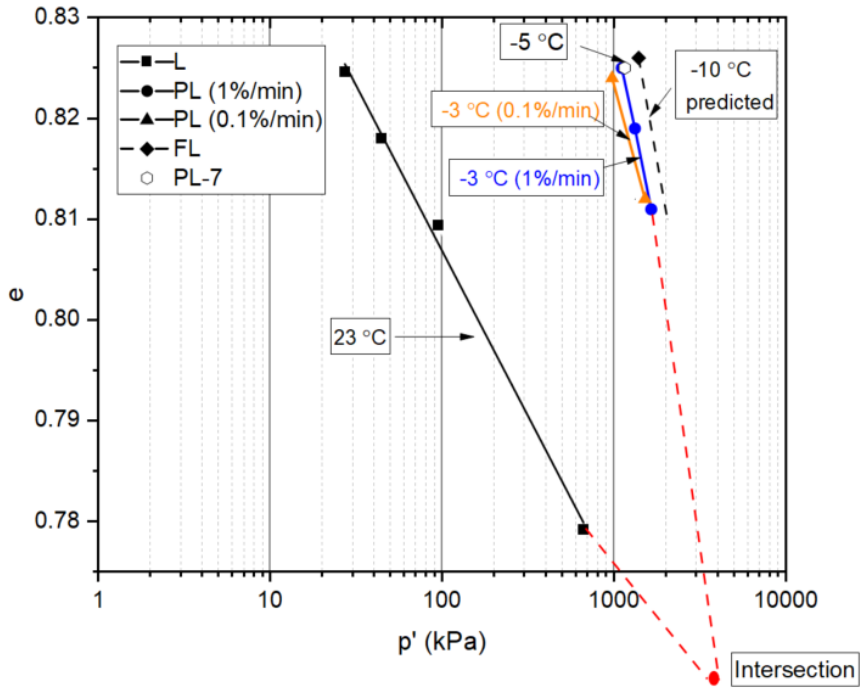

FIG 5-14 State diagram for unfrozen and partially frozen sand

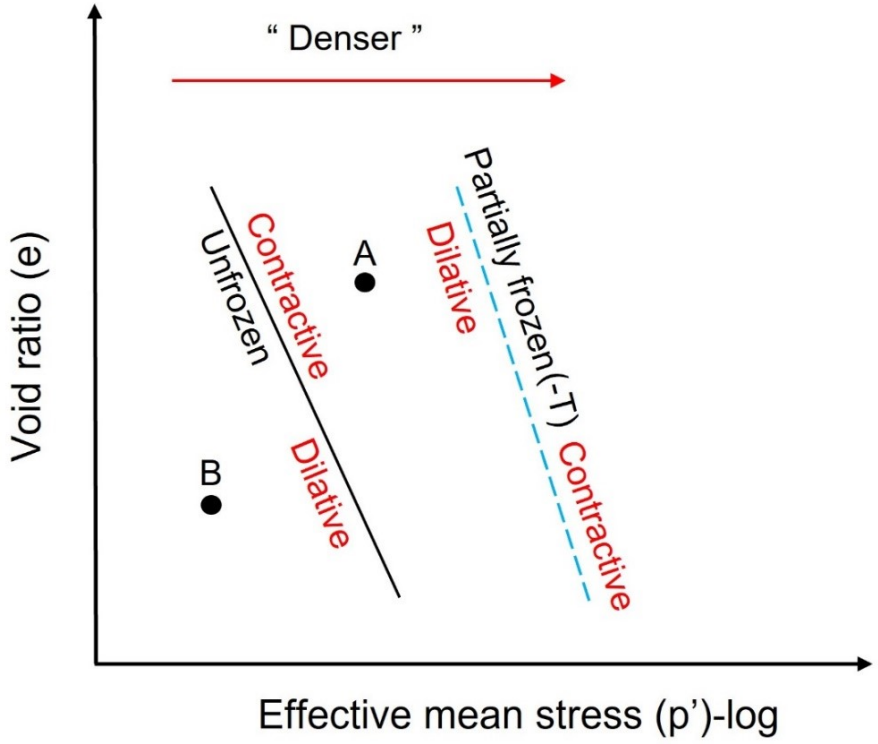

5.8 References

Allard, M., Lemay, M., Barrette, C., L'Hérault, E., Sarrazin, D., Bell, T., and Doré, G. 2012. Permafrost and climate change in Nunavik and Nunatsiavut: Importance for municipal and transportation infrastructures. Nunavik and Nunatsiavut: From science to policy. An Integrated Regional Impact Study (IRIS) of Climate Change and Modernization: 171-197.

Andersen, G.R., Swan, C.W., Ladd, C.C., and Germaine, J.T. 1995. Small-strain behavior of frozen sand in triaxial compression. Canadian Geotechnical Journal, 32(3): 428-451.

Arenson, L.U., and Springman, S.M. 2005a. Mathematical descriptions for the behaviour of ice-rich frozen soils at temperatures close to 0 ºC. Canadian Geotechnical Journal, 42(2): 431-442.

Arenson, L.U., and Springman, S.M. 2005b. Triaxial constant stress and constant strain rate testson ice-rich permafrost samples. Canadian Geotechnical Journal, 42(2): 412-430.

Arenson, L.U., and Sego, D.C. 2006. The effect of salinity on the freezing of coarse-grained

sands. Canadian Geotechnical Journal, 43(3): 325-337.

Been, K., Jefferies, M.G., and Hachey, J. 1991. The critical state of sands. Géotechnique, 41(3):365-381.

Been, K., Conlin, B., Crooks, J., Fitzpatrick, S., Jefferies, M., Rogers, B., and Shinde, S. 1987. Back analysis of the Nerlerk berm liquefaction slides: Discussion. Canadian Geotechnical Journal, 24(1): 170-179.

Blanchard, D., and Fremond, M. 1985. Soils frost heaving and thaw settlement. In Proceedings of the 4th International Symposium on Ground Freezing, Boca Raton, FL, pp. 209–216.

Bragg, R.A., and Andersland, O. 1980. Strain rate, temperature, and sample size effects on compression and tensile properties of frozen sand. Engineering Geology, 18(1-4): 35-46.

Desrues, J., Chambon, R., Mokni, M., and Mazerolle, F. 1996. Void ratio evolution inside shear bands in triaxial sand specimens studied by computed tomography. Géotechnique, 46(3): 529-546.

Ghoreishian Amiri, S., Grimstad, G., Kadivar, M., and Nordal, S. 2016. Constitutive model for rate-independent behavior of saturated frozen soils. Canadian Geotechnical Journal, 53(10): 1646-1657.

Henry, K.S. 2000. A review of the thermodynamics of frost heave. Cold Regions Research and Engineering Laboratory, US Army Corps of Engineers. Report ERDC/CRREL TR-00-16.

Hivon, E., and Sego, D. 1993. Distribution of saline permafrost in the Northwest Territories, Canada. Canadian Geotechnical Journal, 30(3): 506-514.

Hivon, E., and Sego, D. 1995. Strength of frozen saline soils. Canadian Geotechnical Journal, 32(2): 336-354.

Holubec, I. 2008. Flat loop thermosyphon foundations in warm permafrost. Government of the Northwest Territories Asset Management Division of Public Works and Services and the Climate Change Vulnerability Assessment of the Canadian Council of Professional Engineers.

Jefferies, M., and Been, K. 2015. Soil liquefaction: a critical state approach. CRC press.

Jefferies, M., Rogers, B., and Stewart, H. 1988. Island construction in the Canadian Beaufort

sea.In Hydraulic fill structures. ASCE. pp. 816-883.

Jia, J., Zheng, J. and Sun, X. 2021. The critical state parameters of sands from their image-based intrinsic properties. Acta Geotechnica, 16(12): 4081-4092.

Kia, M. 2012. Measuring Pore-water Pressure in Partially Frozen Soils. Ph.D. thesis, Faculty of Graduate Studies and Research, University of Alberta, Edmonton, AB.

Koopmans, R.W.R. 1966. Soil freezing and soil water characteristic curves. Soil Science Societyof America Journal, 30(6): 680-685

Ladanyi, B., and Morel, J.-F. 1990. Effect of internal confinement on compression strength of frozen sand. Canadian Geotechnical Journal, 27(1): 8-18.

Lai, Y., Li, S., Qi, J., Gao, Z., and Chang, X. 2008. Strength distributions of warm frozen clay and its stochastic damage constitutive model. Cold Regions Science and Technology, 53(2): 200-215.

Li, N., Chen, F., Su, B., and Cheng, G. 2002. Theoretical frame of the saturated freezing soil. Cold Regions Science and Technology, 35(2): 73-80.

Li, N., Chen, F., Xu, B., and Swoboda, G. 2008. Theoretical modeling framework for an unsaturated freezing soil. Cold Regions Science and Technology, 54(1): 19-35.

Li, N., Cheng, G.D. and Xu, X.Z., 2001. The advance and review on frozen soil mechanics. Advances in Mechanics, 31(1): 95-102.

Liang Y, Beier N, and Sego DC. 2022a. New Method for Internal Pore-Water Pressure Measurements. Geotechnical Testing Journal, 45(2): 490-502.

Liang Y, Beier N, and Sego DC. 2022b. Continuity of Pore-Water Pressure Measurements in Partially Frozen Sand. (Manuscript submitted for publication)

Lyu, C., Nishimura, S., Amiri, S.A.G., Zhu, F., Eiksund, G.R., and Grimstad, G. 2021. Pore-water pressure development in a frozen saline clay under isotropic loading and undrained shearing. Acta Geotechnica, 16(12): 3831-3847.

Melton, J.S., and Schulson, E.M. 1997. The ductile deformation of columnar (S2) saline ice undertriaxial compression. In The 7th International Offshore and Polar Engineering Conference. OnePetro.

Nishimura, S., and Wang, J. 2019. A simple framework for describing strength of saturated

frozen soils as multi-phase coupled system. Géotechnique, 69(8): 659-671.

Nishimura, S., Gens, A., Olivella, S., and Jardine, R. 2009. THM-coupled finite element analysis of frozen soil: formulation and application. Géotechnique, 59(3): 159-171.

Poulos, S.J., Castro, G., and France, J.W. 1985. Liquefaction evaluation procedure. Journal of Geotechnical Engineering, 111(6): 772-792.

Roscoe, K.H., Schofield, A., and Wroth, a.P. 1958. On the yielding of soils. Géotechnique, 8(1): 22-53.

Sasitharan, S., Robertson, P., Sego, D., and Morgenstern, N. 1993. Collapse behavior of sand. Canadian Geotechnical Journal, 30(4): 569-577.

Sayles, F.H. 1974. Triaxial constant strain rate tests and triaxial creep tests on frozen Ottawa sand. Corps of Engineers, US Army Cold Regions Research and Engineering Laboratory. Technical Report 253.

Schofield, A.N., and Wroth, P. 1968. Critical state soil mechanics. London: McGraw-hill.

Swanson, D., Murphy, D., Temmer, J., and Scaletta, T. 2021. Advancing the Climate Resilience of Canadian Infrastructure: A Review of Literature to Inform the Way Forward. International Institute for Sustainable Development.

Thomas, H.R., Cleall, P., Li, Y.C., Harris, C., and Kern-Luetschg, M. 2009. Modelling of cryogenic processes in permafrost and seasonally frozen soils. Géotechnique, 59(3): 173-184.

Ting, J.M., Torrence Martin, R., and Ladd, C.C. 1983. Mechanisms of strength for frozen sand. Journal of Geotechnical Engineering, 109(10): 1286-1302.

Vaid, Y., and Sivathayalan, S. 1997. Errors in estimates of void ratio of laboratory sand specimens. Canadian Geotechnical Journal, 33(6): 1017-1020.

Wang, J., Nishimura, S., and Tokoro, T. 2017. Laboratory study and interpretation of mechanical behavior of frozen clay through state concept. Soils and Foundations, 57(2): 194-210.

Wood, D.M. 1990. Soil behaviour and critical state soil mechanics. Cambridge university press.

Xu, X., Wang, Y., Bai, R., Fan, C., and Hua, S. 2016. Comparative studies on mechanical behaviorof frozen natural saline silty sand and frozen desalted silty sand. Cold Regions

Scienceand Technology, 132: 81-88.

Yu, F., Guo, P., and Na, S. 2022. A framework for constructing elasto-plastic constitutive modelfor frozen and unfrozen soils. International Journal for Numerical and Analytical Methods in Geomechanics, 46(2): 436-466.

Zhang, Y., and Michalowski, R.L. 2015. Thermal-hydro-mechanical analysis of frost heave and thaw settlement. Journal of Geotechnical and Geoenvironmental Engineering, 141(7): 04015027.

Zhu, Z., Ning, J., and Ma, W. 2010. A constitutive model of frozen soil with damage and numericalsimulation for the coupled problem. Science China Physics, Mechanics and Astronomy, 53(4): 699-711.

6. Summary of the Findings

6.1 Internal PWP measurements in unfrozen and partially frozen sand

A new triaxial testing method that enables the user to track the response and distribution of PWP at the specific zones within a soil was developed. By comparing the PWP measurements between the FRPs and a base transducer in both saturated unfrozen, dense and loose specimens, it is demonstrated that the FRPs provide a reliable PWP response in consolidated, undrained triaxial tests. The comparison improved especially when the pressure is above 400 kPa where the FRPs have a faster response than the base transducer. This method can also provide insight into the local stress variation via the incremental change in the internal PWP.

Since the heavy mineral oil, which is used as the piezometer fluid of the FRPs in unfrozen sand, has a high viscosity, resulting in a low rigidity and conductivity at the sub-zero temperature, a light mineral oil is therefore recommended to fill in the FRPs for measuring the internal PWP of partially frozen sand. Continuity in the water phase within a specimen at the subfreezing temperature is confirmed throughout the tests by the consistent PWP measurements between the FRPs and the base transducer. The pore ice is found to attribute to the shear-induced dilation and the continuous decrease in PWP of partially frozen, loose specimens, while the pore ice has no apparent impact on Skempton's B value in both partially frozen, loose and dense specimens.

6.2 Stress distribution and relationship between the pore ice, unfrozen water, and soil skeleton at -3 °C

The pore ice stress was estimated using Ladanyi and Morel's (1990) postulate that the soil skeleton carries the same amount of stress in both frozen and unfrozen states when the frozen and unfrozen sand specimens share the same strain history. The results of the deviator stress of the pore ice indicate that the behavior of the partially frozen loose, and dense sand is mainly controlled by the pore ice and soil skeleton, respectively. One the other hand, the values of the minor principal stress of the pore ice reveal that the pore ice is under compression in partially frozen, loose sand, but under tension in partially frozen, dense sand (after 4 % of strain).

In partially frozen, loose sand, the pore ice and pore water are in a competitive relationship: the pore ice gradually takes over the applied confining pressure while the PWP continuously decreases until the specimen failure; the change of minor principal stress (hydrostatic) in the pore ice is reflected by an equal change in the PWP. Pore ice strength, soil strength, dilatancy of the pore ice, and structural hindrance are four main mechanisms involved in partially frozen, loose sand.

In partially frozen, dense sand, the pore ice and pore water are in a collaborative relationship: the tension caused by the dilation of the soil skeleton is shared between the pore ice and pore water. Pore ice strength, soil strength, dilatancy of soil skeleton, and structural hindrance are four main mechanisms contributing to the strength of partially frozen, dense sand.

6.3 Effect of pore ice and pore water on the strength of partially frozen sand at -3 ºC

Based on Ladanyi and Morel's (1990) concept of internal confinement in frozen sand, a Mohr–Coulomb model that provides a bridge between unfrozen and partially frozen sand is proposed to estimate the strength of partially frozen sand. The model explains how the PWP (suction) affects the strength of partially frozen, loose sand by increasing the confining pressure, while the pore ice influences the effective cohesion. It also shows how the pore ice affects the peak strength of partially frozen, dense sand by adding an internal confining pressure and by contributing to the effective cohesion.

6.4 CSL of partially frozen sand at -3 ºC

When the ice-sand system is treated as a solid phase, the effective stress is accurately obtained by measuring PWP in partially frozen sand, providing the continuity in the water phase. Then, a unique CSL is established in stress (q-p') and void ratio (e-p') space for partially frozen sand via a series of CID and CIU triaxial tests. It is suggested to only perform the partially frozen, loose specimens under CIU tests to determine CSL in e-p' space, because the specimen exhibits dilatant tendency under the CID condition, and hence cannot expand the range of CSL.

Compared with CSL of unfrozen sand, the CSL of partially frozen sand has a similar slope (M) or critical state friction angle (φ'_{cs}), but a non-zero interception, which is defined as the critical state cohesion resulting from the pore ice. Since both partially frozen, dense and loose sand exhibit or tend to dilate under CID and CIU triaxial conditions, the slope (λ_d) of CSL in e-

p'space represents dilatancy of partially frozen sand.

6.5 Effect of temperature on mechanical properties of partially frozen sand

The temperature has a profound impact on the behavior of partially frozen, loose sand. With a decrease in temperature, the ice content and cementing of pore ice increases, resulting in a more brittle behavior at a colder temperature. Meanwhile, the pore ice in contact with the soil grains contributes to a denser state behavior, so the behavior of partially frozen, loose sand is gradually close to that of partially frozen, dense sand. For example, the stress response and effective stress path of partially frozen, loose specimen, at -5 ºC is similar to that of partially frozen, dense specimen, at -3 ºC. In addition, the effective strength parameter of ice cohesion is strongly dependent on the temperature, but the effective friction angle is independent of the temperature, particularly the residual or critical state friction angle (φ'_{cs}) which is the intrinsic property of soil grains.

6.6 Effect of strain rate on mechanical properties of partially frozen sand

With the decrease in strain rate, the cementing of pore ice gradually decreases as more contacts between the sand grains are created via creep, and the effective ice cohesion will eventually approach zero. Moreover, the specimen become less dilative at a lower strain rate, leading to a lower λ_d than that at a higher strain rate. However, the strain rate has no effect on the effective friction angle of partially frozen sand.

6.7 Practical significance of the findings of this research

- The proposed new testing method is able to capture the PWP at the specific zone, such as the shear band or failure surface, which will help to estimate the shear strength at the failure zone and hence slope stability;
- Validity of the continuity in the water phase within partially frozen soil is the confirmation that effective stress analysis can be carried out in warm permafrost region;
- Stress distribution between the pore ice, unfrozen water, and soil skeleton assists in understanding the influence of each soil phase on the mechanical behavior of partially frozen soil as well as the development of constitutive models;
- The proposed Mohr–Coulomb model bridges the mechanical properties of soil between unfrozen and partially frozen states and can predict the strength of partially frozen soil;
- The method of establishing CSL in partially frozen sand is significant for comprehending critical state behavior of soil in warm permafrost regions.

Overall, this study will be extremely helpful for the engineering community to understand mechanical behavior and mechanism of partially frozen soil and hence to evaluate existing infrastructures as well as design for new soil structures to withstand climate change in warm permafrost regions based on effective stress approach.

7. Limitations

7.1 Internal PWP measurements

Although the continuity in the water phase within partially frozen sand is confirmed by the consistent PWP measurements between the FRPs and the base transducer, there are some erratic measurements from the FRPs due to the blockage of measuring tubes, especially in partially frozen, loose sand. This is because the measuring tubes are continuously compressed in the partially frozen tests even after failure, so the small particles (ice crystals or mineral grains) are likely blocking the tip of the tube. If these anomalies are not recognized and are considered as the true response, it will affect the interpretation of PWP measurements and hence the validity of the continuity in the water phase.

The "coldest" temperature for which the continuous water phase exists is -5 ^{o}C in this study, but this does not mean -5 ^{o}C is the "coldest" temperature for this type of material to have the continuous water phase. So, the minimum unfrozen water content and the corresponding temperature to establish the continuous water phase in partially frozen sand are unclear at present and need further investigation.

7.2 Estimation of pore ice stress

In this study, the term "pore ice stress" is used to represent the overall stress caused by the pore ice. According to Ladanyi and Morel's (1990) postulate that the soil skeleton carries the same amount of stress in both frozen and unfrozen states when the soil has undergone the same strain

history, the pore ice stress is equal to the difference between the effective stress tensor of the partially frozen soil and unfrozen soil. However, the ice strength, and the mechanical interactions between the pore ice and soil skeleton (i.e., dilatancy and hindrance effects) cannot be separately quantified in this way. Additionally, the adhesion strength between the pore ice and soil grains increases with decrease in temperature, and the pore ice stress is not supposed to be separate from the stress of the ice-soil system if the pore ice and soil skeleton deform simultaneously when the adhesion strength is strong enough.

7.3 Determination of critical void ratio

In partially frozen, loose sand, the critical void ratio is considered the same as the global (or average) final void ratio, which is calculated from the final volume of pore water by assuming that the void ratio is not altered during the rapid freezing and subsequent warming processes. However, the shear-induced dilation is observed based on the PWP response and failure mode, and the critical void ratio would not be equal to the global final void ratio if the voids within the shear zones are expanded because of stain localization. Especially, as a shear band forms in a partially frozen, loose sand at temperature of -5 ^{o}C, so the local void ratio rather than global void ratio should be used to represent the critical void ratio. To address this issue, other lab techniques are required to ascertain the local void ratio, such as micro tomography.

7.4 Future scope of the work

- Improving the method to minimize the erratic measurements from the FRPs;
- Investigating minimum unfrozen water content required to establish the continuous

water phase in partially frozen soil;

- Investigating the effect of salinity and ice content on the mechanical properties of partially frozen soil;
- Extending the internal PWP measurements in fine-graded soil close to 0 ^{o}C;
- Technologies, such as micro tomography, are needed to demine the local internal void ratio;

References

Anderson, D.M., and Morgenstern, N.R. 1973. Physics, chemistry, and mechanics of frozen ground : a review. In 2nd International Conference on Permafrost. National Academy of Science, Washington, D.C., Yakutsk, USSR, pp. 257-288.

Anderson, C.D. and Eldridge, T.L. 2012. Critical state liquefaction assessment of an upstream constructed tailings sand dam. 14th International Conference on Tailings and Mine Waste, Vail, CO, United states, pp. 101-112.

Arenson, L.U., and Sego, D.C. 2006. The effect of salinity on the freezing of coarse-grained sands. Canadian Geotechnical Journal, 43(3): 325-337.

Arenson, L.U., and Springman, S.M. 2005. Triaxial constant stress and constant strain rate testson ice-rich permafrost samples. Canadian Geotechnical Journal, 42(2): 412-430.

Alkire, B.D., and Andersland, O.B. 1973. The effect of confining pressure on the mechanical properties of sand–ice materials. Journal of Glaciology, 12(66): 469-481.

Allard, M., Lemay, M., Barrette, C., L'Hérault, E., Sarrazin, D., Bell, T., and Doré, G. 2012. Permafrost and climate change in Nunavik and Nunatsiavut: Importance for municipal and transportation infrastructures. Nunavik and Nunatsiavut: From science to policy. An Integrated Regional Impact Study (IRIS) of climate change and modernization: 171-197.

Allard, M., Gibéryen, T., L'Hérault, E., and Sarrazin, D. 2009. L'impact des changements climatologiques sur laproblématique de la fonte du pergélisol au village de Salluit, Nunavik Rapport d'étape au MAMROT, pp. 41.

Andersen, G.R., Swan, C.W., Ladd, C.C., and Germaine, J.T. 1995. Small-strain behavior of frozen sand in triaxial compression. Canadian Geotechnical Journal, 32(3): 428-451.

Arenson, L.U., and Springman, S.M. 2005a. Mathematical descriptions for the behaviour of ice-rich frozen soils at temperatures close to 0 ºC. Canadian Geotechnical Journal, 42(2): 431-442.

Arenson, L.U., and Springman, S.M. 2005b. Triaxial constant stress and constant strain rate tests on ice-rich permafrost samples. Canadian Geotechnical Journal, 42(2): 412-430.

Arenson, L.U., and Sego, D.C. 2006. The effect of salinity on the freezing of coarse-grained sands. Canadian Geotechnical Journal, 43(3): 325-337.

Atkinson, J. H, and D. Richardson. 1987. The Effect of Local Drainage in Shear Zones on the Undrained Strength of Overconsolidated Clay, Géotechnique 37(3): 393–403.

Baker, T., Jones, S., and Parameswaran, V. 1981. Confined and unconfined compression tests on frozen sands. The Roger JE Brown Memorial Volume. In Proc. 4th Canadian Permafrost Conference, Calgary, Alberta, pp. 2-6.

Barden, L. 1965. Consolidation of compacted and unsaturated clays. Géotechnique, 15(3): 267-286.

Been, K., Conlin, B., Crooks, J., Fitzpatrick, S., Jefferies, M., Rogers, B., and Shinde, S. 1987. Back analysis of the Nerlerk berm liquefaction slides: Discussion. Canadian Geotechnical Journal, 24(1): 170-179.

Been, K., Jefferies, M.G., and Hachey, J. 1991. The critical state of sands. Géotechnique, 41(3): 365-381.

Biermans, M.B.G.M., Dijkema, K.M. and De Vries, D.A. 1978. Water movement in porous media towards an ice front. Journal of Hydrology, 37(1-2):137-148.

Black, P.B. 1995. Applications of the Clapeyron equation to water and ice in porous media. Cold Regions Research and Engineering Laboratory, U. S. Army Corps of Engineers, Hanover, NH, USA, Report 95-6.

Blanchard, D. and Fremond, M. 1985. Soil frost heaving and thaw settlement. In Proceedings of the 4th International Symposium on Ground Freezing, Boca Raton, FL, pp. 209–216.

Bourbonnais, J., and Ladanyi, B. 1985. The mechanical behaviour of frozen sand down to cryogenic temperatures. In Proceedings of 4th International Symposium on Ground Freezing, Boca Raton, FL, pp, pp. 235-244.

Boyle, J., Cunningham, M., and Dekens, J. 2013. Climate Change Adaptation and Canadian Infrastructure: A review of the literature. International Institute for Sustainable Development, Manitoba, Canada.

Bragg, R.A., and Andersland, O. 1980. Strain rate, temperature, and sample size effects on compression and tensile properties of frozen sand. Engineering Geology, 18(1-4):35-46.

Chae, D., Hwang, B., and Cho, W. 2015. Stress-strain-strength characteristics of frozen sands with various fine contents. Journal of the Korean GEO-environmental Society, 16(6): 31-38.

Chamberlain, E., Groves, C., and Perham, R. 1972. The mechanical behaviour of frozen earth materials under high pressure triaxial test conditions. Géotechnique, 22(3): 469-483.

Cheng, X. H. 2004. Localization in Dutch Dune Sand and Organic Clay. PhD diss., Delft University of Technology.

PIEVC. 2008. Adapting to climate change, Canada's first national engineering vulnerability assessment of public infrastructure. Canadian Council of Professional Engineers.

Damm, B., and Felderer, A. 2013. Impact of atmospheric warming on permafrost degradation and debris flow initiation: A case study from the eastern European Alps. E and G Quaternary Science Journal, 62(2): 136-149.

Dash, J.G., Rempel, A.W. and Wettlaufer, J.S. 2006. The physics of premelted ice and its geophysical consequences. Reviews of modern physics, 78(3): 695-741.

Desrues, J., Chambon, R., Mokni, M., and Mazerolle, F. 1996. Void ratio evolution inside shear bands in triaxial sand specimens studied by computed tomography. Géotechnique, 46(3): 529-546.

Du, H., Ma, W., Zhang, S., Zhou, Z., and Liu, E. 2016. Strength properties of ice-rich frozen silty sands under uniaxial compression for a wide range of strain rates and moisture contents. Cold Regions Science and Technology, 123: 107-113.

Eigenbrod, K.D., Knutsson, S., and Sheng, D. 1996. Pore-Water Pressures in Freezing and Thawing Fine-Grained Soils. Journal of Cold Regions Engineering, 10(2): 77-92.

Enokido, M., and Kameta, J. 1987. Influence of water content on compressive strength of frozen sands. Soils and Foundations, 27(4): 148-152.

Ghoreishian Amiri, S., Grimstad, G., Kadivar, M., and Nordal, S. 2016. Constitutivemodel for rate-independent behavior of saturated frozen soils. Canadian Geotechnical Journal, 53(10): 1646-1657.

Government of the Northwest Territories. (2008). NWT climate change impacts and adaptation report. Yellowknife, NWT: Environment and Natural Resources.

Goughnour, R.R., and Andersland, O. 1968. Mechanical properties of a sand-ice system. Journal of the Soil Mechanics and Foundations Division, 94(4): 923-950.

Gylland, A. S., H. P. Jostad, and S. Nordal. 2013. Experimental Study of Strain Localization in Sensitive Clays. Acta Geotechnica. 9(2): 227–40.

Han, C, and I. G. Vardoulakis. 1991. Plane-Strain Compression Experiments on Water-Saturated Fine- Grained Sand. Géotechnique 41 (1): 49–78.

Harris, C., and Davies, M.C.R. Pressures recorded during laboratory freezing and thawing of a natural silt-rich soil. In Seventh International Conference on Permafrost, Yellowknife, NWT, Canada, June. 1998. pp. 23-27.

Hanzawa, H. 1980. Undrained strength and stability analysis for a quick sand. Soils and Foundations , 20(2):17-29.

Hazirbaba, K., Zhang, Y., and Hulsey, J.L. 2011. Evaluation of temperature and freeze–thaw effects on excess pore pressure generation of fine-grained soils. Soil dynamics and earthquake engineering, 31(3): 372-384.

Heginbottom, J., Dubreuil, M., and Harker, P. 1995. Canada, Permafrost. National Atlas of Canada. Geomatics Canada, National Atlas Information Service, and Geological Survey of Canada: Ottawa; Plate 2.1 (MCR 4177).

Henry, K.S. 2000. A review of the thermodynamics of frost heave. Cold Regions Research and Engineering Laboratory, US Army Corps of Engineers. Report ERDC/CRREL TR-0016.

Hivon, E.G. and D.C. Sego. 1993. Distribution of Saline Permafrost in the Northwest Territories, Canada. Canadian Geotechnical Journal. 30(3): 506–14.

Hivon, E., and Sego, D. 1995. Strength of frozen saline soils. Canadian Geotechnical Journal, 32(2): 336-354.

Holubec, I. 2008. Flat loop thermosyphon foundations in warm permafrost. Government of the Northwest Territories Asset Management Division of Public Works and Services and the Climate Change Vulnerability Assessment of the Canadian Council of Professional Engineers.

Imam, S.R., Morgenstern, N.R., Robertson, P.K. and Chan, D.H. 2005. A critical-state constitutive model for liquefiable sand. Canadian geotechnical journal, 42(3): 830-855.

Ishihara, K. 1993. Liquefaction and flow failure during earthquakes. Geotechnique, 43(3): 351-451.

Jefferies, M.G. 1993. Nor-Sand: a simple critical state model for sand. Géotechnique, 43(1): 91-103.

Jefferies, M. and K. Been. 2015. Soil Liquefaction: A Critical State Approach. 2nd ed. Boca Raton, CRC press. US.

Jefferies, M., Rogers, B., and Stewart, H. 1988. Island construction in the Canadian Beaufort sea.In Hydraulic fill structures. ASCE. pp. 816-883.

Jia, J., Zheng, J. and Sun, X. 2021. The critical state parameters of sands from their image-based intrinsic properties. Acta Geotechnica, 16(12): 4081-4092.

Kalifa, P., Ouillon, G., and Duval, P. 1992. Microcracking and the failure of polycrystalline ice under triaxial compression. Journal of Glaciology, 38(128): 65-76.

Kia, M. 2012. Measuring Pore-water Pressure in Partially Frozen Soils. Ph.D. thesis, Faculty of Graduate Studies and Research, University of Alberta, Edmonton, AB.

Kokelj, S., Tunnicliffe, J., Lacelle, D., Lantz, T., Chin, K., and Fraser, R. 2015. Increased precipitation drives mega slump development and destabilization of ice-rich permafrost terrain, northwestern Canada. Global and Planetary Change, 129: 56-68.

Koopmans, R.W.R. 1966. Soil freezing and soil water characteristic curves. Soil Science Societyof America Journal, 30(6): 680-685.

Konrad, J.M. 1989. Pore water pressure at an ice lens: Its measurement and interpretation. Cold Regions Science and Technology, 16(1): 63-74.

Kuerbis, R. H. 1989. The Effect of Gradation and Fines Content on the Undrained Loading Response of Sand. Ph.D. thesis, University of British Columbia.

Kuribayashi, E. 1985. Stress-strain characteristics of an artificially frozen sand in uniaxially compressive tests. Proceedings of the Fourth International Symposium on Ground Freezing, Sapporo, Japan, 2:177-182.

Ladanyi, B., and Morel, J.-F. 1990. Effect of internal confinement on compression strength of frozen sand. Canadian Geotechnical Journal, 27(1): 8-18.

Laxton, S., and Coates, J. 2010. Geophysical and borehole investigations of permafrost conditions associated with compromised infrastructure in Dawson and Ross River, Yukon. Yukon Exploration and Geology: 135-148.

Lai, Y., Li, S., Qi, J., Gao, Z., and Chang, X. 2008. Strength distributions of warm frozen clay and its stochastic damage constitutive model. Cold Regions Science and Technology, 53(2): 200-215.

Lewkowicz A. G., and Harris C. 2005a. Frequency and magnitude of active-layer detachment failures in discontinuous and continuous permafrost, northern Canada.Permafrost and Periglacial Processes, 16(1):115-130

Lewkowicz A. G., and Harris C. 2005b. Morphology and geotechnique of active-layer detachment failures in discontinuous and continuous permafrost, northern Canada. Geomorphology , 69 (1-4):275-297.

Li, N., Chen, F., Su, B., and Cheng, G. 2002. Theoretical frame of the saturated freezing soil. Cold Regions Science and Technology, 35(2): 73-80.

Li, N., Chen, F., Xu, B., and Swoboda, G. 2008. Theoretical modeling framework for an unsaturated freezing soil. Cold Regions Science and Technology, 54(1): 19-35.

Li, N., Cheng, G.D. and Xu, X.Z. 2001. The advance and review on frozen soil mechanics. Advances in Mechanics, 31(1): 95-102.

Lian-hai, Z., Wei, M.A., and Cheng-song, Y. 2015. Pore water pressure measurement for soil subjected to freeze-thaw cycles. Rock and Soil Mechanics, 36(7): 1856-1864.

Liang Y, Beier N, and Sego DC. 2022a. New Method for Internal Pore-Water Pressure Measurements. Geotechnical Testing Journal, 45(2): 490-502.

Liang Y, Beier N, and Sego DC. 2022b. Continuity of pore-water pressure measurements in partially frozen sand. (Manuscript submitted for publication)

Linell, K.A. and Johnston, G.H. 1973. Engineering design and construction in permafrost regions: A review. Permafrost: North American Contribution to the Second International Conference, National Academy of Sciences, pp. 553-575.

Lyu, C., Nishimura, S., Amiri, S.A.G., Zhu, F., Eiksund, G.R., and Grimstad, G. 2021a. Pore-water pressure development in a frozen saline clay under isotropic loading and undrained shearing. Acta Geotechnica, 16(12): 3831-3847.

Lyu, C., Grimstad, G., and Nishimura, S. 2021b. Pore pressure coefficient in frozen soils (Published online). Géotechnique: 1-10.

Marello, S. 2005. Experimental Study of Shear Bands in Fine Grained Soils. In Proceedings of the 11th International Conference on Computer Methods and Advances in Geomechanics, IACMAG, Torino, Italy, 2:119–26.

Mellor, M. 1980. Mechanical properties of polycrystalline ice. In Physics and Mechanics of Ice, International Union of Theoretical and Applied Mechanics, Copenhagen, Springer Verlag, Berlin, pp. 217-245.

Melton, J.S., and Schulson, E.M. The ductile deformation of columnar (S2) saline ice under triaxial compression. In The Seventh International Offshore and Polar Engineering Conference. 1997. OnePetro.

Miyata, Y. and Akagawa, S. 1997. An experimental study on static solid-liquid phase equilibrium in the pores of a porous medium. Heat Transfer-Japanese Research: Co-sponsored by the Society of Chemical Engineers of Japan and the Heat Transfer Division of ASME, 26(2): 69-83.

Muller, S.W. 1946. Permafrost and related engineering problems. AAPG Bulletin, 30(12): 2089-2089.

Nishimura, S., and Wang, J. 2019. A simple framework for describing strength of saturated frozen soils as multi-phase coupled system. Géotechnique, 69(8): 659-671.

Nishimura, S., Gens, A., Olivella, S., and Jardine, R. 2009. THM-coupled finite element analysis of frozen soil: formulation and application. Géotechnique, 59(3): 159-171.

Ogata, N., Yasuda, M., and Kataoka, T. 1983. Effects of salt concentration on strength and creep behavior of artificially frozen soils. Cold Regions Science and Technology, 8(2): 139-153.

Parameswaran, V. 1980. Deformation behaviour and strength of frozen sand. Canadian Geotechnical Journal, 17(1): 74-88.

Parameswaran, V., and Jones, S. 1981. Triaxial testing of frozen sand. Journal of Glaciology, 27(95): 147-155.

Penner, E. 1959. Pressures developed in a porous granular system as a result of ice segregation. Highway Research Board Special Report, (40): 191-199.

Pharr, G., and Merwin, J. 1985. Effects of brine content on the strength of frozen Ottawa sand. Cold Regions Science and Technology, 11(3): 205-212.

Poulos, S.J. 1981. The steady state of deformation. Journal of the Geotechnical Engineering Division, 107(5): 553-562.

Poulos, S.J., Castro, G., and France, J.W. 1985. Liquefaction evaluation procedure. Journal of

Geotechnical Engineering, 111(6): 772-792.

Romanovsky, V.E., Smith, S.L., and Christiansen, H.H. 2010. Permafrost thermal state in the polar Northern Hemisphere during the international polar year 2007–2009: a synthesis. Permafrost and Periglacial Processes, 21(2): 106-116.

Roscoe, K.H., Schofield, A., and Wroth, a.P. 1958. On the yielding of soils. Géotechnique, 8(1): 22-53.

Sasitharan, S., Robertson, P., Sego, D., and Morgenstern, N. 1993. Collapse behavior of sand. Canadian Geotechnical Journal, 30(4): 569-577.

Sayles, F.H. 1974. Triaxial constant strain rate tests and triaxial creep tests on frozen Ottawa sand. Corps of Engineers, US Army Cold Regions Research and Engineering Laboratory. Technical Report 253.

Sayles, F. 1989. State of the art, mechanical properties of frozen soil. In Proceedings of 5th International Symposium on Ground Freezing, Nottingham, England. A.A. Balkema, Rotterdam, pp. 143-165.

Schofield, A.N., and Wroth, P. 1968. Critical state soil mechanics. London: McGraw-hill.

Schrefler, B. A., H. W. Zhang, M. Pastor, and O. C. Zienkiewicz. 1998. Strain Localisation Modelling and Pore Pressure in Saturated Sand Samples. Computational Mechanics, 22 (3): 266–80.

Seto, J., and Konrad, J.-M. 1994. Pore pressure measurements during freezing of an overconsolidated clayey silt. Cold Regions Science and Technology, 22(4): 319-338.

Sheahan, T. C. 1991. An experimental study of the time-dependent undrained shear behavior of resedimented clay using automated stress path triaxial equipment. Ph.D. thesis, Massachusetts Institute of Technology.

Sheeran, D.E., and Yong, R.N. 1975. Water and salt distribution in freezing soils. Proceedings, 1st Conference on Soil-Water Problems in Cold Regions, Calgary, Alta. pp. 58-69

Shiklomanov, N.I., Streletskiy, D.A., Swales, T.B., and Kokorev, V.A. 2017. Climate change and stability of urban infrastructure in Russian permafrost regions: prognostic assessment based on GCM climate projections. Geographical review, 107(1): 125-142.

Shuttle, D.A, and I. M. Smith. 1990. Localisation in the Presence of Excess Porewater Pressure. Computers and Geotechnics, 9(1): 87–99.

Stuckert, B., and Mahar, L. 1984. Role of ice content in the strength of frozen saline coarse grained soils. In Proceedings, Cold Regions Engineering Specialty Conference, Edmonton, AB. Montreal: Canadian Society for Civil Engineering. pp. 579-587.

Swanson, D., Murphy, D., Temmer, J., and Scaletta, T. 2021. Advancing the Climate Resilience of Canadian Infrastructure: A Review of Literature to Inform the Way Forward. International Institute for Sustainable Development.

Thakur, V., S. Nordal, H. P. Jostad, and L. Andresen. 2005. Study on Pore Water Pressure Dissipation during Shear Banding in Sensitive Clays. In 11th International Conference on Computer Methods and Advances in Geomechanics, IACMAG, Torino, Italy, 4: 289- 296.

Thakur, V. 2007. Strain Localization in Sensitive Soft Clays. PhD diss., Norwegian University of Science and Technology.

Thakur, V. 2011. Numerically Observed Shear Bands in Soft Sensitive Clays. Geomechanics and Geoengineering: An International Journal, 6(2): 131–46.

Thakur, V., S. Nordal, G. Viggiani, and P. Charrier. 2018. Shear Bands in Undrained Plane Strain Compression of Norwegian Quick Clays. Canadian Geotechnical Journal, 55 (1): 45-56.

Thomas, H.R., Cleall, P., Li, Y.-C., Harris, C., and Kern-Luetschg, M. 2009. Modelling of cryogenic processes in permafrost and seasonally frozen soils. Géotechnique, 59(3): 173-184.

Ting, J.M., Torrence Martin, R., and Ladd, C.C. 1983. Mechanisms of strength for frozen sand. Journal of Geotechnical Engineering, 109(10): 1286-1302.

Tsarapov, M. 2007. Use of pore pressure to determine strength characteristics of thawing soils. Soil Mechanics and Foundation Engineering, 44(4): 132-136.

Vaid, Y., and Sivathayalan, S. 1997. Errors in estimates of void ratio of laboratory sand specimens. Canadian Geotechnical Journal, 33(6): 1017-1020.

Vardoulakis, I. 1996a. Deformation in Water-Saturated Sand: II. Effect of Pore Water Flow and Shear Banding. Géotechnique, 46(3): 457–72.

Vardoulakis, I. 1996b. Deformation of Water-Saturated Sand: I. Uniform Undrained Deformation and Shear Banding. Géotechnique, 46 (3): 441–56.

Viggiani, G, R J Finno, and W. W. Harris. 1994. Experimental Observations of Strain Localisation in Plane Strain Compression of a Stiff Clay. Localization and Bifurcation Theory for Soils and Rocks, 189–98.

Vincent, W.F., Lemay, M., and Allard, M. 2017. Arctic permafrost landscapes in transition: towards an integrated Earth system approach. Arctic Science, 3(2): 39-64.

Wang, J., Nishimura, S., and Tokoro, T. 2017. Laboratory study and interpretation of mechanical behavior of frozen clay through state concept. Soils and Foundations, 57(2): 194-210.

Williams, P.J. 1966. Pore Pressures at a Penetrating Frost line and their prediction. Géotechnique, 16(3): 187-208.

Wood, D.M. 1990. Soil behaviour and critical state soil mechanics. Cambridge university press.

Xu, J., Liu, H., and Zhao, X. 2017. Study on the strength and deformation property of frozen silty sand with NaCl under triaxial compression condition. Cold Regions Science and Technology, 137: 7-16.

Xu, X., Wang, Y., Bai, R., Fan, C., and Hua, S. 2016. Comparative studies on mechanical behavior of frozen natural saline silty sand and frozen desalted silty sand. Cold Regions Science and Technology, 132: 81-88.

Yamamoto, Y., and Springman, S.M. 2014. Axial compression stress path tests on artificial frozen soil samples in a triaxial device at temperatures just below 0℃. Canadian Geotechnical Journal, 51(10): 1178-1195.

Yuan, J., Q. Zhang, B. Li, and X. Zhao. 2013. Experimental Analysis of Shear Band Formation in Plane Strain Tests on Shanghai Silty Clay. Bulletin of Engineering Geology and the Environment, 72(1): 107–14.

Yu, F., Guo, P., and Na, S. 2022. A framework for constructing elasto‐plastic constitutive models for frozen and unfrozen soils. International Journal for Numerical and Analytical Methods in Geomechanics, 46(2): 436-466.

Zhang, H., Zhang, J., Zhang, Z., and Chai, M. 2016. Investigation of the pore-water pressure of saturated warm frozen soils under a constant load. Journal of Offshore Mechanics and Arctic Engineering, 138(6): 062001

Zhang, L., Ma, W., Yang, C., and Yuan, C. 2014. Investigation of the pore water pressures of

coarse-grained sandy soil during open-system step-freezing and thawing tests. Engineering Geology, 181: 233-248.

Zhang, Y., and Michalowski, R.L. 2015. Thermal-hydro-mechanical analysis of frost heave and thaw settlement. Journal of geotechnical and geoenvironmental engineering, 141(7): 04015027.

Zhou, J., Lee, W. and Zhou, K. 1995. Dynamic properties and liquefaction potential of silts. Proceedings of the International Conference on Earthquake Geotechnical Engineering, Tokyo, Japan, 2:833-838.

Zhu, Z., Ning, J., and Ma, W. 2010. A constitutive model of frozen soil with damage and numericalsimulation for the coupled problem. Science China Physics, Mechanics and Astronomy, 53(4): 699-711.